

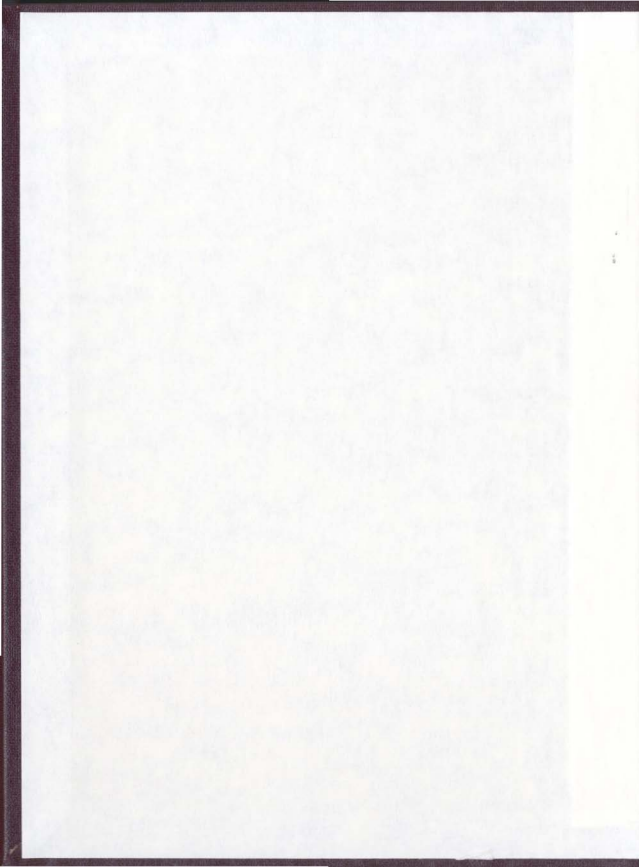
THE THERMODYNAMICS OF (CARBON DIOXIDE +
METHANOL) MIXTURES FROM 25⁰C TO 250⁰C
AND AT PRESSURES UP TO 20 MPA

CENTRE FOR NEWFOUNDLAND STUDIES

**TOTAL OF 10 PAGES ONLY
MAY BE XEROXED**

(Without Author's Permission)

WANDA MARIE AYLWARD



THE THERMODYNAMICS OF (CARBON DIOXIDE + METHANOL) MIXTURES
FROM 25°C TO 250°C AND AT PRESSURES UP TO 20 MPA

By

Wanda Marie Aylward

A thesis submitted to the
School of Graduate Studies
in partial fulfillment of the
requirements for the degree of
Master of Science

Department of Chemistry
Memorial University of Newfoundland

May 2002

St. John's

Newfoundland

Abstract

The presence of carbon dioxide in natural gas, synthetic gas and liquid streams has prompted the industrial community to examine the properties of carbon dioxide mixtures with the intent of finding novel methods for removing this acidic impurity. Carbon dioxide is also of interest to researchers because it possesses a readily accessible critical point. This has stimulated studies of the phase behaviour and thermodynamic properties of supercritical fluid mixtures, particularly in systems used in supercritical fluid chromatography (SFC) and supercritical fluid extraction (SFE). For both of these applications, it is important to obtain information pertaining to the vapour-liquid phase boundaries for the carbon dioxide mixtures and their thermodynamic properties over a wide range of pressure and temperature. The ($\text{CO}_2 + \text{MeOH}$) system is of interest to applied research on fluid properties because the pure liquids have widely differing critical points.

There are many experimental issues associated with supercritical fluids, and laboratory equipment must be specially designed to handle these high pressure, high temperature fluids. A high precision isothermal microcalorimeter has been commissioned to measure the excess molar enthalpy of mixing H_m^E for the mixture at 298.15 K and pressures of 7.5 and 10.0 MPa. A platinum vibrating U-tube densitometer with a specially designed injection system has been used to measure the densities of ($\text{CO}_2 + \text{MeOH}$) mixtures at temperatures from 298.15 K to 523.15 K and pressures up to 20.0 MPa, from which excess molar volumes V_m^E were calculated.

The H_m^E curves display sigmoidal shapes and negative minima in the methanol-rich regions and were observed at both pressures. A positive maximum at high CO_2 mole fraction, x_{CO_2} , was obtained at the higher pressure. These results, along with those obtained for $(CO_2 + MeOH)$ mixtures from Christensen et al. (1987) at higher temperatures were interpreted in terms of the states of the mixtures and pure components.

The volumetric results obtained from the density data showed negative V_m^E results that became much more negative as the temperature was increased. Reduced excess molar volumes $V_m^R = V_m^E / [x(1-x)]$ obtained at high x_{CO_2} showed very large negative deviations from ideal behaviour, indicating strong interactions between supercritical CO_2 and molecular methanol. The V_m^R data were used to determine the apparent molar volumes and the standard partial molar volumes of CO_2 and methanol in the mixtures. Once again, the results were interpreted in terms of phase behaviour of the mixture relative to the pure components.

ACKNOWLEDGEMENTS

First and foremost, I would like to thank Dr. Tremaine for providing me the opportunity to carry out my graduate studies under his guidance. His support and constructive criticism are gratefully acknowledged. I feel that it has been a great honour to have been accepted into his lab group and the experience has opened my eyes to a whole new branch of chemistry.

I would also like to thank everyone in the hydrothermal chemistry lab group for making the experience such an enjoyable one. Thanks are extended to: Rose, for always being a friend that I could rely on and for introducing me to the chemistry society; Jenene, for always being in a good mood and willing to go out for lunch at a moment's notice; Kai, for always being helpful around the lab; and Chris and Richard for many hours of great conversation. A special thanks goes to Liliana and Rodney, without whom I probably wouldn't have made it past my very first week in the program. Randy Thorne and Carl Mulcahy from technical services are greatly acknowledged for their support with equipment problems in the lab. It's always been a pleasure to have an excuse to visit their shops.

Some personal thank-yous go to my family and friends. First to my Mom and Dad for supporting me through my undergraduate schooling and again through this next step of my life. You are a constant source of inspiration to me. My sincere appreciation goes to my sisters, each of whom has played a big part in helping me to get to where I am now. To my sisters: Barbara, who thinks that I am crazy to still be in school; Manda,

whose cheerful mood is so contagious and Jen, who reminds me that a little trouble in life sure is fun! Thank you! And I would also like to thank Jon Kehoe for his constant encouragement and for lightening the load along the way with his comic book and wrestling trivia. And don't forget, Jon, mostly I thank you for your friendship!

Finally I would like to thank Atlantic Accord, the School of Graduate Studies and the chemistry department at M.U.N. for financial support.

Table of Contents

Abstract	ii
Acknowledgement	iv
Table of Contents	vi
List of Figures	ix
List of Tables	xii
List of Symbols	xiv
1. Introduction	1
1.1 The Importance of (Carbon Dioxide + Solvent) Mixtures.....	1
1.2 Thermodynamics of Mixtures.....	3
1.3 Near-Critical Effects.....	8
1.4 (Carbon Dioxide + Solvent) Systems.....	10
1.4.1 Pure Carbon Dioxide.....	10
1.4.2 (Carbon Dioxide + Solvent) Mixtures.....	12
1.5 The (CO ₂ + MeOH) System.....	15
1.5.1 Pure Methanol.....	15
1.5.2 Critical Locus for the (CO ₂ + MeOH) System.....	17
1.6 The Redlich-Kister Equation.....	22
1.7 Solution Flow Calorimetry.....	23
1.7.1 Solution Calorimeters.....	23
1.7.2 Isothermal Flow Calorimeters.....	29
1.8 Vibrating Tube Densitometry.....	35
1.9 Goals and Objectives of this Work.....	36
2. Experimental	38
2.1 Materials.....	38
2.2 Excess Enthalpy of Mixing, H_m^E	39
2.2.1 The Isothermal Flow Heat-of-Mixing System.....	39
2.2.2 Commissioning.....	48
2.2.3 Calibration.....	49
2.2.4 Optimal Conditions.....	53

2.3	Vibrating Tube Densitometry.....	54
2.3.1	Construction	54
2.3.2	Commissioning.....	58
2.3.3	Calibration.....	60
2.3.4	Optimal Conditions	61
2.4	Calculations.....	62
2.4.1	Enthalpy Calculations.....	62
2.4.2	Volumetric Calculations.....	64
2.4.3	Uncertainties in Measurements	66
3.	Enthalpy Results for (CO₂ + MeOH) Mixtures	67
3.1	Introduction	67
3.2	H _m ^E of (CO ₂ + MeOH).....	67
3.2.1	Introduction	67
3.2.2	H _m ^E at 298.15 K	68
3.2.3	H _m ^E vs. Temperature and Pressure for (CO ₂ + MeOH)	69
3.3	Discussion	75
3.3.1	Solute-Solvent Interactions	75
3.3.2	Experimental Insights	76
4.	Volumetric Results for (CO₂ + MeOH) Mixtures.....	79
4.1	Introduction	79
4.2	Calibration of Vibrating U-Tube Densitometer	80
4.2.1	Water and Carbon Dioxide as Calibrating Fluids	80
4.3	Bubble Point Measurements	81
4.4	Molar Volumes for (CO ₂ + MeOH) from Ambient Temperatures to 523.15 K at 12.3 MPa and 19.8 MPa	86
4.4.1	Excess Molar Volumes.....	86
4.4.2	Reduced Excess Molar Volumes.....	103
4.4.3	Reduced Excess Enthalpy for (CO ₂ + MeOH).....	110
4.4.4	Apparent Molar Volumes and Standard Partial Molar volumes	112
5.	Molecular Interpretation	119
6.	Future Work.....	121
	Bibliography	123

Appendix I Scoping Experiments on the CSC 4400 Isothermal Microcalorimeter	130
A.I-1 Calibration of Calorimeter and High Pressure Flow Cells with (Water + Ethanol) Mixtures	130
A.I-2 (Carbon Dioxide + Propylene Carbonate) Mixtures	136
A.I-3 Scoping Experiments on Selected Dilute Systems	138
A.I-3.1 Introduction.....	138
A.I-3.2 (Carbon Dioxide + Aqueous Ethanolamine).....	138
A.I-3.3 (Carbon Dioxide + Aqueous Sodium Dodecyl Sulfate Solutions).....	139
A.I-3.4 (Carbon Dioxide + Water)	143
Appendix II Experimental Results for the (CO₂ + MeOH) Mixtures	146

LIST OF FIGURES

Figure 1.1	The critical locus for (CO ₂ + MeOH) as a function of temperature and pressure as determined by Brunner et al. (1985, 1987) and Ziegler et al. (1995).....	19
Figure 1.2	Three-dimensional plot of (CO ₂ + MeOH) vapour-liquid phase behaviour as a function of pressure, temperature and composition from 298.15 K to 373.15 K. As determined by Reighard et al. (1996).....	20
Figure 1.3	Isothermal phase equilibrium of (xCO ₂ + (1-x)MeOH). Re-plotted from Brunner et al. (1987).....	21
Figure 1.4	Schematic diagram of a heat-flow calorimeter.....	28
Figure 1.5	Schematic diagram of a power-compensated isothermal calorimeter.....	30
Figure 1.6	Schematic diagram of a flow-mixing cell.....	31
Figure 1.7	Schematic diagram of a differential flow calorimeter.....	33
Figure 2.1	Schematic diagram of the CSC 4400 isothermal microcalorimeter.....	42
Figure 2.2	Schematic diagram of the flow injection system used with the CSC 4400 isothermal microcalorimeter.....	43
Figure 2.3	Schematic diagram of the high-pressure viewing cell.....	47
Figure 2.4	Schematic representation of the pulse calibration method.....	51
Figure 2.5	Schematic representation of the steady-state calibration method.....	52
Figure 2.6	Schematic diagram of the injection system used with the vibrating U-tube densitometer.....	57
Figure 2.7	Schematic diagram of the mixer constructed for this work to use with the vibrating U-tube densitometer.....	59
Figure 3.1	Comparisons of the experimental results with literature values for the (CO ₂ + MeOH) system at 298.15 K.....	70
Figure 3.2	H _m ^E values for (CO ₂ + MeOH) at three temperatures at 7.5 MPa as obtained from Christensen et al. (1987).....	72

Figure 3.3	H_m^E values for (CO ₂ + MeOH) at three temperatures at 12.5 MPa as obtained from Christensen et al. (1987).....	73
Figure 4.1a	Excess molar volumes for (CO ₂ + MeOH) mixtures at 12.3 MPa.....	89
Figure 4.1b	Enlargement of excess molar volumes for (CO ₂ + MeOH) mixtures at 12.3 MPa and temperatures below 323.15 K.....	90
Figure 4.2	Excess molar volumes for (CO ₂ + MeOH) mixtures at 19.8 MPa.....	91
Figure 4.3	Excess molar volumes obtained at 323.15 K for (CO ₂ + MeOH) mixtures by Goldfarb et al. (1999).....	98
Figure 4.4	The relationship of the V_m^E curve at 298.15 K for (0.5 CO ₂ + 0.5 MeOH) to the molar volumes of (1) V_{m,CO_2}^* , pure carbon dioxide, (2) $V_{m,MeOH}^*$, pure methanol, and (4) $V_{m,soln}$, the mixture.....	99
Figure 4.5	The relationship of the V_m^E curve at 308.15 K for (0.5 CO ₂ + 0.5 MeOH) to the molar volumes of (1) V_{m,CO_2}^* , pure carbon dioxide, (2) $V_{m,MeOH}^*$, pure methanol, and (4) $V_{m,soln}$, the mixture.....	100
Figure 4.6	The relationship of the V_m^E curve at 498.15 K for (0.25 CO ₂ + 0.75 MeOH) to the molar volumes of (1) V_{m,CO_2}^* , pure carbon dioxide, (2) $V_{m,MeOH}^*$, pure methanol, and (4) $V_{m,soln}$, the mixture.....	101
Figure 4.7	The relationship of the V_m^E curve at 523.15 K for (0.5 CO ₂ + 0.5 MeOH) to the molar volumes of (1) V_{m,CO_2}^* , pure carbon dioxide, (2) $V_{m,MeOH}^*$, pure methanol, and (4) $V_{m,soln}$, the mixture.....	102
Figure 4.8	Reduced excess molar volume results obtained at 12.3 MPa at low temperatures (298.15 K ≤ T ≤ 323.15 K) for the carbon dioxide-rich region of the mole fractions.....	105
Figure 4.9	Reduced excess molar volume results obtained at 12.3 MPa at high temperatures (373.15 K ≤ T ≤ 523.15 K) for the carbon dioxide-rich region of the mole fractions.....	106
Figure 4.10	Reduced excess molar volume results obtained at 12.3 MPa at several temperatures for the methanol-rich region of the mole fractions.....	107
Figure 4.11	Reduced excess molar volume results obtained at 19.8 MPa at several temperatures for the carbon dioxide-rich region of the mole fraction.....	108

Figure 4.12	Reduced excess molar volume results obtained at 19.8 MPa at several temperatures for the methanol-rich region of the mole fraction	109
Figure 4.13	Reduced excess enthalpy and reduced excess volume for (CO ₂ + MeOH) at 308.15 K and 12.5 MPa	113
Figure 4.14	Reduced excess enthalpy and reduced excess volumes for (CO ₂ + MeOH) at 473.15 K and 12.5 MPa	114
Figure 4.15	Reduced excess enthalpy and reduced excess volumes for (CO ₂ + MeOH) at 523.15 K and 12.5 MPa	115
Figure 4.16	V _{CO₂} ^o as a function of temperature and pressure.....	117
Figure 4.17	V _{MeOH} ^o as a function of temperature and pressure.....	118
Figure A-1	CSC 4400 isothermal microcalorimeter power output for a 50-50 (water + ethanol) mixture at 298.15 K and 0.4 MPa as a function of flow rates	133
Figure A-2	(Water + ethanol) results for a 50-50 volume mixture at 298.15 K and 0.4 MPa and a total flow rate of 0.600 cm ³ ·min ⁻¹ taken during two different runs.....	134
Figure A-3	Excess enthalpy results for the (carbon dioxide + propylene carbonate) system over the entire mole fraction range at 298.15 K and 7.5 MPa.....	137
Figure A-4	Signal obtained from a one molal aqueous solution of SDS mixed with carbon dioxide at 298.15 K and 7.5 MPa.....	142
Figure A-5	Signal obtained for (carbon dioxide + water) at 298.15 K and 7.5 MPa	145

LIST OF TABLES

Table 1.1	Critical properties for pure carbon dioxide.....	11
Table 1.2	Critical properties for pure methanol.....	16
Table 2.1	Calibration of flow rates for injection system using water at 298.15 K and atmospheric pressure.....	45
Table 3.1	Summary of results for (CO ₂ + MeOH) at 298.15 K and 7.5 MPa and 10.0 MPa.....	71
Table 4.1	Molar volumes of CO ₂ : From densitometer calibration based on water and methanol.....	83
Table 4.2	Molar volumes of methanol: From densitometer calibration based on water and carbon dioxide.....	84
Table 4.3	Bubble point pressures for water, methanol and two (CO ₂ + MeOH) mixtures measured with the vibrating U-tube densitometer.....	85
Table 4.4	Density (ρ) of the (CO ₂ + MeOH) mixtures compared with results from the literature.....	88
Table 4.5	Parameters for the modified Redlich-Kister equation for (CO ₂ + MeOH) mixtures and standard deviations s for V_m^E	92
Table 4.6	Fitting parameters used in the linear portion of the excess volume curves in the two phase region at 12.3 MPa.....	93
Table 4.7	Comparison of the VLE data obtained in this work with Brunner et al. (1987).....	94
Table 4.8	Summary of the standard partial molar volumes obtained for methanol and carbon dioxide at 12.3 and 19.8 MPa.....	116
Table A-1	Commissioning results for the (water + ethanol) mixtures on the CSC 4400 isothermal microcalorimeter at $x_{H_2O} = 0.50$ and at 298.15 K and 0.4 MPa.....	135

Table A-2	Volumetric results for (CO ₂ + MeOH) mixtures at 298.15 K and 12.5 MPa.....	146
Table A-3	Volumetric results for (CO ₂ + MeOH) mixtures at 308.15 K and 12.5 MPa.....	147
Table A-4	Volumetric results for (CO ₂ + MeOH) mixtures at 323.15 K and 12.5 MPa.....	149
Table A-5	Volumetric results for (CO ₂ + MeOH) mixtures at 373.15 K and 12.3 MPa.....	151
Table A-6	Volumetric results for (CO ₂ + MeOH) mixtures at 373.15 K and 19.8 MPa.....	153
Table A-7	Volumetric results for (CO ₂ + MeOH) mixtures at 473.15 K and 12.3 MPa.....	155
Table A-8	Volumetric results for (CO ₂ + MeOH) mixtures at 473.15 K and 19.8 MPa.....	157
Table A-9	Volumetric results for (CO ₂ + MeOH) mixtures at 498.15 K and 12.3 MPa.....	159
Table A-10	Volumetric results for (CO ₂ + MeOH) mixtures at 498.15 K and 19.8 MPa.....	161
Table A-11	Volumetric results for (CO ₂ + MeOH) mixtures at 523.15 K and 12.3 MPa.....	163
Table A-12	Volumetric results for (CO ₂ + MeOH) mixtures at 523.15 K and 19.8 MPa.....	165

LIST OF SYMBOLS

A	Constant characteristic to the vibrating tube densitometer
ASME	American Society of Mechanical Engineers
CO ₂	Carbon Dioxide
C _p	Heat capacity
CSC	Calorimetry Sciences Corp
DEA	Diethanolamine
EtOH	Ethanol
K	Constant characteristic to the vibrating tube densitometer
K _H	Henry's Law constant
MDEA	Methyldiethanolamine
MeOH	Methanol
NIST	National Institute of Standards and Technology
P	Power
p _c	Critical pressure
p _{sat}	Saturation pressure
q	Heat
s	Standard deviation
SFC	Supercritical Fluid Chromatography

SFE	Supercritical Fluid Extraction
T_c	Critical temperature
V_c	Critical volume
Y_m^E	Excess molar property
Y_n^*	Thermodynamic property for pure n
Y_n^o	Standard partial molar property of solute n
\bar{Y}_n	Partial molar property of component n
Y_m^R	Reduced excess molar property
Y_{soln}	Total property of the solution
$Y_{\phi,n}$	Apparent molar property of solute n
α	Isobaric thermal expansivity
α_c	Critical exponent
β_c	Critical exponent
ρ	Density
ρ_c	Critical density
τ	Period of vibration
ec	Calorimetric calibration constant

Chapter 1: Introduction

1.1 The Importance of (Carbon Dioxide + Solvent) Mixtures

The properties of binary carbon dioxide mixtures have attracted considerable attention in recent years. The presence of this acidic gas in natural gas, synthetic gas (refinery gas) and liquid streams has prompted the studies of (CO₂ + solvent) mixtures. It is desirable to remove acidic impurities (CO₂, hydrogen sulfide, sulfur dioxide) from gas streams, as they can poison catalysts vital in subsequent gas processing. Specifications of product quality related to end-use and environmental standards also require the removal of these impurities. Carbon dioxide is the most widely used solvent for the critical extraction of natural products because of its easily obtainable critical point and non-toxic properties. It is also of interest to researchers seeking to study the fundamental phase behaviour and thermodynamic properties of mixtures in the near critical and supercritical regions.

The removal of carbon dioxide from gas streams must be accomplished at high pressure and may be done so through absorption or chemical reaction treatment processes. Absorption involves the transfer of carbon dioxide from the gaseous phase to the liquid phase by dissolution into a polar organic solvent. These solvents are known as "physical" solvents. The second class of treatment processes involves chemical reactions of an acid-base type between the acidic gas and a chemical base, usually an amine, in aqueous solution. These "chemical" solvents have large heats of regeneration and limited

absorption capacities. The chemical solvents are also usually more costly, corrosive, environmentally unfriendly and may cause undesirable side reactions. It would be desirable for gas processing industries to find an absorbent that would selectively and successfully remove carbon dioxide impurities from gas streams while reducing the cost for regeneration of the absorbent and eliminating caustic purchasing and disposal costs. The choice of solvent depends on the design constraints associated with the carbon dioxide removal process. Physical solvents are preferred when the partial pressure of acidic gas is high, whereas the chemical solvents are preferred under conditions of lower partial pressures. The tendency in recent years has been to favour physical rather than chemical solvents. The solubilities of acidic gases in physical solvents, along with thermodynamic data for the solutions that are related to temperature and pressure are fundamental quantities needed for the design and evaluation of absorption systems (Kohl and Riesenfeld, 1974). Methanol is an example of a good physical solvent and is commonly employed in a gas purification technique called the "Rectisol Process" in which the methanol is used to remove CO₂, and other impurities, by physical absorption (Kohl and Riesenfeld, 1974).

A recent development in the characterization of raw material is the use of supercritical fluids in supercritical fluid chromatography (SFC) and supercritical fluid extraction (SFE). Due in part to its easily accessible critical point and its natural abundance, carbon dioxide is the most commonly used fluid in SFC and SFE. Despite this, carbon dioxide is still greatly limited in its ability to function as an ideal solvent in supercritical fluid work. It is unable to solvate or efficiently extract large or polar

molecules. The solubility of polar species in supercritical carbon dioxide may be altered or enhanced by adding small amounts of a second solvent, known as a modifier, to the mixture. Methanol is one such modifier (Taylor et al., 1997).

It is essential in SFC and SFE that the system pressure is kept sufficiently high to ensure that a one-phase mixture ensues. Therefore, information pertaining to the vapour-liquid phase boundaries for the (CO₂ + modifier) and its thermodynamic properties over a range of pressure and temperature is essential. The enthalpy of mixing data for the (CO₂ + solvent) mixtures presented in this thesis have been collected using a commercial CSC 4400 isothermal microcalorimeter (Calorimetric Science Corporation), similar to the flow calorimeters used in Christensen's laboratory at Brigham Young University (see for example, Christensen et al., 1983). As well, a vibrating U-tube densitometer, similar to the one used by Albert and Wood (1984) for fluids at high temperature and pressure, was used in this work to measure the densities and volumes of (CO₂ + methanol) mixtures from which equations of state can be derived.

1.2 Thermodynamics of Mixtures

Mixing is the process that occurs when two liquids are combined together to form a solution, and is described as follows:



where the letters represent the different components of the mixture and n_i is the number of moles of component i . Mixing is a spontaneous process that serves to lower the Gibbs energy of the mixture:

$$\Delta_{\text{mix}}G = RT \sum n_i \ln a_i \quad (1.2)$$

where a_i is the activity in solution and is calculated as:

$$a_i = \gamma_{R,i} x_i \quad (1.3)$$

The term $\gamma_{R,i}$ from eq 1.3 refers to the Raoult's law activity coefficient of component i and x_i is the mole fraction. For an ideal solution, $\gamma_{R,i} = 1$ and the Gibbs energy for one mole of solution is represented as:

$$\Delta_{\text{mix}}G_m^{\text{id}} = RT \sum x_i \ln x_i \quad (1.4)$$

Other thermodynamic properties of the ideal mixture are easily calculated from eq 1.4:

$$\Delta_{\text{mix}}S_m^{\text{id}} = -R \sum x_i \ln x_i \quad (1.5)$$

$$\Delta_{\text{mix}}H_m^{\text{id}} = 0 \quad (1.6)$$

$$\Delta_{\text{mix}} U_m^{\text{id}} = 0 \quad (1.7)$$

$$\Delta_{\text{mix}} V_m^{\text{id}} = 0 \quad (1.8)$$

In ideal solutions, the molecules A and B are of similar size and the A-A, B-B and A-B interactions are of equal strength and energy (Ott and Boerio-Gates, 2000).

Real solutions deviate from Raoult's law since the energies associated with the A-A and B-B interactions are not the same as those for A-B interactions. The difference on forming one mole of mixture and one mole of ideal mixture is expressed as the excess property (Y_m^E) of that mixture.

$$Y_m^E = \Delta_{\text{mix}} Y_m - \Delta_{\text{mix}} Y_m^{\text{id}} \quad (1.9)$$

Real solutions may also be expressed in terms of their partial molar properties, which represent the change in an extensive property per mole of solute 'i' caused by an infinitesimal addition of the solute. They can also be viewed as the change in the molar property of the solution upon the addition of one mole of solute to a very large amount of solution at constant temperature and pressure and are given by:

$$\bar{Y}_1 = (\partial Y / \partial n_1)_{P,T,n_2}; \bar{Y}_2 = (\partial Y / \partial n_2)_{P,T,n_1} \quad (1.10)$$

where \bar{Y}_n is the partial molar property of component n . In this case, the volume of the solution is so large that the addition of one mole of the solute has no effect on the concentration. The total property of the real solution (Y_{soln}) is a function of the partial molar properties of the components and is expressed as follows:

$$Y_{\text{soln}} = n_1 \bar{Y}_1 + n_2 \bar{Y}_2 + \dots \quad (1.11)$$

Partial molar properties are often determined by measuring the apparent molar property of the solute, $Y_{\phi,2}$:

$$Y_{\phi,2} = (Y_{\text{soln}} - n_1 Y_1^*) / n_2 \quad (1.12)$$

where Y_{soln} is the total thermodynamic property, Y_1^* is the property value for the pure solvent and n_1 and n_2 are the number of moles of solvent and solute respectively. At infinite dilution, the apparent molar quantity is equal to the standard partial molar quantity of the solute, Y_2° :

$$\lim_{n_2 \rightarrow 0} Y_{\phi,2} = Y_2^\circ \quad (1.13)$$

From the definitions of excess properties and apparent molar properties, it follows that the two quantities are interrelated (Perron and Desnoyers, 1992). These relationships are shown in eqs 1.14 and 1.15:

$$Y_m^E/[x_2(1-x_2)] = (Y_{\phi,2} - Y_2^*)/x_1 = (Y_{\phi,1} - Y_1^*)/x_2 \quad (1.14)$$

$$\lim_{x_2 \rightarrow 0} \{Y_m^E/[x_2(1-x_2)]\} = Y_2^0 - Y_2^*; \quad \lim_{x_2 \rightarrow 1} \{Y_m^E/[x_2(1-x_2)]\} = Y_1^0 - Y_1^* \quad (1.15)$$

Although excess properties may be beneficial in illustrating the magnitude of deviation from ideality, interactions at low compositions may be hidden. Reduced excess properties, which are more sensitive to the composition, are useful in investigating dilute regions of mixtures (Perron and Desnoyers, 1992). A reduced excess property is defined as:

$$Y_m^R = Y_m^E/[x_2(1-x_2)] \quad (1.16)$$

Reduced excess functions are related to the apparent molar properties by eq 1.14. Extrapolating to the two ends of the mole fraction range ($x_2 = 0$ and 1), as shown in eq 1.15, will provide the two standard partial molar properties Y_1^0 at infinite dilution from the intercepts, $Y_1^0 - Y_1^*$.

Thermodynamic properties such as enthalpy and volume are known for many systems at ambient conditions. However, since not all naturally occurring and industrially designed processes take place under such conditions, knowledge of how these properties change with temperature, pressure and composition is required.

1.3 Near-Critical Effects

A pure fluid possesses a liquid-vapour critical point that is uniquely defined by temperature, pressure and density. The critical temperature, T_c , is the temperature above which the fluid cannot exist as a liquid, and the critical pressure, p_c , is the minimum pressure needed to liquefy a gas at its critical temperature (Atkins, 1997). Above the critical point, it is no longer possible to distinguish between the liquid and vapour forms of the fluid and phase separation is therefore not possible. This occurs because the thermal motions of the molecules are able to overcome any attractions between them. Just above the critical point, a highly compressible fluid known as a supercritical fluid is formed. This fluid has both gas-like and liquid-like characteristics. Below the critical temperature and at the saturation pressure (p_{sat}) a coexisting saturated vapour and saturated liquid describe the equilibrium state. At higher pressures, $p > p_{sat}$ and $T < T_c$, only the liquid or solid phase is stable.

Long range correlations between the molecules at the critical point cause density fluctuations and critical opalescence in the fluid as increasingly larger domains of the

fluid experience density fluctuations. Theoretical critical exponents, e.g. β_c and α_c , are used in equations of state to describe the critical behaviour of the solvent (Ott and Boerio-Gates, 2000). For example, the strong discontinuities in density (ρ) and heat capacity (C_p), that occur at the critical point, are described by the expressions

$$(\rho_l - \rho_g) \propto (|T - T_c|/T_c)^{\beta_c} \quad (1.17)$$

$$C_p \propto (|T - T_c|/T_c)^{-\alpha_c} \quad (1.18)$$

These effects cause other thermodynamic variables to undergo singularities at the critical point. For example, the thermal expansivity, compressibility and heat capacity all become infinite at the critical point.

Chemical mixtures also exhibit critical behaviour similar to that of the pure fluids. The dependence of the critical point on pressure, temperature and composition ($p_{c,x}$ and $T_{c,x}$ vs. x_c , where the subscript c denotes a critical property) is called the "critical locus". A complete critical locus for a mixture is a plot showing regions of supercritical and subcritical behaviour. The critical behaviour of the mixtures can be classified into five "types" that arise from the nature of the components of which the mixture consists (van Konynenburg and Scott, 1980).

If the experimental conditions are such that the temperature lies between the critical temperatures of the two pure solvents and the pressure is below the critical locus, liquid-vapour phase separation at the saturation pressure, p_{sat} , is possible for all Type I mixtures. If phase separation has occurred, increasing the temperature will cause the

composition of the two phases to approach each other until the critical point of the mixture is reached. At this point the two phases merge and a single phase is observed. Depending on the behaviour of the mixture, “lower” and “upper” critical solution temperatures and pressures can exist (Ott and Boerio-Goates, 2000).

1.4 (Carbon Dioxide + Solvent) Systems

1.4.1 Pure Carbon Dioxide

The large volume of pVT data collected for carbon dioxide have made it possible to accurately describe carbon dioxide by an equation of state. NIST represents the thermodynamic surface of carbon dioxide by an empirical multiparameter classical equation of state (McCarthy and Arp, 1986). This treatment is based on a modified Benedict-Webb-Rubin equation of state (MBWR) which describes fluids more accurately than the more familiar cubic equations of state (e.g. the van der Waals equation). The formulation for this equation of state consists of an equation for the Helmholtz energy (per unit mass) as a function of temperature and density. All other thermodynamic properties can be obtained by differentiating the Helmholtz energy surface. Conditions of vapour-liquid equilibrium can be established by finding a pressure where the vapour and liquid phases have identical fugacities (i.e. identical chemical potentials). The critical properties for carbon dioxide are listed in Table 1.1.

Table 1.1 Critical Properties for Pure Carbon Dioxide*

Critical Property	Value
Temperature, T_c / K	304.2
Pressure, p_c / MPa	7.376
Volume, $V_c / \text{cm}^3 \cdot \text{mol}^{-1}$	93.9
Density, $\rho_c / \text{mol} \cdot \text{cm}^{-3}$	0.01063

* Angus et al., 1976

1.4.2 (Carbon Dioxide + Solvent) Mixtures

Excess molar enthalpies, H_m^E , have been measured for binary mixtures of (CO_2 - hydrocarbon), (CO_2 + alkanol), and (CO_2 + aqueous amine) using flow calorimeters, especially by Christensen's group at Brigham Young University (1983, 1984, 1985, 1986, 1987, 1988). The various (CO_2 + hydrocarbon) mixtures that have been measured include decane, cyclohexane, toluene, and pentane at temperatures from 293.15 K to 573.15 K and up to 12.50 MPa, depending on the hydrocarbon. The mole fraction dependence of H_m^E and V_m^E is very dependent on the phase behaviour of the system. The sign and magnitude of H_m^E have been interpreted by comparing the states of the mixtures relative to those of the two pure components. Transitions from a low-density to a high-density supercritical fluid, and phase changes below the critical locus can produce large changes in H_m^E . When the states and densities of both components are similar, H_m^E are negative or slightly positive. When the states are different, the sign and magnitude of H_m^E depends on the state of the resulting mixture. Low-density fluids and gases that form high-density or liquid mixtures result in negative H_m^E values. On the other hand, positive H_m^E are the result of high-density or liquid components forming low-density or gaseous mixtures (Christensen et al., 1986). All hydrocarbons show linear excess enthalpy behaviour in CO_2 -rich mixtures under certain p and T conditions corresponding to two phase mixtures, and large negative H_m^E values near carbon dioxide's critical temperature (Zhao, 1996). This arises from the large changes in $C_{p,m}$, V_m and isobaric thermal

expansivity (α) that occur in supercritical CO_2 near the critical point (Levelt-Sengers, 1991). In their work with (CO_2 + decane), Christensen experienced problems with mixing and reproducibility (1986).

H_m^E results for carbon dioxide mixtures with methanol, n-propanol, n-butanol, and n-octanol were published together in a single paper in which Christensen et al. (1988) compared the effects of alkanol chain length. As the chain length of the alkanol increased, Christensen showed that the maximum value of the excess enthalpy decreased and occurred at increasingly higher carbon dioxide content. A modified Soave equation of state was used to represent H_m^E over the temperature and pressure range used. To minimize the standard deviation obtained by fitting the equation to experimental data, Christensen introduced an interaction parameter k_{ab} , which was varied with temperature and pressure to improve the fitting. Ideally, k_{ab} should be zero. However, Christensen's group found interaction parameters that were as high as 1.3 in some cases. This shows the very non-ideal behaviour of (CO_2 + alcohol) mixtures.

(CO_2 + amine) mixtures represent the class of "chemical" solvents, because carbon dioxide reacts with the amines to form carbamates (Kohl and Riesenfeld, 1974). In studies such as those of Oscarson et al. (1989) the calorimeter results were used to determine the saturated loading point of carbon dioxide (i.e., the mols of CO_2 absorbed per mol of amine) and to measure the enthalpy of absorption, $\Delta H_{\text{absorbed}}$. In work done with diethanolamine, DEA, (Oscarson et al., 1989) and methyldiethanolamine, MDEA (Merkely et al., 1987), it has been found that $\Delta H_{\text{absorbed}}$ is independent of the amount of

carbon dioxide absorbed below the saturation loading point and that it approaches zero asymptotically past the saturation point. Chemical equilibrium was ensured by checking to see that no flow rate dependency existed. The effects of x , p , and T varied with the type of amine.

The ($\text{CO}_2 + \text{H}_2\text{O}$) system has been extensively studied due to its importance as a model for steam injection and combustion processes, geothermal water systems, various pollution control problems, and seawater and blood chemistry. Barbero et al. (1983) and Hnedkovsky et al. (1996) reported volumetric data for the ($\text{CO}_2 + \text{H}_2\text{O}$) system as a function of temperature and pressure while solubility data have been published by Wiebe and Gaddy (1940) and Crovetto and Wood (1992). The ($\text{CO}_2 + \text{H}_2\text{O}$) system is described as follows:



Following this step, dissolved carbon dioxide reacts with the solvent water to form carbonic acid:



Often the speciation of aqueous carbon dioxide is represented by a single neutral "species" H_2CO_3^* where:



The neutral species is also in equilibrium with $\text{HCO}_3^{\ominus}(\text{aq})$ and $\text{CO}_3^{\ominus 2}(\text{aq})$.

The equilibrium distribution of carbon dioxide between the water and the air is described by Henry's Law and is expressed by the Henry's Law constant, K_{H} :

$$K_{\text{H}} = [\text{H}_2\text{CO}_3^*] / p\text{CO}_2 \quad (1.22)$$

where K_{H} has been determined to be $0.0347 \text{ mol}\cdot\text{L}^{-1}\cdot\text{atm}^{-1}$ at 298.15 K and 1 atm (Palmer and van Eldik, 1983). Reviews by Palmer and van Eldik (1983) and Gallagher et al. (1993) describe the carbon dioxide and water system and its thermodynamic behaviour in more detail.

1.5 The ($\text{CO}_2 + \text{MeOH}$) System

1.5.1 Pure Methanol

Methanol is a very polar solvent with hydrogen bonded networks and chains in the liquid phase. It forms H-bonded complexes in nonpolar liquid solvents. Its critical properties are listed in Table 1.2.

Methanol is highly hygroscopic and aqueous impurities reduce its vapour pressure

Table 1.2 Critical Properties for Pure Methanol

Critical Property	Value
Temperature, T_c / K	512.65
Pressure, p_c / MPa	7.99
Volume, V_c / $\text{cm}^3 \cdot \text{mol}^{-1}$	118
Density, ρ_c / $\text{mol} \cdot \text{cm}^{-3}$	0.00860

* de Reuck and Craven, 1993

and increase its density (Cheng and Kung, 1994). While much care was taken to avoid moisture in this work, eliminating all water impurities in methanol is virtually impossible. Methanol also adsorbs easily onto many surfaces, creating a potential source of error. Polymerization of methanol in the vapour state is another troublesome phenomenon for researchers working at high temperatures (Goodwin, 1987). The pVT properties of methanol are described by a virial equation of state that is constrained to the formulated coexistence boundary (de Reuck and Craven, 1993). This isochoric equation of state gives pressure as a function of temperature along paths of constant density which originate on the liquid-vapour critical locus. Because of its small size and large anisotropy, methanol is a difficult molecule to treat theoretically, and comparison with experimental data shows that Goodwin's equation of state is not valid under high temperature and pressure conditions (Friend, 2001).

1.5.2 Critical Locus for the (CO₂ + MeOH) System

A knowledge of the critical locus of the (CO₂ + MeOH) system is important to ensure that our measurements lie in the critical and single-phase fluid region. Most of the literature studies to determine the critical locus for the (CO₂ + MeOH) system employed specially designed sight gauges or view cells. The critical loci were determined visually by observing the disappearance and reappearance of gas-liquid meniscus or bubbles in a closed cell upon changing temperatures and pressures (Brunner, 1985; Gurdial et al.,

1993; Reighard et al., 1996). When visual cells are not sufficiently accurate or when convenience dictated, inverse gas chromatographic methods can be employed in novel ways to determine the critical locus (Brunner, 1987; Ziegler et al., 1995).

Studies on the p-T plane of the critical locus for the (CO₂+MeOH) system at elevated temperatures show the system to display Type I phase behaviour according to van Konyenburg and Scott's classification (Section 1.3). Type I phase behaviour describes a critical locus that smoothly and continuously joins the two critical end points of the pure liquids. It is observed for binary mixtures with components of similar chemical type or of similar critical properties. The critical boundary shown in Figure 1.1, taken from a paper by Ziegler (1995), is a continuous mixture critical curve connecting the critical points of the pure carbon dioxide and methanol. Above this curve, a single supercritical fluid phase exists. The area below the curve represents the region where one-phase liquid, one-phase vapour and liquid-vapour phases are possible. The phase behaviour below this curve is determined by the composition of the mixture. A thorough study on the p-T-x plane for (CO₂+MeOH) mixtures at temperatures up to 373 K by Reighard et al. (1996) provided more detailed information about this system. Reighard's three-dimensional plot for the vapour-liquid phase behaviour for the (CO₂ + MeOH) mixture is shown in Figure 1.2 and Brunner's isothermal phase equilibrium plot is given in Figure 1.3. As before, the region above the curve represents the one phase liquid or supercritical fluid phase. The area under the curve is the two-phase liquid-vapour region. At very low pressures, a single-phase vapour region also occurs.

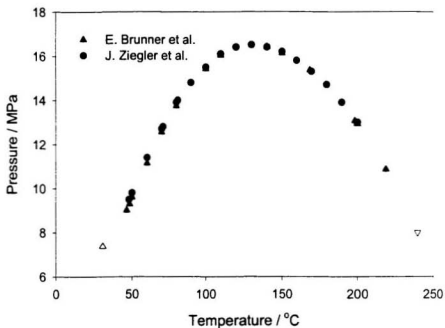


Figure 1.1 The critical locus for (CO₂ + MeOH) as a function of temperature and pressure as determined by Brunner et al. (1985, 1987) and Ziegler et al. (1995). Δ, pure CO₂; ∇, pure methanol.

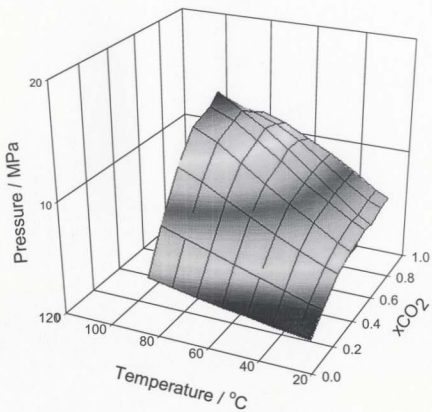


Figure 1.2 Three-dimensional plot of (CO₂ + MeOH) vapour-liquid phase behaviour as a function of pressure, temperature and composition from 298.15 K to 373.15 K. As determined by Reighard et al. (1996).

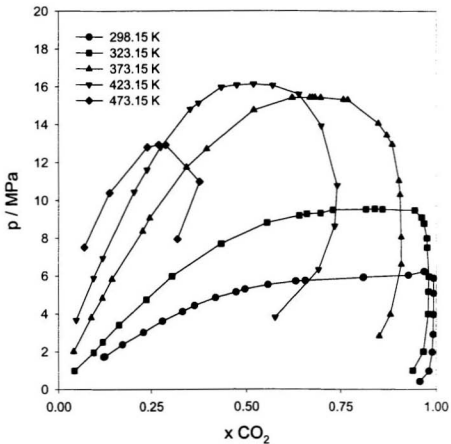


Figure 1.3 Isothermal phase equilibrium of $(x\text{CO}_2 + (1-x)\text{MeOH})$. Re-plotted from Brunner et al. (1987).

1.6 The Redlich-Kister Equation

Excess property data for fluid mixtures is often expressed by the Redlich-Kister equation (Redlich and Kister, 1948). This equation provides a convenient method for representing the excess properties and classifying different types of solvent-solvent interactions in liquid solutions. The Redlich-Kister equation is an expanded form of the Margules equation, having the form:

$$Y_m^E = x_2 (1-x_2) \sum A_i (2x_2-1)^i \quad (1.23)$$

where the interaction terms, A_i , are least-squares parameters. The Margules equation ($i=0$) is symmetric in x_2 and produces a parabola when Y_m^E is plotted against x_2 . The shape of the parabola is controlled by the value of the interaction parameter used. The Redlich-Kister equation is a more flexible fitting function. The even-powered correction terms (A_2, A_4, \dots), are symmetric in x_2 and are used to flatten or sharpen the parabola. The parameters of odd power are inserted into the equation to skew the parabola either to the left or to the right. They are able to do so because of their asymmetric relationship to x_2 . In practice, an adequate number of terms are applied to obtain the most statistically significant "best" fit of the Redlich-Kister equation to experimental data. One must be careful when fitting data to equations of this type, as correlations may be meaningless if too many parameters are needed to adequately fit the curve. Generally no more than four

parameters should be required in the correlation (Perron et al., 1992). If more terms are needed, an alternative approach should be considered. An alternative, more general form of the Redlich-Kister equation has been used extensively by research groups working with binary and ternary carbon dioxide mixtures. Christensen and co-workers (1984, 1985, and 1986) have adapted the use of rational functions (ratios of polynomials) as the method of choice for expressing excess properties of carbon dioxide. The ratio is expressed by Van Ness and Abbott (1982) as:

$$Y_m^E = \{x_2 (1-x_2)\} \{A_0 + [\sum A_n (2x-1)^n]\} / \{1 + [\sum B_m (2x-1)^m]\} \quad (1.24)$$

This was the form of the equation used to obtain the best fits to data measured in this work.

1.7 Solution Flow Calorimetry

1.7.1 Solution Calorimeters

Solution chemistry is the study of physical properties and chemical reactions occurring between species in the liquid phase. It embraces systems of chemical, biological and physical interest. Calorimetry is an important tool in solution chemistry because many thermodynamic properties of solutes may be obtained by solution

calorimetry. Since 1960, the use of calorimetry in solution studies has been extended to systems under extreme conditions of temperature and pressure (Somsen, 1994). The development of flow calorimeters by thermochemical research groups, such as those at Brigham Young University and the University of Delaware, introduced new methods for obtaining accurate enthalpies of mixing, dilution, or reaction, and partial molar heat capacities (Somsen, 1994). Flow calorimetry has also made a substantial contribution to the collection of data for supercritical fluids. In heat of mixing flow calorimetry, two liquids flow continuously through a mixing chamber at constant flow rate and pressure. The heat change measured in the mixing chamber is proportional to the known flow rate and the heat released from the chemical reaction. Heat capacity flow calorimeters measure the power required to impose a fixed temperature increment on a flowing sample of solution relative to that for pure water. A further advancement in solution calorimetry was the development of highly sophisticated microcalorimeters of various designs, most often used for biophysical purposes. These are able to measure accurate enthalpy changes for very small samples on short time scales.

Calorimeters are classified by the methods they use to measure the heats evolved during the process. The three most widely used calorimeters are (1) adiabatic calorimeters, (2) isoperibol calorimeters and (3) isothermal calorimeters. Other calorimeter designs are also available.

(1) Adiabatic Calorimeters

An adiabatic calorimeter consists of an insulated reaction vessel and a heat shield placed within a thermostatted water bath. The heat shield surrounds the reaction vessel and is maintained at the same temperature to prevent the exchange of heat between the reaction vessel and the surrounding, i.e. $q = 0$. The temperature of the surrounding is kept constant by a thermostatted bath while the temperature of the calorimeter vessel itself changes as heat is evolved during the reaction. The enthalpy of reaction can be calculated from the temperature change in the reaction vessel. The precision of adiabatic calorimeters is about 0.02 per cent (Cordfunke and Ouweltjes, 1994) but this advantage is offset by their complicated construction and instrumentation, and their expense.

(2) Isoperibol Calorimeters

An isoperibol calorimeter also consists of an insulated calorimetric vessel placed inside a constant temperature water bath, but in this case there is no temperature-controlled heat shield present to ensure that no heat flows between the reaction vessel and the bath. While most of the heat evolved is accumulated in the reaction vessel, some heat is exchanged with the surrounding. The enthalpy of reaction is calculated from the temperature change during the chemical process, as measured with high-sensitivity thermistors. Although the accuracy of isoperibolic calorimeters is not as great as that of the adiabatic ones (within 0.2 per cent), they have the advantage of being simpler in construction and operation (Albert and Archer, 1994) and are most suitable for fast reactions.

(3) Isothermal Calorimeters

An isothermal calorimeter consists of a reaction vessel placed inside a constant temperature water bath where complete heat exchange between the vessel and the surrounding is allowed. The heats of mixing are measured by monitoring the energy needed to maintain the reaction vessel at the same temperature as its surrounding:

$$T_{\text{surrounding}} = T_{\text{vessel}} = \text{Constant} \quad (1.25)$$

Isothermal calorimeters are among the most widely used calorimeters for determining heats of mixing in research and have the advantage that slow reactions may be studied since heat leaks are minimized.

Isothermal calorimeters consist of two types based on either the "heat flux" or "power-compensated" design principle. "Heat Flux" or "Heat Flow" calorimeters are passive calorimeters that monitor the heats of reaction by placing a large constant temperature heat sink, such as a copper plate, in contact with the reaction vessel. The heat sink must be a good enough conductor, so that all of the heat exchange occurs along the heat sink, instead of through the insulated reaction vessel walls into the surrounding water bath. Thermopiles, or other measuring devices, are placed between the plate and the reaction vessel to monitor the flow of heat between the reaction vessel and the heat sink.

A schematic diagram of a typical heat-flow calorimeter is illustrated in Figure 1.4. In a heat-flow calorimeter, thermopiles or solid state Peltier devices are connected to the reaction vessel to provide a means of measuring the energy flow from the cell into a heat sink at the same temperature as the reaction vessel. These are mounted in a cylindrical construction around the reaction vessel or at the base of the vessel in contact with the heat sink, with a defined thermal resistance between the vessel and the sink. The heat released or consumed during the mixing process initially causes a temperature change between the vessel and the surroundings and is immediately followed by a relaxation process in which the heat flows in or out of the cell to re-establish isothermal conditions. A record of the time dependence of this temperature difference allows us to measure the heat flow according to the following:

$$q = 1/R_{th} \int \Delta T(t) \quad (1.26)$$

This equation takes into account the small time-dependent temperature difference between the vessel wall and the heat sink ($\Delta T(t)$) and thermal resistance (R_{th}) of the thermopile (Zhao, 1996).

“Power-compensated” calorimeters are active calorimeters in which the vessel temperature is actively controlled by regulating a series of electrical heaters and coolers. By using a Peltier device to add heat to or remove heat from the vessel, the temperature difference between the vessel and surroundings is minimized and isothermal conditions

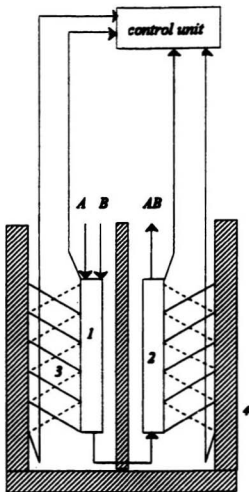


Figure 1.4 Schematic diagram of a heat-flow calorimeter. (1) reaction vessel, (2) reference cell, (3) thermopiles and (4) heat sink.

are maintained. The heating or cooling power required by the Peltier device to maintain the vessel at constant temperature is used to measure the heats of mixing in power-compensated calorimeters.

A schematic illustration of a power-compensated isothermal calorimeter is shown in Figure 1.5. For this type of calorimeter, isothermal conditions are maintained by means of either a negative heat flux or a positive heat flux provided by a Peltier device, depending on whether exothermic or endothermic mixing has occurred in the reaction vessel. That is to say that the temperature of the vessel is forced to follow that of the surroundings at all times. If we define the power generated by the mixing process $P_1(t)$ and that of the compensating heater power $P_2(t)$ the condition that the calorimeter follows is:

$$P_1(t) + P_2(t) = 0 \quad (1.27)$$

1.7.2 Isothermal Flow Calorimeters

The simplest way of achieving good mixing between two components without the use of mechanical stirrers, for which heat corrections must be applied, is to use a flow cell (Somsen, 1994). Flow cells typically consist of a T-piece at which two fluids are brought together, such as the one shown in Figure 1.6. The fluids flow into the cell through separate tubing and are allowed to come to thermal equilibrium with the

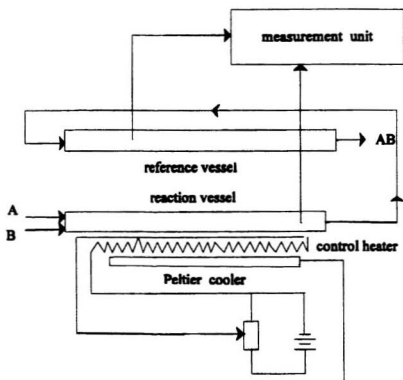


Figure 1.5 Schematic diagram of a power-compensated isothermal calorimeter.

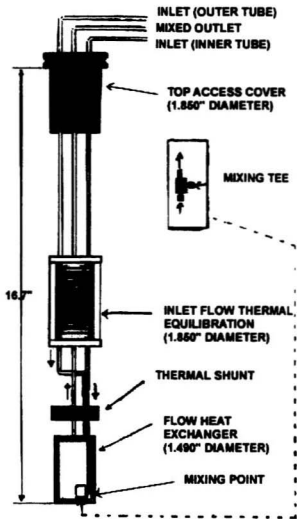


Figure 1.6 Schematic diagram of a flow-mixing cell. The cell shown here is a CSC flow-mixing cell.

surrounding bath before reaching the tee piece. The two fluids arrive at the tee joint at separate entrances and mixing occurs inside the tee piece. A homogeneous mixture flows out through the remaining pathway and is carried away from the calorimeter through a third tube called the outlet. Flow cells are usually designed to operate at low flow rates in order to conserve the sample material. Flow cells have the advantages of eliminating the time-consuming steps of weighing and filling calorimeter vessels. Also, the time needed to reach thermal equilibrium prior to measurement is greatly reduced.

To achieve greater sensitivity and stability, two identical calorimeter flow cells can be connected in a differential mode known as a twin arrangement (Ott and Wormald, 1994). The sample is pumped through one of the cells while a reference fluid is pumped through the other. Since it is virtually impossible to maintain truly isothermal conditions, this arrangement is used to eliminate some of the noise caused by temperature fluctuations in the water bath and produces more stable signals.

The general principle of differential flow calorimetry is illustrated in Figure 1.7. As described above, the reactant fluids A and B are flowed separately into the calorimeter vessel at constant flow rate and brought together in a mixing chamber. Mixture AB leaves the calorimeter through another piece of tubing placed after the mixing tee. A duplicate flow system, through which a fluid of similar heat capacity (shown here as mixture AB) is circulated, is used as a reference.

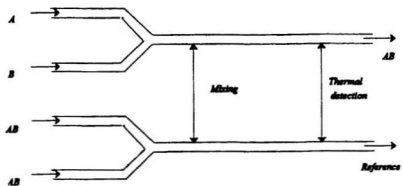


Figure 1.7 Schematic diagram of a differential flow calorimeter.

It is essential in flow calorimetry to have reliable flow pumps because lack of a constant and reproducible flow is often a major source of error. Reciprocating and syringe pumps developed for high pressure and liquid chromatography (HPLC) have been widely used for this application. Care must also be taken to ensure constant pressure conditions during a calorimetric run. While excess enthalpies may be measured for mixtures near a critical point using a flow calorimeter, the accuracy of the results depends on the accuracy of pressure, temperature and flow rate readings.

At temperatures and pressures within one per cent of the critical locus, problems associated with the high compressibility of the sample fluid may be expected (Ott and Wormald, 1994). The small pressure gradient that is required to make a fluid flow will result in large thermodynamic differences near the critical point. As well, the time required to reach equilibrium for near-critical fluids may be longer than the residence time in the calorimeter. Another problem is that associated with the presence of impurities within the mixing components.

1.8 Vibrating Tube Densitometry

It was first demonstrated in 1969 by Kratky et al. that the density of a fluid can be obtained by measuring the natural vibrational frequency of a tube containing that fluid. The oscillation frequency of the U shaped tube is dependent on the total mass of the tube, and hence the density of the liquid flowing through it, according to the relationship:

$$\rho = A + K\tau^2 \quad (1.28)$$

where A and K are constants characteristic to the vibrating tube assembly. K is calculated from the time periods (τ) and known densities (ρ) of two reference solutions:

$$K = (\rho_2 - \rho_1) / (\tau_2^2 - \tau_1^2) \quad (1.29)$$

Once the densitometer has been calibrated, the density of a solution can be determined by the equation:

$$\rho_{\text{soln}} - \rho_w = K(\tau_{\text{soln}}^2 - \tau_1^2) \quad (1.30)$$

where ρ_{soln} and ρ_w are the densities of the solution and solvent and τ_{soln} and τ_1 are the corresponding resonance time periods.

Densitometers of the type used in our work consist of a U-tube mounted in a support block such that a permanent magnet rests between the arms of the tube through which the solution is circulated. Two inconel rods attached to the U-tube are positioned between the poles of the magnet. One is used to carry a controlled alternating electrical current to the U-tube and which causes the tube to vibrate. The vibration of the second rod in the magnetic field of the magnet induces an AC current that is carried back to a feedback amplifier to sense the frequency of the vibration. A lock-in amplifier maintains the vibrations at the resonance frequency of the U-tube. HPLC flow systems are used to inject the sample solution into the vibrating tube. Vibrating U-tube densitometers used in high pressure and temperature work are not commercially available and only a few research instruments have been built. The high temperature and pressure densitometer used in this work was constructed in our lab by Xiao (1997), based on a design by Albert and Wood (1984). A complete description of the densitometer used in this work can be found in Section 2.3.

1.9 Goals and Objectives of This Work

As previously described, thermodynamic properties of carbon dioxide mixtures are of importance to the gas processing industry and in the extraction of solutes from raw materials via SFE and SFC. The effects of temperature and pressure on phase equilibria, excess properties, and reduced properties are of particular interest.

Although many data have already been collected for the (CO₂+MeOH) system at low temperatures and pressures, the results are incomplete, and the temperature ranges studied do not extend up to or beyond the critical point of methanol. In some cases, there is poor agreement between the results obtained from experiments carried out under similar conditions by different researchers. This has been attributed to the difficulties of working with supercritical fluids (Ziegler et al., 1995).

The goal of this work is to obtain accurate thermodynamic data for (CO₂+MeOH) mixtures that will extend the existing literature database to include the entire mole fraction range at temperatures up to and beyond the critical temperature of methanol. A significant part of this work is in the commissioning, modification and application of the instrumentation (microcalorimeter and densitometer) to obtain accurate thermodynamic results for supercritical mixtures.

Thus, the objectives of this work are:

- (1) Commissioning of a commercial microcalorimeter and flow injection cell, new to our laboratory, that is capable of measuring accurate heats of mixing for supercritical fluids.
- (2) Measurement of the excess enthalpies and volumes for (CO₂+MeOH) mixtures over the whole mole fraction range, and the application of the Redlich-Kister equation to represent the data.
- (3) Determination of standard partial molar properties, where possible, from a treatment based on reduced excess volumes.

Chapter 2: Experimental

2.1 Materials

The gaseous carbon dioxide used throughout this work was obtained from Canada Liquid Air ($\geq 99.7\%$). An extra high-pressure nitrogen tank (used with a regulator rated at 6000 psi), also obtained from Canada Liquid Air, was used to pressurize the systems in this work. ACS grade methanol (99.8%) and anhydrous ethanol were obtained from BDH and Aldrich respectively. HPLC grade propylene carbonate (99.7%) was obtained from Sigma-Aldrich. All solvents were used as is. The ethanolamine and the surfactant lauryl sulfate (commonly referred to as sodium dodecyl sulphate or simply SDS), used during the scoping calorimetry experiments on aqueous amines and surfactants respectively, were obtained from the Aldrich Chemical Company and Sigma. Both were sold as 99-% purity grade and no further purifications were considered necessary. Aqueous solutions of the amine and surfactant were prepared by mass, using nanopure water having a resistivity of $< 18 \text{ M}\Omega\text{-cm}^{-1}$. Prior to use, the water was boiled to remove any dissolved carbon dioxide and sealed in polyethylene bottles. This water was also used as a reference fluid in the densitometry work.

2.2 Excess Molar Enthalpy of Mixing, H_m^E

2.2.1 The Isothermal Flow Heat-of-Mixing System

The calorimeter used in this work is a Calorimetry Sciences Corp. CSC 4400 isothermal microcalorimeter. The design of this calorimeter allows for reliable measurements of power outputs as low as $\pm 0.1 \mu\text{Watts}$ with an accuracy of $\pm 0.2\%$ on a $100 \mu\text{Watt}$ signal. The CSC Model 6238 water bath surrounding the measuring unit of the calorimeter provides a temperature range of 0 to 100°C . The flow cells are designed to withstand pressures up to 13.8 MPa. The microcalorimeter measures the heat flux (P) occurring during a reaction and relates it to the product of the molar flow rate through the cell (dn/dt) and the enthalpy change of the reaction, ΔH .

$$P = (dn/dt) \cdot \Delta H \quad (2.1)$$

The overall design of this calorimeter is shown as a block diagram in Figure 2.1. The bulk of the calorimeter consists of a large aluminium heat sink, and incorporates two or four test wells (depending on the model) to make up the measuring unit. The high-pressure flow cell shown in Figure 1.6 is specially designed to fit tightly into the test wells of the calorimeter with approximately $10 \mu\text{m}$ clearance between the walls of the cell and those of the well. Thermal shunts made of nickel plated aluminium are fitted at

different levels along the measurement cavity access tube as a means of allowing two inlet tubes to reach thermal equilibrium with the bath. The fluids enter the flow cell via the inlet tubes and are allowed to reach thermal equilibrium before mixing in a tee joint at the bottom of the cell. During the mixing process, any heat that is produced or absorbed in the flow cell is completely exchanged with the heat sink, which is kept at constant temperature, through the test well walls. Passive thermoelectric sensors (Peltier devices) located between the sample and the aluminium block, generate a voltage that is proportional to the temperature gradient (heat flux) across the sensors. The microcalorimeter is designed so that it can be run with a reference cell in a twin cell arrangement. The reference cell is used to minimize the effects of electronic noise, temperature fluctuations in the bath, and imperfect thermal equilibration. The differential signal from the sample and the reference wells provides the measurement of the heat change occurring in the sample.

Two Isco 260D syringe pumps were filled with the fluids used for the experiments. The Isco pumps have a flow rate range of $1.00 \mu\text{L}\cdot\text{min}^{-1}$ to $90 \text{ mL}\cdot\text{min}^{-1}$ with an accuracy of $\pm 0.5\%$ and a pressure range of $0.07 \text{ MPa} \leq p \leq 51.7 \text{ MPa}$ at temperatures of $273.15 \text{ K} \leq T \leq 313.15 \text{ K}$. The first pump contained solvent. Carbon dioxide was placed in the second Isco pump. The carbon dioxide was maintained as a liquid at 6°C by circulating a water/anti-freeze solution from an Isotemp 1013 water bath ($\pm 0.01^\circ\text{C}$) through the outer walls of the pump reservoir containing the carbon dioxide.

The injection system is shown in Figure 2.2. Corrosive or hard to handle samples (amine, surfactant and propylene carbonate) were not placed directly into the Isco pumps. Rather a displacement-cell injection system has been designed for use with the first Isco pump. The injection system consisted of two four-port valves, a six-port valve, a long ~150 mL Teflon bag and a ConstaMetric HPLC pump from Milton Roy. The bag was sealed at each end around a Teflon plug with an inlet or outlet line constructed of PEEK tube according to the method of Busey et al. (1984). It was placed inside a water-filled high-pressure cylinder, so that, when water was pumped into the bottom of the cylinder from the Isco pump, it increased the pressure around the Teflon bag and forced the sample inside of it out through PEEK outlet tubing. The bag could be refilled by turning the six-port valve to "Refill" and pumping the sample (which is placed in the ConstaMetric pump) into the bag. Turning the three valves to their various positions allowed either the solvent from the Isco pump, or the sample from the injection bag, to be pumped into the calorimeter so that it mixed with the carbon dioxide from the second Isco pump. The resulting mixture exited the calorimeter via an outlet tube into a stainless steel vessel (rated for 2000-2500 psi) whose pressure was held constant by an overpressure of gas from a high-pressure nitrogen cylinder. The pressure was monitored by an Omegadyne PX01K1-5KG5T pressure transducer rated for 5000 psi and was maintained by a Tescom model 26-1762 backpressure regulator. An Omega DP41-E process indicator displayed the system pressure. As an added security device, a rupture disk rated at 1500-2500 psi was connected to the outlet pressure vessel.

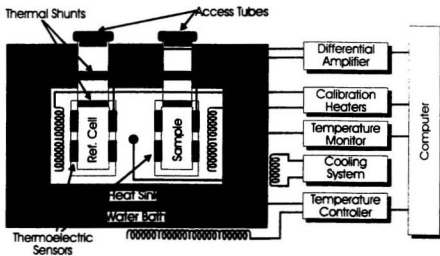


Figure 2.1 Schematic diagram of the CSC 4400 isothermal microcalorimeter.

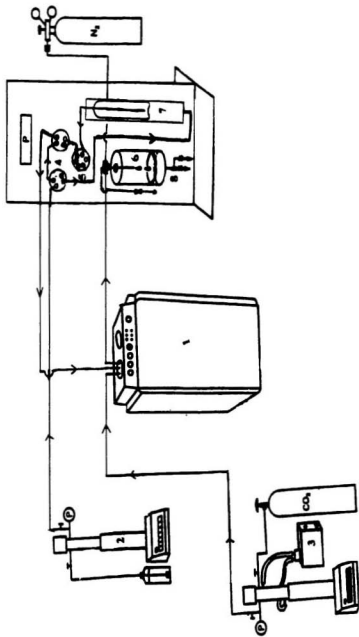


Figure 2.2 Schematic diagram of flow injection system used with the CSC 4400 isothermal microcalorimeter. (1) CSC 4400 isothermal microcalorimeter, (2) Isco syringe pump; (3) Circulating water bath; (4) Four-port valves; (5) Six-port valves; (6) Pressurized waste vessel; (7) Pressurized cylinder containing the Teflon bag; (8) Security rupture disk.

The excess molar enthalpy H_m^E obtained from the CSC 4400 isothermal microcalorimeter is dependent on the molar flow rates entering the microcalorimeter. For this reason it was necessary to calibrate the flow rates of the solutions flowing out of the Teflon bag in our injection system and from the Isco pumps.

The Teflon bag was filled with water and placed inside the high-pressure cylinder, which was then filled with water from the Isco pump that served to pressurize the cylinder. Once the cylinder was completely filled with water and the system pressure began to rise, the water inside the Teflon bag was forced to flow out of the cylinder. At the first appearance of this, a clock was started and the time required to collect 5 cm^3 of water was recorded. The water collected was weighed and, using the density of water to determine the exact volume of water, the flow rate of the injection system was determined. This procedure was repeated several times for several flow rates to get an average flow rate calibration factor, r , of 1.01 with a standard deviation of 0.02. The calibration results are listed in Table 2.1.

Table 2.1 Calibration of flow rates for injection system using water at 298.15 K and atmospheric pressure.

Pump Flow Rate	Time	Mass	System Flow Rate	r^3
$\text{cm}^3 \cdot \text{min}^{-1}$	Seconds	g	$\text{cm}^3 \cdot \text{min}^{-1}$	
5.0	55	4.6265	5.04	1.008
4.0	74	5.0358	4.08	1.020
3.0	100	5.0721	3.04	1.013
2.0	153	5.0021	1.96	0.980
1.0	296	5.0132	1.02	1.020
0.6	474	5.0002	0.63	1.050

³ Calibration factor $r = \text{experimental flow rate} / \text{nominal flow rate}$

Due to the low solubility of CO₂ in water a high-pressure viewing cell was placed in-line with the microcalorimeter in order to determine whether a gas phase was present during experiments on (CO₂ + water). The viewing cell, designed by Trevani et al. (2001), was constructed from a titanium cylinder with a cylindrical channel machined along the principal axis. The central portion of the channel acted as the sample compartment and sapphire windows at each end of the compartment allowed us to view the sample as it flowed through the compartment. Teflon washers provided a seal between the sapphire windows and the titanium flow cell. Each sapphire window was secured in place by a titanium disc that was bolted to the end of the cylindrical titanium body. Titanium tubing (1/16 inch o.d.) was used as an inlet and outlet for the solution. A schematic of the viewing cell is shown in Figure 2.3.

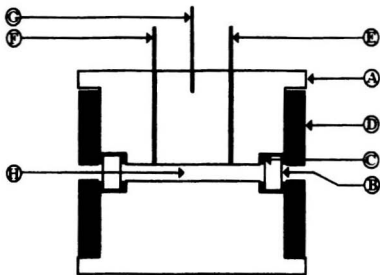


Figure 2.3 Schematic diagram of the high-pressure viewing cell. A, cylindrical titanium flow cell; B, sapphire window; C, Teflon washer; D, titanium disc; E, sample solution outlet; F, sample solution inlet; G, Chromega-Alomega thermocouple; H, sample compartment.

2.2.2 Commissioning

In addition to designing and constructing the injection system, further work was needed to ensure that reliable data were obtained from the microcalorimeter, since it is a relatively new piece of equipment to our laboratory and had not been previously used with the flow cells. The objective of the commissioning work was to reproduce known data for fluid mixtures and then to extend the usage to include carbon dioxide systems. Heats of mixing were measured as a function of temperature, pressure, flow rate and composition. The results will be discussed in detail in Chapter 3. The first runs on the calorimeter were on a single-phase fluid mixture of liquid water and ethanol at 7.5 MPa and 298.15 K, since this system is well documented in the literature. Varying the pump flow rate ratio from 0 to 1 at a total flow rate of $0.500 \text{ cm}^3 \cdot \text{min}^{-1}$ allowed us to examine the entire mole fraction range of the mixture. These measurements were successful in reproducing literature data (Christensen et al., 1986), and are presented in Section 3.2. Thereafter, work with the carbon dioxide mixtures began. A calorimetric study of the system ($\text{CO}_2 + \text{propylene carbonate}$) had been performed in this lab on an older calorimeter by a former student (Zhao, 1996), and an attempt to reproduce the data was made here. Scoping studies on this and various other carbon dioxide systems were performed in the same manner as described above. Results for the scoping experiments and initial results for the ($\text{CO}_2 + \text{MeOH}$) system did not agree with literature results.

Extensive tests showed that the problems resulted from a flaw in the design of the mixing component of the flow cell and in the limited working range of the calorimeter itself.

The biggest issues identified during the commissioning runs involved poor mixing of the components in the flow cell and the need to extend the range of the calorimeter, which was limited to $\pm 100\,000\ \mu\text{W}$ as purchased from Calorimetric Sciences Corp. Both problems required modifications to the instrument by the manufacturer.

2.2.3 Calibration

Electrical calibration of a heat conduction calorimeter such as the CSC 4400 is performed using built-in calibration heaters by either of two means: (i) the pulse calibration method or (ii) the steady state calibration method. For the former, shown in Figure 2.4, a known pulse of electrical energy is added to the sample well to simulate the heat of a reaction. The observed signal is used to determine a calibration constant (ϵ_c) from the area of the signal response (A_{tot}) and the electrical energy input (q_e):

$$\epsilon_c = q_e / A_{\text{tot}} \quad (2.2)$$

In the steady state calibration method, shown in Figure 2.5, electrical energy is added at a constant rate (dq_e/dt) to the calorimeter until a constant output signal is obtained. The calibration constant is determined as follows:

$$\epsilon_c = (dq_c/dt)/(S_{\text{heater}}-S_{\text{base}}) \quad (2.3)$$

where $(S_{\text{heater}}-S_{\text{base}})$ is the difference in the output signal with the calibration heater turned on, and at a point where the heater is turned off and the baseline signal is stable.

In an experiment where the pulse yields a signal that returns to baseline, the total heat measured is simply:

$$q_{\text{measured}} = \epsilon_c \cdot A_{\text{tot}} \quad (2.4)$$

When the sample signal (S_{measured}) is significantly different from the baseline (S_{baseline}).

the heat rate (dq_{measured}/dt) at any point of the experiment is calculated as follows:

$$dq_{\text{measured}}/dt = \epsilon_c (S_{\text{measured}}-S_{\text{base}}) \quad (2.5)$$

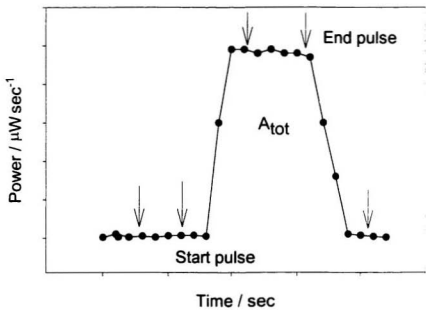


Figure 2.4 Schematic representation of the pulse calibration method. Arrows show the range used in the measurement.

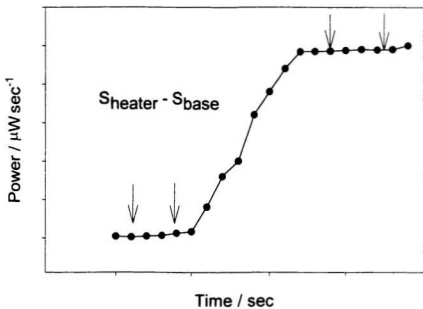


Figure 2.5 Schematic representation of the steady-state calibration method. Arrows show the range used in the measurements.

2.2.4 Optimal Conditions

The most important operating parameter to be optimized while using the microcalorimeter is the flow rate. Since the amount of heat released inside the flow cell depends on the amount of substance present, the output signal will vary in proportion to the flow rates and mixing ratio of the two Isco pumps. As mentioned previously, the calorimeter has a maximum working range of $\pm 100\,000\ \mu\text{W}$ with an accuracy of $\pm 0.2\%$ on a $100\ \mu\text{W}$ signal. Flow rates must be chosen to provide the correct pump ratio for a given mole fraction, so that the mixing reaction will produce a large, steady signal on screen without exceeding the maximum range of detector response. Also, when mixing fluids of very different viscosity, turbulent flow is required to reduce the risk of viscous fingering and this can only be achieved by running the pumps at high velocity. The operator must choose between high molar flow rates, resulting in high power outputs that could saturate the detectors, and low flow rates which may result in laminar flow that causes poor mixing inside the flow cell mixing chamber. For the ($\text{H}_2\text{O}+\text{EtOH}$) system, a total flow rate in the range of 0.400 to $0.600\ \text{cm}^3\text{-min}^{-1}$ gave flow-rate independent results.

This problem of finding an optimal flow rate is further aggravated when one of the fluids is carbon dioxide. A total flow rate of $0.500\ \text{cm}^3\text{-min}^{-1}$ was successful in reproducing literature values for the carbon dioxide mixtures only in the mole fraction range of $0.7 \leq x_{\text{CO}_2} \leq 1.0$. As the flow rate for the carbon dioxide pump was decreased to maintain the necessary pump ratio, inadequate mixing occurred, as was evident by the

unstable output signals. Carbon dioxide is an extremely compressible liquid and a higher flow rate was required to ensure smooth flow from the pump. Therefore, it was not convenient to set the pump flow rates according to the previous rule of having a total flow rate of 0.400 to 0.600 $\text{cm}^3\text{min}^{-1}$ to achieve the desired mole fractions. Instead, it was necessary to ensure that the carbon dioxide pump always flowed at 0.300 $\text{cm}^3\text{min}^{-1}$ or greater and make the necessary adjustments to the flow rate of the other pump to achieve the desired mixture mole fraction.

2.3 Vibrating Tube Densitometry

2.3.1 Construction

Two vibrating tube densitometers were used to measure the densities of all mixtures. The principle behind the vibrating U-tube densitometer is based on the properties of a mechanical oscillator and is described in Section 1.8.

A platinum vibrating-tube densitometer designed in our laboratory by Xiao (1996) was used for the high temperature work. The core of the densitometer consists of an iridium-alloy U-tube (90% platinum + 10% iridium) mounted in a cylindrical copper block. Two inconel rods were cemented on to the two arms of the tube and positioned between the poles of a permanent horseshoe magnet that also rested between the arms. A fine silver wire attached to the first inconel rod carried the electrical current needed to

drive the U-tube to vibrate. Since the second rod is cemented to the arm of the now vibrating U-tube, it too vibrates. An induced electric current, produced by the presence of the vibrating rod in a magnetic field, is sent to a feedback amplifier through another silver wire attached to the second rod. The frequency of the vibration was measured by the feedback amplifier, which then changed the electric current sent to the first rod in order to achieve the resonance frequency of the two rods. The temperature of the cylinder was measured by a 100 Ω platinum RTD (resistance temperature device) and was monitored by a Hewlett-Packard 3478A multimeter. The RTD was previously calibrated by measuring the ice point of water and the freezing points of tin and lead, supplied by NIST as standard reference materials. The core of the densitometer was placed in an oven, which consisted of a cylindrical brass block which had two strands of insulated heating wire wound around it in a symmetrical counter-current configuration surrounded by a stainless steel container. The temperature of the oven was controlled by an Omega CN2011P2-D3 temperature controller and was measured by a 100 Ω platinum RTD located near the outer rim of the large brass cylinder. At the entrance to the oven core, where the exposed inlet and outlet ends of the U-tube are located, was a small pre-heater. This Chromalox pre-heater consisted of an aluminium cylinder whose temperature was independently controlled by an Omega HBA-103027 nozzle heater and an Omega CN7600 PID temperature controller surrounding the aluminium cylinder. The pre-heater was wrapped in insulation to prevent heat loss. Frequencies were measured

using a Hewlett-Packard 5316A universal counter and an electronic circuit based on the phase-locked loop described by Wood et al. (1989).

For the low temperature density work ($298.15 \text{ K} \leq T \leq 323.15 \text{ K}$) the densitometer measuring unit was placed in a Tronac 1250 bath and connected to a Sodev models PC-B and CT-L high stability control unit and circulating pump. The temperature was monitored by a thermistor that was placed in the circulating fluid lines from the temperature bath the frequencies of vibration were recorded using a Hewlett-Packard model 5316A universal counter.

The sample injection system shown in Figure 2.6 consisted of two Isco 260D pumps and 1/8" o.d. PEEK tubing ($\sim 13 \text{ cm}^3$) for an injection loop. The first pump was filled with the solvent (methanol) and the loop was filled with water using a syringe. Two four-port valves and one six-port valve were used in series to deliver either the methanol or the water to the densitometer. Carbon dioxide from the second pump was sent directly to the densitometer from the pump. A high-pressure nitrogen cylinder and a Tescom model 26-1722-24 back-pressure regulator maintained the pressure of the flow system. The pressure was monitored by an Omega PX623 pressure transducer rated for 5000 psi and displayed on an Omega DP41-E process indicator.

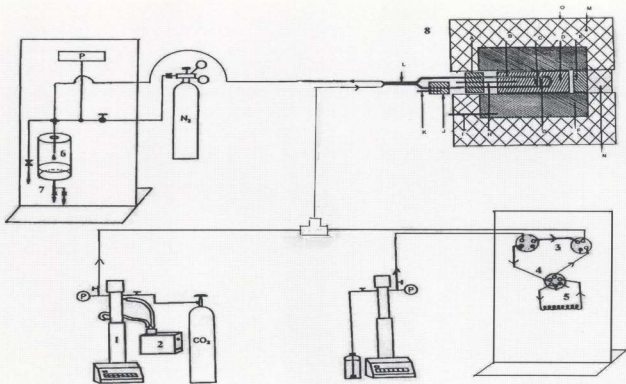


Figure 2.6 Schematic diagram of the injection system used with the vibrating U-tube densitometer. (1) Isco syringe pump; (2) Circulating water bath; (3) Four-port valve; (4) Six-port valve; (5) Injection loop; (6) Pressurized waste vessel; (7) Rupture disk; (8) Densitometer. The densitometer consists of (A) Aluminum heat shield; (B) Platinum U-shaped vibrating tube; (C) Inconel rods for sensing and driving current; (D) Densitometer cell body; (E) Brass heat shield; (F) Brass oven; (G) Permanent magnet; (H) RTD; (I) RTD; (J) Aluminum pre-heater; (K) RTD; (L) Heat exchanger; (M) Thermal insulation; (N) Thermal insulation; (O) Stainless steel container.

2.3.2 Commissioning

Previous work done in the lab with the densitometer involved simply injecting previously prepared solutions into the densitometer. Since it is not feasible to prepare bench-top carbon dioxide mixtures in advance, a method for mixing the two fluids together had to be developed. A home-made “mixer” was constructed and placed within the injection assembly at a point before the fluids reach the densitometer.

The mixer designed for this project was a modified high-pressure 1/8" Swagelock Tee joint. The hole between the two horizontal openings of the tee piece was widened so that a 1/16" PEEK tubing could be fed all the way through one end and out the other through which the carbon dioxide could flow. At the end with the protruding PEEK tubing, a stainless steel tubing of 1/8" o.d. was connected so that the PEEK tubing lay inside the stainless steel tube. The solvent entered from the remaining vertical opening of the tee through a 1/8" Peek tube and was forced to flow out through the stainless steel tube, which contained flowing carbon dioxide. Three pieces of twisted small-diameter stainless steel wire were placed inside the larger-diameter stainless steel tube at its end to ensure that turbulent mixing between the carbon dioxide and the solvent occurred. A schematic of the mixer is shown on Figure 2.7.

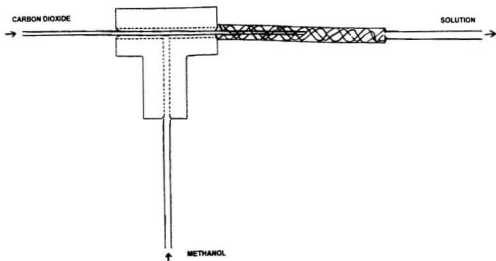


Figure 2.7 Schematic diagram of the mixer constructed for this work to use with the vibrating U-tube densitometer

2.3.3 Calibration

The vibrating U-tube densitometer must be calibrated using two fluids of known density, in order to carry out the calculations described in Section 1.7. In this work, the frequencies of vibration for pure water and carbon dioxide were measured daily under the experimental temperature and pressure conditions. The densities were obtained from equations of state provided by NIST [ASME Steam Properties Database 10 (Harvey et al., 1996) and NIST Standard Reference Database 12 (McCarty and Arp, 1986)].

The pressure transducer and display monitor had been calibrated by the manufacturer using standards traceable to NIST. The precision and stated accuracy of the gauge is ± 0.1 psi ($\pm 7 \cdot 10^{-4}$ MPa) and $\pm 0.10\%$ of its span. Further calibrations were conducted late in the project by connecting an Ashcroft 1000 psi (6.89 MPa) Bourdon pressure gauge which had been calibrated against a dead weight system, to verify the readings on the pressure transducer. The pressure reading on the transducer was lower than the Ashcroft gauge by approximately 26 psi (0.18 MPa). We have corrected the observed pressures by this amount, and assigned an uncertainty of ± 0.2 MPa to all pressure readings. The precision of the measurements has been assumed to remain at $\pm 7 \cdot 10^{-4}$ MPa.

2.3.4 Optimal Conditions

As discussed in Section 2.2.4, complete mixing is best achieved through turbulent flow. Unlike the calorimeter, the densitometer does not have the problems associated with oversaturating the instrument's response signal since density is not a function of the flow rate of the fluid sample. It was not desirable to allow the mixture to flow too quickly through the densitometer since there is a very large temperature difference between the injected room-temperature fluids and the measurement temperature inside the densitometer oven. Slow flow rates on the order $0.050 \text{ cm}^3\cdot\text{min}^{-1}$ were necessary for the fluids to come to thermal equilibrium.

It was found that the best way to avoid this problem was to force the fluids to mix turbulently by running the pumps at high flow rates, on the order of 1 to $1.5 \text{ cm}^3\cdot\text{min}^{-1}$, to ensure that complete mixing occurred inside the home-made mixer. However, once the arms of the U-tube were completely filled with solution, the flowrates of the two pumps were reduced dramatically so that the mixture flowed very slowly in the tube. The final flow rates used were of the order of 0.05 to $0.100 \text{ cm}^3\cdot\text{min}^{-1}$ and the signals achieved by this means were very stable. Carbon dioxide was run as the baseline and the density values were obtained from equations of state provided in NIST Standard Reference Database 12. A typical run required approximately 20 minutes to run the baseline and the mixture. However, for mixtures with extremely large carbon dioxide content, more time was required to achieve the same kind of stable signal shown for the lower mole fraction

mixtures. This may be because more time was required for the gas-like mixture to completely sweep away the previous solution, water or methanol that was in the U-tube. Approximately 30 to 40 minutes were required. If the signal did not stabilize within this time frame, it was assumed that a two-phase mixture was present. In these cases, the measurements had larger uncertainties and, although the calculations were carried out, the data points were omitted from the volume vs. x_{CO_2} curves. The critical locus for the (CO_2 +MeOH) system, determined by Ziegler et al. (1995) and Brunner (1985), is consistent with the possibility that two-phase fluids might form under the conditions where they were encountered in this work. Similar behaviour has been noted by Christensen et al. (1988) for several (carbon dioxide + an alkanol) mixtures.

2.4 Calculations

2.4.1 Enthalpy Calculations

The power output, P_T , given in $\mu\text{J}\cdot\text{sec}^{-1}$ displayed on the CSC 4400 isothermal microcalorimeter is the integrated signal of the temperature gradient that the thermoelectric sensors detect between the sample cell and the aluminium heat sink. A baseline value, P_B , obtained by running pure solvent through the calorimeter prior to every measurement, was subtracted from P_T to take into account any heat flux associated

with the flow of the pure fluids into the calorimeter. This leaves us with a measurement of the heat change due solely to the mixing of the solution, P_{soln} :

$$P_{\text{soln}} = P_T - P_B \quad (2.6)$$

The molar flow rates (f_m) of the individual fluids were calculated from the volumetric flow rates, f , in $\text{cm}^3\text{-sec}^{-1}$ of the two pumps, the density of the fluids at their respective pump temperatures, ρ , and the molar masses of the fluids, MM , as:

$$f_{m,\text{CO}_2} = (f_{\text{CO}_2}) \cdot (\rho_{\text{CO}_2}) / MM_{\text{CO}_2} \quad (2.7)$$

$$f_{m,\text{MeOH}} = (f_{\text{MeOH}}) \cdot (\rho_{\text{MeOH}}) / MM_{\text{MeOH}} \quad (2.8)$$

The total molar flow rate ($f_{m,\text{total}}$), in $\text{mol}\text{-sec}^{-1}$, is the sum of the individual molar flowrates of the two pumps:

$$f_{m,\text{total}} = \sum f_{m,i} \quad (2.9)$$

Dividing the power output of the mixture by the total molar flow rate yields the excess molar enthalpy of mixing with the units $\text{J}\text{-mol}^{-1}$:

$$H_m^E = (P_{\text{soln}}) \cdot (1\text{J} / 10^6 \mu\text{J}) / (f_{m,\text{total}}) \quad (2.10)$$

2.4.2 Volumetric Calculations

The relationship between the density of the solution and the densitometer frequency is described in Section 1.8. Knowing the calibration constant of the densitometer, the frequency and density for the carbon dioxide standard and the frequency of the solution, we can calculate the difference in density between the solution relative to pure carbon dioxide at the same temperature and pressure.

$$\rho_{\text{soln}} - \rho_{\text{CO}_2} = K (\tau_{\text{soln}}^2 - \tau_{\text{CO}_2}^2) \quad (2.11)$$

The molar volumes of the solutions, $V_{\text{m,soln}}$, were calculated from the density and mole fractions, x , as:

$$V_{\text{m,soln}} = (1/\rho_{\text{soln}}) \cdot (x_{\text{CO}_2} \cdot \text{MM}_{\text{CO}_2} + x_{\text{MeOH}} \cdot \text{MM}_{\text{MeOH}}) \quad (2.12)$$

where MM is the molar mass of CO_2 or MeOH. The molar excess volumes of the solutions, V_m^E , were determined by subtracting the contribution of the molar volumes of the pure components from the molar volume of the solution:

$$V_m^E = V_{\text{m,soln}} - (x_{\text{CO}_2} \cdot V_{\text{m,CO}_2}^* - (x_{\text{MeOH}} \cdot V_{\text{m,MeOH}}^*)) \quad (2.13)$$

where V_{m,CO_2}^* is the molar volume of pure carbon dioxide and was taken from the NIST Standard Reference Database 12 and $V_{m,MeOH}^*$ is the molar volume of pure methanol and was calculated as follows:

$$V_{m,MeOH}^* = (1/\rho_{MeOH}) \cdot MM_{MeOH} \quad (2.14)$$

The reduced excess molar volumes, V_m^R , were determined by dividing the experimental excess molar volumes by the product of the mole fractions of the two fluids present in the mixture.

$$V_m^R = V_m^E / \{x_{CO_2}(1-x_{CO_2})\} \quad (2.15)$$

Extrapolating the reduced excess volumes to infinite dilution using the Redlich-Kister fitting equation allowed us to determine the values for V_i^0 , the standard partial molar volume of component i at infinite dilution:

$$\lim_{x_{CO_2} \rightarrow 0} V_m^R = V_{CO_2}^0 - V_{CO_2}^* \quad (2.16)$$

$$\lim_{x_{CO_2} \rightarrow 1} V_m^R = V_{MeOH}^0 - V_{MeOH}^* \quad (2.17)$$

where V_i^0 is the volume of the pure component i .

The apparent molar volumes were determined from the following formula:

$$V_{\phi} = [1000(\rho - \rho_{\text{soln}})(m \cdot \rho_{\text{soln}})] + (MM_2/\rho_{\text{soln}}) \quad (2.18)$$

where ρ and ρ_{soln} are the densities of the solution and the solvent respectively, m is the molarity of the solution and MM_2 is the molar mass of the solute.

2.4.3 Uncertainties in Measurements

For the calorimetric study, the errors associated with measurements were attributed to fluctuations in heat response, flow rate and cell temperature and the accuracy of the calibration factor. The CSC 4400 isothermal microcalorimeter provides reliable data with an accuracy of $\pm 0.2\%$ on a $100 \mu\text{W}$ signal.

For the volumetric study, the errors associated with density measurements came from the random errors associated with the fluctuations of temperature and pressure, the calibration constant, and periods of frequencies measured for carbon dioxide and the solutions. The error limits of densities in the temperature range of interest were in the order of $\pm 10^{-4} \text{ g}\cdot\text{cm}^{-3}$ in the one-phase regions and $\pm 10^{-3} \text{ g}\cdot\text{cm}^{-3}$ in the two-phase regions. This resulted in an error of $\pm 0.4 \text{ cm}^3\cdot\text{mol}^{-1}$ in V_{ϕ} at the low carbon dioxide mole fraction and $\pm 4 \text{ cm}^3\cdot\text{mol}^{-1}$ at the high carbon dioxide mole fraction range.

Chapter 3: Enthalpy Results for (CO₂ + MeOH) Mixtures

3.1 Introduction

In this chapter, we report the excess enthalpy results obtained for (CO₂+MeOH) mixtures over the entire mole fraction range at 298.15 K and two pressures. The results determined in this work were compared with results taken from literature, to commission the calorimeter and to ensure that reliable data for supercritical carbon dioxide mixtures were obtainable.

Since the CSC 4400 isothermal microcalorimeter had never been used in our lab before with a flow cell, extensive commissioning work had to be carried out beforehand to determine the ideal working conditions when using supercritical fluids. Results for the calibration of the microcalorimeter and flow cell along with the results for several (CO₂ + solvent) scoping experiments can be found in the appendix.

3.2 H_m^E of (CO₂ + MeOH)

3.2.1 Introduction

The excess enthalpy of (CO₂ + MeOH) over the entire mole fraction range has been studied previously in our lab by Zhao (1996) using a Tronac calorimeter at 298.15 K

and 308.15 K and pressures between $7.5 \leq p \leq 12.5$ MPa. Her results have been published together with results obtained from Hauser (Hauser et al., 1996). Christensen's group has performed a study of the same system (Christensen et al., 1988) covering the temperature range of $308.15 \text{ K} \leq T \leq 573.15 \text{ K}$.

3.2.2 H_m^E at 298.15 K

Excess enthalpies were obtained for the ($\text{CO}_2 + \text{MeOH}$) system at 298.15 K and 7.5 MPa and 10.0 MPa, for comparison with the results obtained previously in our lab. Figure 3.1 shows these results. Our experimental values for H_m^E of ($\text{CO}_2 + \text{MeOH}$) at $p = 7.5$ MPa and 10.0 MPa were within experimental limits of Zhao's (1996) values obtained on the Tronac calorimeter, $\pm 25 \text{ J mol}^{-1}$. At 10.0 MPa, there were no difficulties in obtaining values for H_m^E over the entire mole fraction range. However, at the lower pressure, 7.5 MPa, values could not be obtained between $0.09 < x_{\text{CO}_2} < 0.30$. Very large negative thermal effects occur in this region and the magnitude of the signal was larger than the working range of the calorimeter ($-1.2 \cdot 10^5 \mu\text{W}$). Although the changes made to the flow cell during the commissioning trials and the addition of a gain switch to the microcalorimeter did extend the working range of the instrument (see appendix), there is still a limit to the data that can be obtained on this microcalorimeter. Systems that display very large thermal changes upon mixing and mixtures of components with very different viscosities are not suitable for this equipment.

A summary of the results obtained from our work on the CSC 4400 isothermal microcalorimeter may be found on Table 3.1.

3.2.3 H_m^E vs. Temperature and Pressure for (CO₂ + MeOH)

In the 1980's and early 1990's, Christensen's group at Brigham Young University carried out a long-term program to measure the excess molar enthalpies of carbon dioxide mixtures in the vicinity of the critical locus and in the supercritical region. Curves obtained for the (CO₂+MeOH) system over the entire mole fraction range by Christensen et al. (1987) as a function of temperature and pressure are shown in Figure 3.2 and Figure 3.3.

The results from our work at 298.15 K, discussed in the previous section, are similar to those obtained by Christensen et al. at 308.15 K. The H_m^E mixing curves for (CO₂ + MeOH) at both temperatures have a sigmoidal shape. Negative minima in the range $0.25 \leq x_{CO_2} \leq 0.50$ were observed at both pressures and a positive maximum was observed in the range $0.90 \leq x_{CO_2} \leq 1.0$ for the curve obtained at 10.0 MPa. As is apparent from Figures 3.2 and 3.3, extremely large negative values were obtained for H_m^E at 308.15 K and 7.5 MPa but, as the pressure was increased, the magnitude of the heat of mixing decreased. Increasing the temperature of the mixtures resulted in H_m^E curves with sigmoidal shapes having positive maxima.

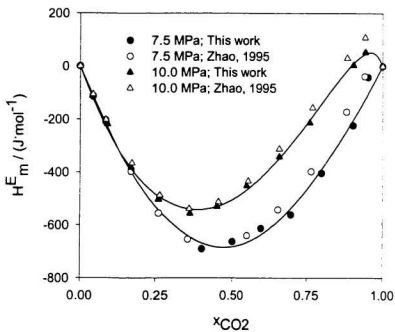


Figure 3.1 Comparisons of the experimental results with literature values for the $(\text{CO}_2 + \text{MeOH})$ system at 298.15 K . Solid curves are from the Redlich-Kister equation for our values.

Table 3.1 Summary of results for (CO₂ + MeOH) at 298.15 K and 7.5 MPa and 10.0 MPa

Pressure	x_{CO_2}	H_m^E
MPa		J·mol ⁻¹
7.5	0.00	0.00
	0.04	-115.06 ± 0.03
	0.08	-210.31 ± 0.04
	0.17	Saturated output signal
	0.30	Saturated output signal
	0.39	-692.48 ± 0.01
	0.50	-663.36 ± 0.03
	0.59	-612.70 ± 0.03
	0.70	-561.50 ± 0.02
	0.80	-403.79 ± 0.03
	0.90	-223.81 ± 0.10
	0.94	-42.41 ± 0.04
	1.00	0.00
10.0	0.00	0.00
	0.04	-112.61 ± 0.03
	0.09	-218.72 ± 0.02
	0.17	-381.67 ± 0.03
	0.26	-503.44 ± 0.10
	0.36	-556.19 ± 0.02
	0.45	-530.23 ± 0.04
	0.55	-451.58 ± 0.06
	0.66	-342.12 ± 0.05
	0.76	-213.01 ± 0.30
	0.90	3.10 ± 0.04
	0.94	52.40 ± 0.10
	1.00	0.00

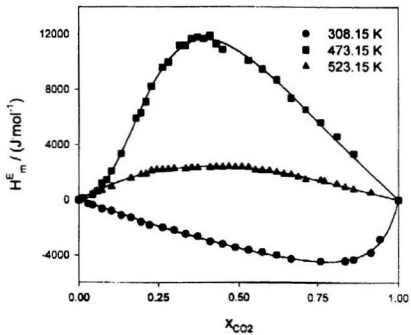


Figure 3.2 H_m^E values for ($\text{CO}_2 + \text{MeOH}$) at three temperatures at 7.5 MPa as obtained from Christensen et al. (1987).

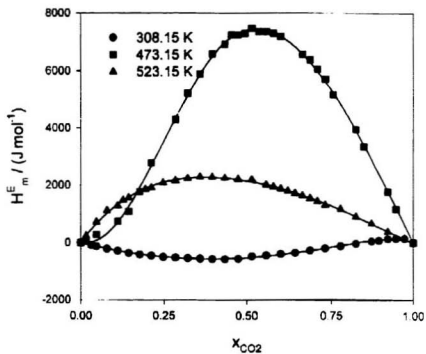


Figure 3.3 H_m^E values for ($\text{CO}_2 + \text{MeOH}$) at three temperatures at 12.5 MPa as obtained from Christensen et al. (1987).

At 298.15 K two liquid components are mixed to produce a liquid-like mixture. Since the states and densities of the two starting components are similar, we would expect the H_m^E curve to be negative or slightly positive, as described in Section 1.4.2. The curves shown in Fig 3.1 do indeed show negative values, with a slightly positive maximum at high x_{CO_2} at 10 MPa. As the temperature is increased to 308.15 K, carbon dioxide becomes a high-density supercritical fluid. The resulting mixture of CO_2 with liquid methanol is a liquid, as indicated by the isothermal phase equilibrium diagram shown in Fig 1.3. Once again the sign and magnitude of H_m^E is determined by the similar states of the starting fluids. However, since carbon dioxide is now a supercritical fluid, rather than a liquid, we would expect the H_m^E curve to be more negative than that produced at 298.15 K. At 473.15 K carbon dioxide is a low-density supercritical fluid and therefore behaves as a gas, a fluid being defined here as supercritical when $V \leq 1.5V_c$ and defined as being "gas-like" when $V \geq 2V_c$. It mixes with the liquid methanol to produce a low-density supercritical fluid at $x_{CO_2} > 0.3$. We now have a situation where a supercritical fluid and a liquid mix to produce a low-density fluid mixture. According to Christensen et al. (1986) such mixtures yield large positive H_m^E curves, as shown in Figs 3.2 and 3.3. As we continue to increase the temperature to 523.15K, we exceed methanol's critical point and are now mixing two supercritical fluids to produce a low-density supercritical mixture. Since the two components have similar states, we would expect the curve to be negative or slightly positive. The curves obtained from

Christensen show slightly positive H_m^E values for this temperature. Increasing the pressure has the effect of reducing the magnitude of the results.

3.3 Discussion

3.3.1 Solute-Solvent Interactions

The H_m^E behaviour for ($\text{CO}_2 + \text{MeOH}$) over the temperature and pressure range discussed throughout this chapter is similar to that observed for studies on other (carbon dioxide + polar solvent) systems. Data obtained in this work at 298.15 K and pressures of 7.5 and 10.0 MPa suggest the presence of a void-filling mechanism in the hydrogen-bonded network formed by the methanol (Hauser et al., 1996). The temperature and pressure dependence of H_m^E for these systems may be explained in terms of the classical near-critical effects associated with the pure fluid properties of carbon dioxide and methanol.

The change in excess enthalpy with temperature at constant pressure can be expressed as follows:

$$\left(\frac{\partial H_m^E}{\partial T}\right)_p = C_{p,m}^E = C_{p,m}(\text{mixture}) - xC_{p,m}(\text{CO}_2) - (1-x)C_{p,m}(\text{solvent}) \quad (3.1)$$

where C_p^E is the excess molar heat capacity at constant pressure. The change in excess enthalpy with pressure at constant temperature can be expressed as follows:

$$(\partial H_m^E / \partial p)_T = V_m^E - T(\partial V_m^E / \partial T)_p \quad (3.2)$$

where V_m^E is the excess molar volume of the mixture.

It has been shown that, at temperatures and pressures near the critical region, large changes in the values of H_m^E may be expected (Levelt Sengers, 1991). These changes show themselves in the large values of H_m^E observed by Christensen's group at 308.15 K and 523.15 K at 7.5 MPa, conditions that approach the critical points of pure carbon dioxide and pure methanol. The signs and magnitude of the curves have been interpreted in terms of the states of the components and the mixtures.

3.3.2 Experimental Insights

In the work presented here, a CSC 4400 isothermal microcalorimeter with a flow cell and Isco syringe pumps was used to measure the excess molar enthalpy of (CO_2 + methanol) mixtures. Several test systems were first measured to define the useful working ranges of the instrument, in terms of molar flow rates and power limitations of the microcalorimeter. A high-temperature, high-pressure injection system was designed to handle the problems associated with working with supercritical fluids. The injection

system also allowed us to use solutions that could not be placed directly into the Isco pumps.

The efficiency of mixing was of great concern in this work. Turbulent conditions were needed to ensure that complete mixing occurred and the only way to achieve turbulence with this instrument was to run the Isco pumps at high velocity. This problem was further complicated by the compressibility of the carbon dioxide in the second pump. A high flow rate was needed for this pump to ensure that the flow of carbon dioxide was smooth and continuous. It was determined that the best mixing occurred with the carbon dioxide flowing at a rate above $0.300 \text{ cm}^3 \cdot \text{min}^{-1}$ and the total flow rate of the system remaining above $0.500 \text{ cm}^3 \cdot \text{min}^{-1}$. This restriction limited the range of mole fractions that could be studied with the microcalorimeter.

The second concern was the working limit of the microcalorimeter. Scoping work with high molar flow rates showed that the microcalorimeter detectors saturated above $\pm 1.1 \cdot 10^5 \mu\text{W} \cdot \text{sec}^{-1}$. Since the power signals detected on the microcalorimeter are dependent on the amount of fluid entering the flow cells, this problem is related to the flow rate. Decreasing the flow rates of the pumps to obtain a measurable signal from the microcalorimeter could not guarantee a good measurement if complete mixing did not occur inside the flow cell. This is an ironic instance where the high sensitivity of the instrument became a source of difficulty.

It was necessary to obtain a re-designed flow mixing cell and an attenuator for the microcalorimeter to overcome these problems. The improved mixing chamber and

longer thermal equilibration chamber of the new flow cell allowed us to achieve complete mixing with fluids at slower flow rates. Due to the compressibility of carbon dioxide, it was still necessary to maintain a relatively high flow rate from the CO₂ pump. Good mixing was achievable so long as the carbon dioxide flow rate remained above 0.300 cm³·min⁻¹.

The gain switch added to the microcalorimeter extended the working range of the instrument from $\pm 1.1 \cdot 10^5 \mu\text{W}$ to $\pm 1.2 \cdot 10^5 \mu\text{W}$. This allowed us to measure systems with large excess enthalpies, such as (CO₂ + MeOH). However, measurements between $0.08 \leq x_{\text{CO}_2} \leq 0.39$ for the mixtures at 298.15 K and 7.5 MPa could not be obtained, even with the addition of these modifications. Microcalorimeters are excellent tools for measuring accurately very small enthalpy changes on short time scales. Modifications of the instrument and the flow cells are needed before microcalorimeters can be used efficiently to measure the large enthalpy changes associated with near-critical fluids.

Chapter 4: Volumetric Results for (CO₂ + MeOH) Mixtures

4.1 Introduction

Much work has been done to study the volumetric properties of aqueous solutions, particularly dilute solutions, using the high temperature, high pressure vibrating U-tube densitometer built in our laboratory. Vibrating U-tube densitometers are widely used near ambient conditions because they are reliable and easy to operate. However, extending the range of the vibrating U-tube densitometer to high-temperature, high-pressure conditions requires the design and construction of a specialized instrument and injection system, and the development of reliable experimental methods. Densitometers of this sort are not available commercially.

A new application for our densitometer is its use in studying carbon dioxide mixtures under conditions of extreme temperature and pressure. Data for the density, excess volume and reduced excess volume have been obtained for the (CO₂ + MeOH) system as a function of temperature, pressure and composition, and are presented in this chapter. As well, data for the apparent volumes and standard partial molar volumes at infinite dilution are presented and discussed here.

4.2 Calibration of Vibrating U-Tube Densitometer

4.2.1 Water and Carbon Dioxide as Calibrating Fluids

The vibrating U-tube densitometer must be calibrated daily using two fluids of known density to obtain a value for the calibration constant K . With this calibration constant, it is possible to determine the densities of unknown mixtures from the resonant vibration frequency of the U-tube containing the mixture.

The injection system was designed so that the two Isco syringe pumps could be used to inject a continuous flow of carbon dioxide and methanol. The nanopure water used to calibrate the instrument was contained in the injection loop. Initially it was thought that pure water and methanol could be used for the calibration, to avoid the use of a supercritical fluid as a calibrating fluid. Density values for pure water and methanol were obtained from the NIST Standard Reference Databases (Harvey et al., 1996) and an equation of state from Goodwin (1987). Calculations using calibration constants obtained in this manner resulted in large errors for the molar volumes of pure carbon dioxide at elevated temperatures compared to values from the NIST fluid database (McCarthy and Arp, 1986). This was a major concern since carbon dioxide is a well-studied fluid and literature data for its pVT properties should be more reliable than the data for methanol. A summary of these results is shown in Table 4.1. As a result, data for pure methanol were not obtained from the databases, but rather, they were

obtained experimentally. Consequently, water and carbon dioxide were selected as the calibrating fluids. To measure the density of supercritical carbon dioxide, a longer time was needed to completely flush the previous solution out of the arms of the U-tube. The carbon dioxide was injected at a high flow rate for 15 minutes before reducing the flow rate to $0.010 \text{ cm}^3\text{-min}^{-1}$ to measure the frequency of vibration. Table 4.2 shows the volumetric results obtained for methanol using water and carbon dioxide as the calibrating fluids.

4.3 Bubble Point Measurements

The phase boundaries for supercritical carbon dioxide mixtures have been studied by several labs using high pressure, high temperature viewing cells (Reighard et al., 1996 and Brunner, 1985) similar to that described in Section 2.2.1. Recently chromatographic methods for determining phase boundaries have also been employed (Ziegler et al., 1995 and Brunner et al., 1987). Our method is based on a study done by Crovetto and Wood (1992) that describes the determination of the solubility of carbon dioxide in water using a vibrating U-tube densitometer. In this procedure, the system was equilibrated at the desired temperature with pure fluid or fluid mixture flowing through the vibrating tube at a pressure higher than the known bubble pressure. Once τ_w was constant, the flow was greatly reduced so that the fluid was almost at rest in the U-tube. The amplitude and behaviour of the period of vibration was noted at pressure, p_1 . The pressure was then

decreased to p_2 , and the steady state period observed once again. In this manner, the pressure was continuously reduced until a point was reached where the amplitude of τ_w was abruptly reduced and the behaviour of the signal became erratic, indicating the first appearance of the vapour phase. The pressure at which this occurred was noted. The system pressure was then increased slightly until the signal became normal once again, showing that the bubbles had disappeared. The pressure was reduced once more in smaller steps until an erratic signal was again displayed. This pressure "titration" method was repeated with increasingly smaller pressure changes until the pressure at which the bubbles appeared in the forward direction matched that at which the bubbles disappeared in the reverse direction. This pressure was taken as the bubble point.

This procedure was carried out at 473 K and 523 K for water, and at 473 K for pure methanol. The bubble point pressures obtained in this work were compared with those taken from the NIST Standard Reference Databases as a means of calibrating the system pressure. Bubble points for two ($\text{CO}_2 + \text{MeOH}$) solutions were also determined at 473 K in this work. Literature values for the ($\text{CO}_2 + \text{MeOH}$) solutions were obtained from the isothermal phase equilibrium curves for the mixture determined by Brunner et al. (1987) by optical methods. Results are shown in Table 4.3 and Brunner's isothermal vapour-liquid phase diagram for the ($\text{CO}_2 + \text{MeOH}$) mixtures is shown on Figure 1.3. The results of the bubble point experiments show once again that the pressure displayed for the system reads lower than the actual system pressure. The re-calibrated pressure scale was used throughout the volumetric calculations.

Table 4.1 Molar volume of CO₂: From densitometer calibration based on water and methanol

Temperature	Pressure	V _{CO₂} [*] (Expt)	V _{CO₂} [*] (Lit) ^a
K	MPa	cm ³ ·mol ⁻¹	cm ³ ·mol ⁻¹
298.15	2.5	51.7	51.79
308.15	12.5	54.9	56.59
323.15	12.5	71.4	71.63
373.15	12.3	166.0	175.90
	19.8	95.4	92.46
473.15	12.3	258.0	287.27
	19.8	151.4	171.58
498.15	12.3	337.5	310.15
	19.8	160.3	187.52
523.15	12.3	146.7	332.40
	19.8	119.4	202.72

^a McCarthy and Arp, 1986

Table 4.2 Molar volume of methanol: From densitometer calibration based on water and carbon dioxide

Temperature	Pressure	V_{MeOH}^* (Expt)	V_{MeOH}^* (Lit) ³
K	MPa	$\text{cm}^3\cdot\text{mol}^{-1}$	$\text{cm}^3\cdot\text{mol}^{-1}$
298.15	12.5	40.16	40.15
308.15	12.5	40.54	40.63
323.15	12.5	41.31	41.31
373.15	12.3	44.00	44.02
	19.8	43.14	43.17
473.15	12.3	54.50	53.99
	19.8	53.95	51.87
498.15	12.3	56.75	59.75
	19.8	57.44	55.81
523.15	12.3	81.36	72.98
	19.8	121.11	61.90

³ McCarthy and Arp, 1986

Table 4.3 Bubble-point pressures for water, methanol and two (CO₂ + MeOH) mixtures measured with the vibrating U-tube densitometer.

System	Temperature	Pressure (Lit.)	Pressure (Expt.)
	K	MPa	MPa
Water	473.15	1.555 ^a	1.39 (± 0.7)
	523.15	3.976	3.85 (±0.7)
Methanol	473.15	4.025 ^b	4.01 (±0.3)
x _{CO₂} = 0.30	473.15	7.94 ^c	7.30 (±0.4)
x _{CO₂} = 0.75	473.15	Above T _c	-

^a Harvey et al., 1996

^b deReuck and Craven, 1993

^c Brunner et al., 1987

4.4 Molar Volumes for (CO₂ + MeOH) From Ambient Temperatures to 523.15 K at 12.5 MPa and 20.0 MPa

4.4.1 Excess Molar Volumes

This section presents volumetric results for (CO₂ + MeOH) mixtures over the whole mole fraction range as a function of temperature. The densities for (CO₂ + MeOH) mixtures from $298.15 \leq T \leq 523.15$ K are listed in Table 4.4 at two pressures, 2.3 and 19.8 MPa. The density values obtained by Galicia-Luna and Renon (1994) with a commercial vibrating tube densitometer at temperatures up to 373.15 K are included in the table for comparison. The table shows excellent agreement between our results and those from the literature.

The excess molar volumes for the (CO₂ + MeOH) mixtures were calculated from the density data using eq 2.13. The excess molar volumes are tabulated in the appendix and plotted in Figures 4.2 and 4.3. The modified Redlich-Kister equation (eq 1.19) was fitted to the data by the method of least squares. The "best" fits were taken to be those that provided the lowest overall standard deviation in which the standard deviations of the fitting parameters were less than 10 percent. No more than four parameters were used for each curve. The fitted excess molar volumes are shown as solid curves in Figures 4.2 and 4.3. Linear portions for the curves shown for 373.15 K ($0.40 \leq x_{\text{CO}_2} \leq 0.95$) and 473.15 K ($0.21 \leq x_{\text{CO}_2} \leq 0.59$) represent regions where phase separation is believed to have occurred. This interpretation is based on the observation that, while in

these regions, the densitometer signal did not behave as expected. Signals took significantly longer to stabilize in the two-phase regions and the density results showed a linear dependence on the mole fraction. Comparison with the vapour-liquid equilibrium (VLE) data obtained by Brunner et al. (1987) confirms the presence of a two-phase region. Table 4.5 lists the parameters obtained from the curve fitting to eq 1.24, while Table 4.6 lists the parameters obtained from the straight line portions of the curve where phase separation is believed to have occurred. Data for the VLE points are listed in Table 4.7.

The excess molar volume data obtained at 298.15 K and 308.15 K at 12.3 MPa showed curves with positive V_m^E values in the low x_{CO_2} regions and negative values in the high x_{CO_2} regions. As the temperature was increased, the excess molar volumes became negative over the entire mole fraction range and their magnitude increased with temperature. Similar behaviour, although less pronounced, was observed at 19.8 MPa.

The data scattering in Figs 4.2 and 4.3 is due to experimental uncertainties and shows the difficulty that was encountered in obtaining volumes for supercritical carbon dioxide mixtures.

Table 4.4 Density (ρ) of (CO₂ + MeOH) mixtures compared with results from the literature.

Temp	Literature Results*			Experimental Results		
	Pressure	x_{CO_2}	ρ	Pressure	x_{CO_2}	ρ
	MPa		g·cm ⁻³	MPa		g·cm ⁻³
323.15	12.5	0.0	0.77511	12.5	0.0	0.7756
		0.0961	0.79906		0.1003	0.7988
		0.3524	0.82465		0.3501	0.8241
		0.7467	0.78635		0.7499	0.7859
373.15	12.5	0.0	0.72812	12.3	0.0	0.7281
		0.0961	0.73902		0.1004	0.7381
		0.3524	0.72674		0.3503	0.7264
	20.0	0.0	0.73752	19.8	0.0	0.7329
		0.0961	0.75204		0.1004	0.7607
		0.3524	0.75438		0.3498	0.7579

* Galicia-Luna and Renon, 1994

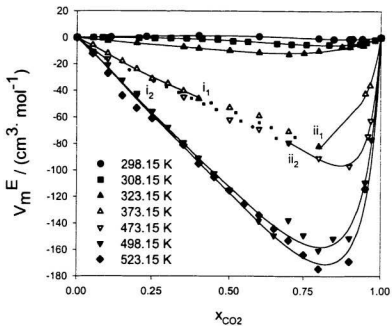


Figure 4.1-a Excess molar volumes for $(\text{CO}_2 + \text{MeOH})$ mixtures at 12.3 MPa. Points on plot represent experimental values and solid lines represent the solutions to the modified Redlich-Kister equation. Dashed lines represent regions of phase separation. Refer to the discussion in the text of Section 4.4.1 for definition of points i_1 , i_2 , ii_1 and ii_2 .

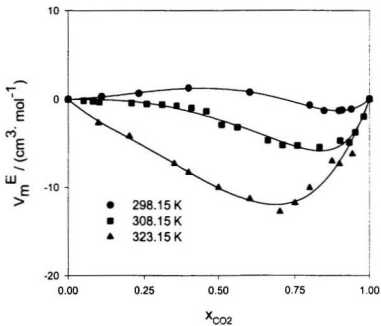


Figure 4.1-b Enlargement of excess molar volumes for ($\text{CO}_2 + \text{MeOH}$) mixtures at 12.3 MPa and temperatures below 323.15 K. Points on plot represent experimental values and solid lines represent the solutions to the modified Redlich-Kister equation.

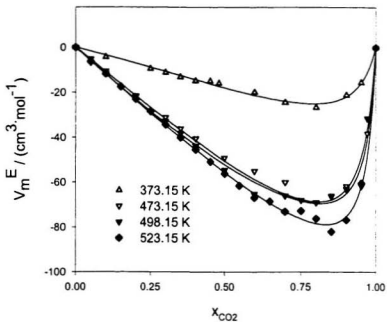


Figure 4.2 Excess molar volumes for ($\text{CO}_2 + \text{MeOH}$) mixtures at 19.8 MPa. Points on plot represent experimental values and solid lines represent the fits to the modified Redlich-Kister equation.

Table 4.5 Parameters for the modified Redlich-Kister equation for (CO₂ + MeOH) mixtures and standard deviations (s) for V_m^E.

P	T	A ₀	A ₁	A ₂	B ₁	s
MPa	K					cm ³ ·mol ⁻¹
12.5	298.15	4.7	-7.0	-10.6	-0.59	0.7
	308.15	-9.3	-15.3	-5.5	-0.72	2.3
	323.15	-40.3	-37.7	-23.3	0.10	17.6
	373.15	-216.7	-28.7	0	-0.88	8.5
	473.15	-411.5	-21.8	0	-0.84	0.8
	498.15	-451.0	-23.0	0	-0.88	9.9
	523.15	-468.7	-34.2	0	-0.90	14.3
19.8	373.15	-71.7	-9.3	0	-0.84	3.3
	473.15	-201.3	15.2	0	-0.92	5.9
	498.15	-208.5	25.9	0	-0.93	10.2
	523.15	-222.3	8.7	0	-0.93	8.2

Table 4.6 Fitting parameters used in the linear portions of the excess volume curves in the two phase region at 12.3 MPa.

Temperature	A	B	s
K			$\text{cm}^3 \cdot \text{mol}^{-1}$
373.15	-96.03	-5.08	0.09
473.15	-97.70	-10.71	0.13

Table 4.7 Comparison of the VLE data obtained in this work with Brunner et al. (1987). Mole fraction values listed in this table describe the regions of phase separation.

Temperature	Pressure	x_{CO_2} (This work)	x_{CO_2} *
K	MPa		
298.15	12.3	No phase separation	Single phase
308.15	12.3	No phase separation	Single phase
323.15	12.3	No phase separation	Single phase
373.15	12.3	0.40 to 0.95	0.397 to 0.905
	19.8	No phase separation	Single phase
473.15	12.3	0.2 to 0.7	0.24 to 0.47

* Brunner et al., 1987

The excess molar volumes shown in Figs 4.1 and 4.2 can be explained in terms of the states of the two components and of the mixtures. At 298.15 K both carbon dioxide and methanol are liquid, and the resulting mixture is liquid. The small excess volumes are due to the interactions between carbon dioxide and methanol in solution. At temperatures 308.15 K and 323.15 K we use supercritical carbon dioxide and liquid methanol to produce a liquid mixture. The resulting excess volumes are negative because of the carbon dioxide supercritical fluid effect without a major contribution from phase changes (Wormald, 1986; Zhao, 1996). At 373.15 K carbon dioxide behaves as a gas-like supercritical fluid (see the definition in Section 3.2.3). The mixture formed with methanol under these circumstances is liquid-like at $x_{\text{CO}_2} < 0.35$ and gas-like at $x_{\text{CO}_2} > 0.85$. A similar situation is observed at 473.15 K, where the resulting mixtures are liquid at $x_{\text{CO}_2} < 0.20$ and gaseous at $x_{\text{CO}_2} > 0.3$. The V_m^E curves obtained under these circumstances reflect this phase behaviour. At low x_{CO_2} , subtraction of a large gaseous carbon dioxide volume from a smaller liquid mixture volume gives negative V_m^E values that decrease with carbon dioxide content. As $x_{\text{CO}_2} \rightarrow 1$ the solution becomes a gas-like supercritical fluid. We are now subtracting the same carbon dioxide volume from a gaseous mixture volume. The result is a curve that becomes less negative as we approach $x_{\text{CO}_2} = 1$. The same situation occurs at 498.15 K, except that there are no two-phase regions present. As we increase the temperature to 523.15 K we have passed the critical point for methanol and are now subtracting two large volumes (that of CO_2 and methanol) from the volume of the mixture. As we increase the pressure we compress the

fluids and move further away from the critical locus of the mixture so that all solutions are supercritical. The same effect is noticed, but damped.

The straight lines observed in Fig 4.1 at 373.15 K and 473.15 K at 12.5 MPa and between $0.35 \leq x_{\text{CO}_2} \leq 0.90$ represent regions where two phases were detected in the mixture. The compositions of the two phases in equilibrium are given by the breaks in the curve at points (i_n) and (ii_n). Increasing the mole fraction of carbon dioxide from $x_{\text{CO}_2} = 0$ results in a single phase mixture with strong interactions between the methanol and carbon dioxide (Smith et al., 1991; Taylor et al., 1997) leading to large negative volumetric effects. This continues until point (i_n) is reached where vapour-liquid phase separation occurs. If, instead, we start at $x_{\text{CO}_2} = 1.0$, pure supercritical carbon dioxide, and add methanol to the fluid, a single phase mixture is formed until point (ii_n) is reached. At this point vapour-liquid phase separation occurs.

The linear behaviour of V_m^E curve between points i_n and ii_n arises because no changes occur in the composition of the liquid phase if carbon dioxide is added at point (i_n) to increase the overall composition towards that at (ii_n). Rather, the amount of the liquid phase with composition i_n decreases while the amount of vapour phase with composition ii_n increases (Ott and Boerio-Gates, 2000). The measured V_m^E in this range is a weighted average of the values of V_m^E at points (i_n) and (ii_n). Increasing the pressure or temperature on this system produced data completely in the one-phase region.

The excess molar volumes found in this work are similar to those reported by Goldfarb et al. (1999) who have also found very asymmetric and negative V_m^E values

over the whole mole fraction range at 323.15 K. Their work also found that the effect of pressure on the (CO₂ + MeOH) mixtures was to decrease the magnitude of V_m^E . Their results are shown in Figure 4.3.

Figures 4.4 to 4.7 illustrate the behaviour of V_m^E as a function of T, p for (CO₂ - MeOH). The plots show the molar volumes for pure carbon dioxide and methanol, V_{m,CO_2}^* and $V_{m,MeOH}^*$, and the molar volumes for the mixture, $V_{m,soln}$, at $x_{CO_2} = 0.5$ where $V_m^E = V_{m,soln} - [x_{CO_2}V_{m,CO_2}^* + (1-x_{CO_2})V_{m,MeOH}^*]$. At 298.15 K and pressures above 7.0 MPa, the two pure components and the mixture at $x_{CO_2} = 0.50$ are all in the liquid state and the excess volumes are small. As we increase the temperature to 308.15 K, carbon dioxide becomes supercritical at 7.4 MPa while methanol and the mixture are still liquids. Since carbon dioxide is a dense supercritical fluid at this temperature, the curve behaves much the same as that at 298.15 K but the magnitude of V_m^E is slightly larger. At 498.15 K, carbon dioxide behaves as a gas-like supercritical fluid and the large negative V_m^E values obtained at 498.15 K are due to the large difference in volume between the liquid methanol and the gaseous carbon dioxide, and are illustrated in Fig 4.6. The mixture in Fig 4.6 is at $x_{CO_2} = 0.25$ in order to obtain a mixture that was a dense-supercritical one. Fig 4.7 shows the excess volumes obtained with gaseous CO₂ and supercritical methanol.

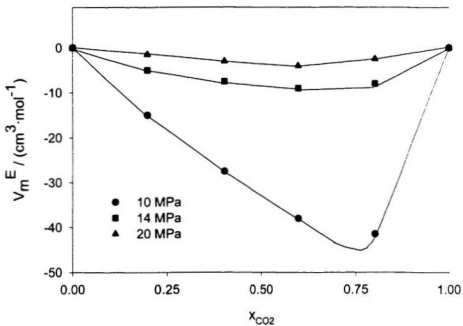


Figure 4.3 Excess molar volumes obtained at 323.15 K for ($\text{CO}_2 + \text{MeOH}$) mixtures by Goldfarb et al (1999).

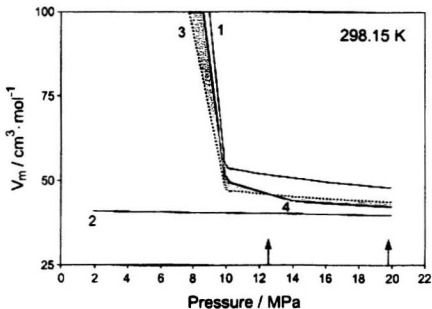


Figure 4.4 The relationship of the V_m^E curve at 298.15 K for (0.5 CO₂ + 0.5 MeOH) to molar volumes (1) V_{m,CO_2}^* , pure carbon dioxide, (2) $V_{m,MeOH}^*$, pure methanol, and (4) $V_{m,soln}$, the mixture. The dashed curve (3) is $[0.5 V_{m,CO_2}^* + 0.5 V_{m,MeOH}^*]$. The shaded area between (3) and (4) is the excess molar volume for the mixture, $V_m^E = V_{m,soln} - [0.5 V_{m,CO_2}^* + 0.5 V_{m,MeOH}^*]$. The arrows indicate the experimental pressures used in this work.

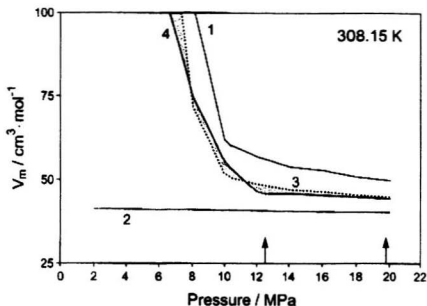


Figure 4.5 The relationship of the V_m^E curve at 308.15 K for (0.5 CO₂ + 0.5 MeOH) to the molar volumes of (1) V_{m,CO_2}^* , pure carbon dioxide, (2) $V_{m,MeOH}^*$, pure methanol, and (4) $V_{m,soln}$, the mixture. The dashed curve (3) is $[0.5 V_{m,CO_2}^* + 0.5 V_{m,MeOH}^*]$. The shaded area between (3) and (4) is the excess molar volume for the mixture, $V_m^E = V_{m,soln} - [0.5 V_{m,CO_2}^* + 0.5 V_{m,MeOH}^*]$. The arrows indicate the experimental pressures used in this work.

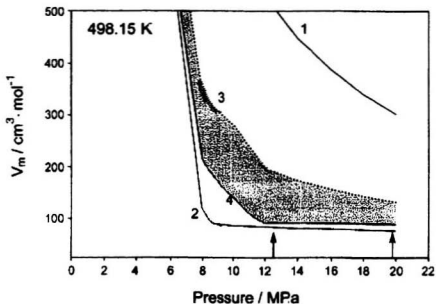


Figure 4.6 The relationship of the V_m^E curve at 498.15 K for (0.25 CO_2 + 0.75 MeOH) to the molar volumes of (1) V_{m,CO_2}^* , pure carbon dioxide, (2) $V_{m,\text{MeOH}}^*$, pure methanol, and (4) $V_{m,\text{soln}}$, the mixture. The dashed curve (3) is $[0.25 V_{m,\text{CO}_2}^* + 0.75 V_{m,\text{MeOH}}^*]$. The shaded area between (3) and (4) is the excess molar volume for the mixture, $V_m^E = V_{m,\text{soln}} - [0.25 V_{m,\text{CO}_2}^* + 0.75 V_{m,\text{MeOH}}^*]$. The arrows indicate the experimental pressures used in this work.

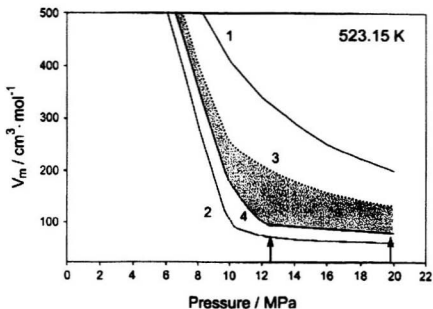


Figure 4.7 The relationship of the V_m^E curve at 523.15 K for (0.5 CO₂ + 0.5 MeOH) to the molar volumes of (1) V_{m,CO_2}^* , pure carbon dioxide, (2) $V_{m,MeOH}^*$, pure methanol, and (4) $V_{m,soln}$, the mixture. The dashed curve (3) is $[0.5 V_{m,CO_2}^* + 0.5 V_{m,MeOH}^*]$. The shaded area between (3) and (4) is the excess molar volume for the mixture, $V_m^E = V_{m,soln} - [0.5 V_{m,CO_2}^* + 0.5 V_{m,MeOH}^*]$. The arrows indicate the experimental pressures used in this work.

4.4.2 Reduced Excess Molar Volumes

Reduced excess molar volumes are obtained when the excess molar volumes are divided by the product of the mole fractions, as described in Section 1.2. They are used to characterize the non-ideality of mixtures as a function of mole fraction (Desnoyers and Perron, 1997) and show limiting behaviour as $x \rightarrow 0$ or $x \rightarrow 1$.

The reduced excess molar volumes obtained in this work are shown in Figures 4.8 to 4.12 for both the carbon dioxide-rich and methanol-rich regions as a function of temperature and pressure. The curves were obtained by fitting the modified Redlich-Kister equation to the V_m data. For regions where phase separation was observed, V_m^R values were omitted from the plots. Negative and asymmetric V_m^R curves were obtained at all temperatures and pressures over the entire mole fraction range, with very large negative deviations from ideal behaviour in the carbon dioxide-rich regions. These deviations extend beyond five litres per mole at 12.3 MPa, and beyond three litres per mole at 19.8 MPa. The effect of increasing pressure on the system is to reduce the magnitude of V_m^R .

Due to experimental difficulties in obtaining density values for x_{CO_2} larger than approximately 0.95, the Redlich-Kister extrapolation to infinite dilution for CO_2 -rich mixtures is questionable, particularly at higher temperatures. At temperatures of 498.15 K and 523.15 K the densities of the carbon dioxide-rich mixtures took longer to obtain, as the mixtures behaved like gases (see Figure 1.3). For these reasons, the

extrapolations to infinite dilution were not performed at high x_{CO_2} . Instead, the experimental data obtained at $x_{\text{CO}_2} = 0.9$ was taken as the infinite dilution value, using the relationship:

$$V_m^R(x_{\text{CO}_2} = 0.9) = V_{\phi, \text{MeOH}} - V_{\text{MeOH}}^* \quad (4.1)$$

to obtain V_{MeOH}^0 by the assumption that :

$$V_{\text{MeOH}}^0 = V_{\phi, \text{MeOH}}(x_{\text{CO}_2}=0.90) \quad (4.2)$$

The experimental uncertainties in these values are shown in the appendix, with questionable data shown in square brackets.

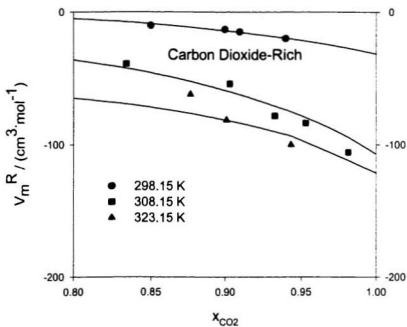


Figure 4.8 Reduced excess molar volume results obtained at 12.3 MPa at low temperatures ($298.15 \text{ K} \leq T \leq 323.15 \text{ K}$) for the carbon dioxide-rich region of the mole fractions. Symbols represent experimental V_m^R data and curves are obtained from the modified Redlich-Kister equation.

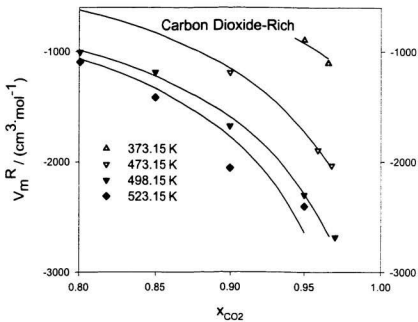


Figure 4.9 Reduced excess molar volume results obtained at 12.3 MPa at high temperatures ($373.15 \text{ K} \leq T \leq 523.15 \text{ K}$) for the carbon dioxide-rich region of the mole fractions. Symbols represent experimental V_m^R data and curves are obtained from the modified Redlich-Kister equation.

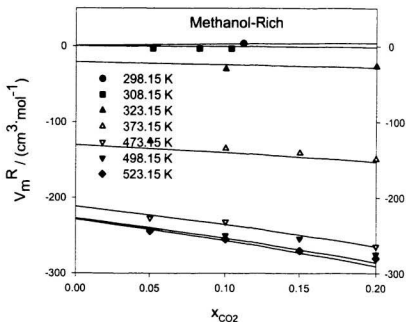


Figure 4.10 Reduced excess molar volume results obtained at 12.3 MPa at several temperatures for the methanol-rich region of the mole fractions. Symbols represent experimental V_m^R data and curves are obtained from the modified Redlich-Kister equation.

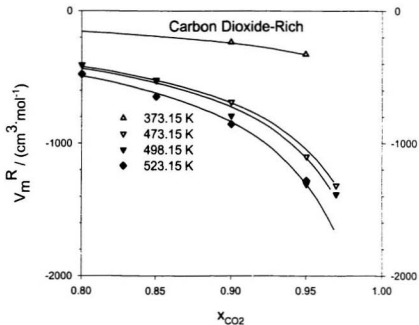


Figure 4.11 Reduced excess molar volume results obtained at 19.8 MPa at several temperatures for the carbon dioxide-rich region of the mole fractions. Symbols represent experimental V_m^R data and curves are obtained from the modified Redlich-Kister equation.

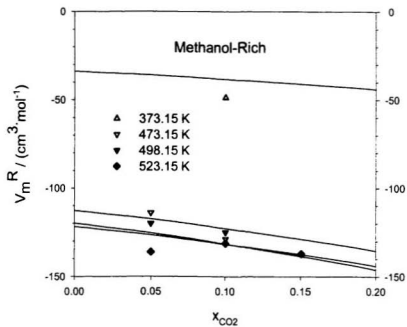


Figure 4.12 Reduced excess molar volume results obtained at 19.8 MPa at several temperatures for the methanol-rich region of the mole fractions. Symbols represent experimental V_m^R data and curves are obtained from the modified Redlich-Kister equation.

4.4.3 Reduced Excess Enthalpy for (CO₂ + MeOH)

Reduced excess enthalpies were calculated from Christensen's data (1988) at temperatures of 308.15, 473.15 and 523.15 K and a pressure of 12.5 MPa. These are shown in Figures 4.13 to 4.15, along with the reduced excess volumes obtained in this work, and correspond to the H_m^E data shown in Fig 3.8.

Comparisons among the H_m^R curves in Figs 4.13 to 4.15 are not as straightforward as comparing the V_m^R data in the previous section since enthalpies are not absolute values and need to be referenced to a standard. We measure:

$$H_m^R = (H_1^*(\text{pure liquid at } T, p) - H_{1,4}) / x_2 \quad 4.3$$

which gives us:

$$\lim_{x_1 \rightarrow 0} H_m^R = H_1^* - H_1^0(\text{soln}) \quad 4.4$$

$H_1^0(\text{soln})$ is the standard partial molar enthalpy of the solute at infinite dilution and H_1^* is the enthalpy of the pure liquid which changes as T and p change. These limits can be used to interpret solvation enthalpies. We can use the Lee-Kesler equation of state, using

the reduced temperatures and pressures of Reid et al. (1987), to determine approximate values for $H_1^{\circ}(\text{g}) - H_1^*$.

Combining this with eqn 4.4 we can calculate the enthalpy of solvation:

$$\Delta_{\text{solvation}}H = H_1^{\circ}(\text{soln}) - H_1^{\circ}(\text{g}) \quad 4.5$$

Figure 4.13 shows the reduced excess properties of the mixture at 308.15 K near carbon dioxide's critical temperature. As $x_{\text{CO}_2} \rightarrow 1.0$ the mixture is in a liquid state and the H_m^R upward curving plot increases sharply to a value of 10 kJ mol⁻¹ at the intercept. The Lee-Kesler residual enthalpy calculated at this T and p is 21.6 kJ mol⁻¹. This gives us a solvation enthalpy value of -31.6 kJ mol⁻¹. At 473.15 K, Fig 4.14, the methanol-rich liquid mixture is near its critical point and the H_m^R shows the same upward curvature as at 308.15 K. As carbon dioxide is added, a two-phase mixture is produced. The addition of even more CO₂ results in a progression from a dense gaseous mixture at $x_{\text{CO}_2} \cong 0.30$ to gaseous carbon dioxide at $x_{\text{CO}_2} = 1.0$. This is reflected in the downwards slope of the curve at $x_{\text{CO}_2} > 0.50$. The intercept at $x_{\text{CO}_2} = 1.0$ is 22 kJ mol⁻¹ and the Lee Kesler value is calculated to be 17.0 kJ mol⁻¹, to give a solvation enthalpy of -39.0 kJ mol⁻¹. At 523.15 K supercritical methanol is mixed with gaseous CO₂ to produce a dense gas mixture well above its critical pressure. As more CO₂ is mixed in, the mixture becomes less dense. This accounts for the downward curving plot shown in Fig 4.15. The intercept at $x_{\text{CO}_2} =$

1.0 is approximately 6 kJ mol^{-1} and the Lee Kesler value is 14.6 kJ mol^{-1} . This gives us a solvation enthalpy of $-20.6 \text{ kJ mol}^{-1}$.

4.4.4 Apparent Molar Volumes and Standard Partial Molar Volumes

A summary of the apparent molar volumes for carbon dioxide and methanol from this work as a function of temperature and pressure is shown in the appendix. Eqns 2.15 and 2.16 show the relationship between reduced molar volumes and standard partial molar volumes. Standard partial molar volumes provide measurements for the change in volume per mole of component for an infinitesimal addition of solute. In effect, they are a measure of the solute-solvent interactions occurring at infinite dilution in the mixture. Table 4.8 lists the values obtained for V_{MeOH}° and $V_{\text{CO}_2}^{\circ}$ from this work based on the assumptions made in Section 4.4.1. The same results are shown in Figures 4.16 and 4.17. The standard partial molar volumes for carbon dioxide in methanol were found to be positive and to increase with increasing temperature. Conversely, the standard partial molar volumes for methanol in CO_2 were found to be large negative values that become more negative with increasing temperature. These large negative values of V_{MeOH}° are evidence that there is a strong attraction between the methanol and carbon dioxide at elevated temperatures which results in a high solvation number of CO_2 (solvent) molecules around each methanol (solute) molecule at infinite dilution. This is supported by the values of the solvation enthalpies discussed in Section 4.4.3.

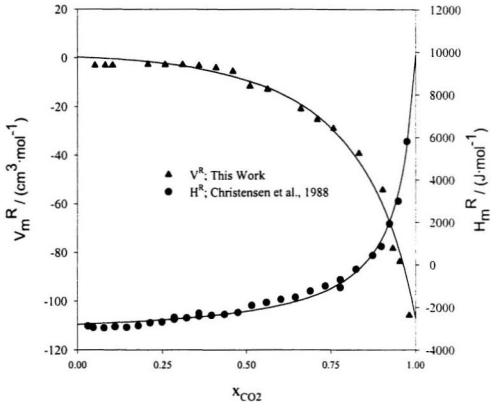


Figure 4.13 Reduced excess enthalpy and reduced excess volume for $(\text{CO}_2 + \text{MeOH})$ at 308.15 K and 12.5 MPa .

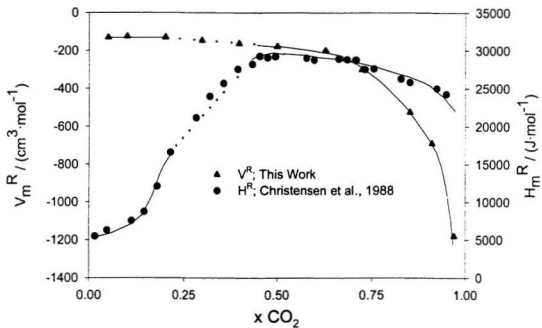


Figure 4.14 Reduced excess enthalpy and reduced excess volume for ($\text{CO}_2 + \text{MeOH}$) at 473.15 K and 12.5 MPa.

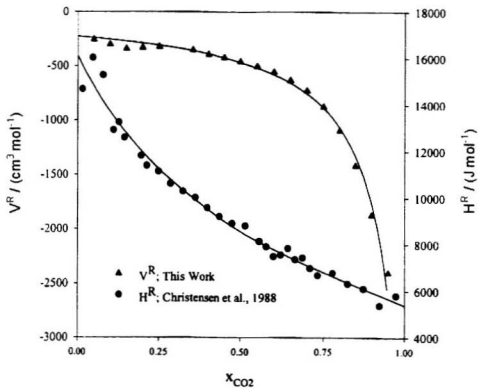


Figure 4.15 Reduced excess enthalpy and reduced excess volume for $(\text{CO}_2 - \text{MeOH})$ at 523.15 K and 12.5 MPa.

Table 4.8 Summary of the standard partial molar volumes obtained for methanol and carbon dioxide at 12.3 and 19.8 MPa.

Temp	$V^R_{X=0.90}$	V^*_{MeOH}	V^0_{MeOH}	$V^R_{X \rightarrow 0}$	$V^*_{CO_2}$	$V^0_{CO_2}$
K	$cm^3 mol^{-1}$	$cm^3 mol^{-1}$	$cm^3 mol^{-1}$	$cm^3 mol^{-1}$	$cm^3 mol^{-1}$	$cm^3 mol^{-1}$
12.3 MPa						
298.15	-15.07 ± 0.03	40.20	26 ± 1	0.648 ± 0.003	51.649	52.3 ± 0.2
308.15	-54.12 ± 0.07	40.53	-8 ± 2	-0.327 ± 0.006	56.583	56.3 ± 0.8
323.15	-81.31 ± 0.06	41.30	-642 ± 2	-12.64 ± 0.06	71.631	58.99 ± 0.06
373.15	-894 ± 5	44.01	-806 ± 50	-110.422 ± 0.3	175.899	65.5 ± 0.2
473.15	-1068 ± 40	56.50	-1050 ± 10	-211.7 ± 0.2	287.271	75.6 ± 0.2
498.15	-1675 ± 5	56.75	-1452 ± 20	-227.4 ± 0.1	310.148	82.7 ± 0.1
523.15	-2056 ± 6	81.40	-1769 ± 100	-248.6 ± 0.4	332.402	83.8 ± 0.3
19.8 MPa						
373.15	-235.0 ± 0.1	43.14	-168 ± 8	-33.827 ± 0.007	92.458	58.631 ± 0.002
473.15	-686.82 ± 0.05	53.95	-763 ± 10	-112.7 ± 0.7	171.579	58.9 ± 0.3
498.15	-791.1 ± 0.7	57.44	-655 ± 10	-121.73 ± 0.07	187.516	65.79 ± 0.04
523.15	-854 ± 1	70.04	-699 ± 10	-119.83 ± 0.08	202.718	82.89 ± 0.03

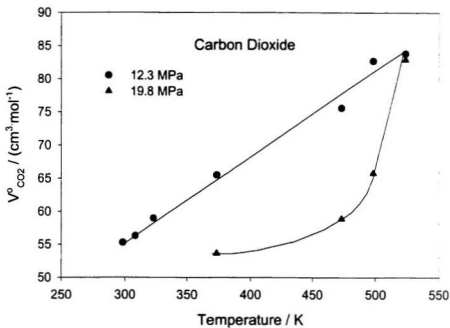


Figure 4.16 $V_{CO_2}^o$ as a function of temperature and pressure. Symbols represent values calculated from experimental data.

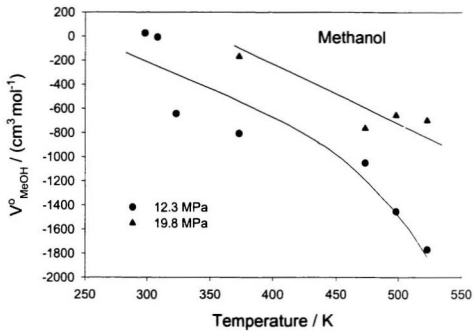


Figure 4.17 V_{MeOH}° as a function of temperature and pressure. Symbols represent values calculated from experimental data.

Chapter 5: Molecular Interpretation

The sigmoidal excess volume curves obtained at $298.15 \text{ K} \leq T \leq 308.15 \text{ K}$ at 12.5 MPa are in good agreement with the excess enthalpy curves presented in Chapter 3 for the ($\text{CO}_2 + \text{MeOH}$) mixtures at 298.15 K and represent data obtained near the critical curve of pure carbon dioxide. Positive deviations from ideality found between $0.10 \leq x_{\text{CO}_2} \leq 0.60$ are thought to be indicative of the presence of a methanol hydrogen-bonded network in the solvent (Hauser et al., 1996). This network results in an expansion of the mixture and therefore, a positive excess molar volume. The negative values of V_m^E found between $0.75 \leq x_{\text{CO}_2} \leq 0.90$ may reflect the breakdown of the hydrogen-bonded network as the amount of carbon dioxide in the mixture is increased. At high x_{CO_2} the hydrogen-bonded networks are broken (Hauser et al., 1996) and the carbon dioxide solvent attracts the methanol molecules towards itself and a collapse of the mixture results. This accounts for the negative excess molar volumes in this region.

At temperatures greater than 308.15 K, increasingly large volumetric effects were observed with increasing temperatures. These may result from the formation of methanol multimers and carbon dioxide-methanol aggregates in the methanol-rich regions and of the strong interactions between the carbon dioxide quadrupoles and the methanol dipoles in the highly compressible carbon dioxide-rich region (Taylor et al., 1997). In the methanol-rich regions it has been proposed by Roskar et al. (1992) that methanol multimers and carbon dioxide-methanol pair wise aggregates form. In the carbon

dioxide-rich regions, the unusually high quadrupole-dipole interactions between the molecules may account for the extremely large negative standard partial molar volumes for methanol. The unusually high solubility of methanol in carbon dioxide at high carbon dioxide composition is also consistent with the extreme behaviours shown above (Reighard et al., 1996).

Chapter 6: Future Work

This work reports measurements of the excess molar enthalpies, H_m^E , for (CO₂ - MeOH) mixtures at 298.15 K made on a newly commissioned microcalorimeter and flow cell. The results have been compared to several literature sources. H_m^E values for this system are reported by Christensen et al. (1988) to temperatures above 500 K. It would be beneficial to the lab for the next student to measure H_m^E values for (CO₂ + MeOH) mixtures up to 473 K, the temperature limit of the calorimeter using an oil bath, and to compare the values with those from Christensen. This would ensure that the microcalorimeter and flow cell provide accurate data at elevated temperatures.

Experiments were begun on (CO₂ + aqueous amine) mixtures, also important in gas processing, but were cut short because of time constraints. Unfortunately, pre-calculations on several amines show that they produce large heats of mixing and cannot be measured with our microcalorimeter. However, no volume data were found for (CO₂ + amine) mixtures in the literature searches done for this work. It would be good to find an amine suitable for measuring on our microcalorimeter, if possible, and to carry out a complete volumetric study on the mixtures.

Also of interest would be to study heats of mixing and volumes of carbon dioxide ternary mixtures, such as (CO₂ + H₂O + MeOH). This system would compliment the volumetric and density studies of (MeOH + H₂O) mixtures performed in our lab by Xiao

(1997) and those of ($\text{CO}_2 + \text{MeOH}$) presented here. It would also provide a useful test system for developing equations of state for polar H-bonded system.

In future work, the densitometer could also be used to determine bubble points, as shown in Section 4.3, in order to construct complete critical loci for these mixtures.

Bibliography

Albert and Archer (1994) in *Solution Calorimetry*. Marsh K.N. and O'Hare P.A., eds. Blackwell Scientific Publications, Chapter 5.

Albert H.J., and Wood R.H. (1984). High-precision densimeter for fluids at temperatures to 700 K and pressures to 40 MPa. *Rev. Sci. Instrum.* **55**, 589-593.

Angus S., Armstrong B., and deReuck K.M. (1976). *International Thermodynamic Tables of the Fluid State, Vol. 3. Carbon Dioxide*. Pergamon Press, Oxford.

Atkins P. and Jones L. *Chemistry. Molecules, Matter, and Change*, 3rd Edition, (1997). Chapter 10: Liquid and Solid Materials. W.H. Freeman and Company, New York. 377-381.

Barbero J.A., Hepler L.G., McCurdy K.G. and Tremaine, P.R. (1983). Thermodynamics of aqueous carbon dioxide and sulfur dioxide: heat capacities, volumes, and the temperature dependence of ionization. *Can. J. Chem.*, **61**, 2509-2519.

Brunner E. (1985). Fluid mixtures at high pressures I. Phase separation and critical phenomena of 10 binary mixtures of (a gas + methanol). *J. Chem. Thermodynamics* **17**, 671-679.

Brunner E., Hultenschmidt W., and Schlichtharle G. (1987). Fluid mixtures at high pressures IV. Isothermal phase equilibria in binary mixtures consisting of (methanol - hydrogen or nitrogen or methane or carbon monoxide or carbon dioxide). *J. Chem. Thermodynamics* **19**, 273-291.

Busey R.H., Holmes H.F., and Mesmer R.E. (1984). The enthalpy of dilution of aqueous sodium chloride to 673 K using a new heat-flow and liquid-flow microcalorimeter. Excess thermodynamic properties and their pressure coefficients. *J. Chem. Thermodynamics*, **16**, 343-372.

Cheng W-H. and Kung H.H. (1994) in *Methanol Production and Use*. Cheng W-H and Kung H.H., eds. Marcel Dekker Inc., New York, Chapter 1.

Christensen J., Christensen S., Schofield R., Faux P., Harding P., Izatt R. (1983). The Excess Enthalpies of (carbon dioxide + cyclohexane) at 308.15, 358.15, and 413.15 K from 7.50 to 12.50 MPa. *J. Chem. Thermodynamics* **15**, 1151-1157.

Christensen J., Christensen S., Schofield R., Faux P., Harding P., Izatt R. (1984). The Excess Enthalpies of (carbon dioxide + pyridine) at 308.15, 358.15 and 413.15 K from 7.50 to 12.50 MPa. *J. Chem. Thermodynamics* **16**, 249-255.

Christensen J., Zebolsky D., Izatt R. (1985). The Excess Enthalpies of (carbon dioxide + pyridine) at 470.15 and 573.15 K from 7.50 to 12.50 MPa. *J. Chem. Thermodynamics* **17**, 785-795.

Christensen J., Cordray D., Izatt R. (1986). The Excess Enthalpies of (carbon dioxide + decane) from 293.15 to 573.15 K at 12.50 MPa. *J. Chem. Thermodynamics* **18**, 53-61.

Christensen J., Faux P., Cordray D., Izatt R. (1986). The Excess Enthalpies of (carbon dioxide + pentane) at 348.15, 373.15, 413.15, 470.15, and 573.15 K from 7.58 to 12.45 MPa. *J. Chem. Thermodynamics* **1986**, 1053-1064.

Christensen J., Walker T., Cordray D., Izatt R. (1987). The Excess Enthalpies of (carbon dioxide + cyclohexane) at 470.15, 553.15, and 573.15 K from 7.50 to 12.50 MPa. *J. Chem. Thermodynamics* **19**, 47-56.

Christensen J., Cordray D.R., Oscarson J.L., Izatt R.M. (1988). The excess enthalpies of four (carbon dioxide + an alkanol) mixtures from 308.15 to 573.15 K at 7.50 to 12.50 MPa. *J. Chem. Thermodynamics* **20**, 867-875.

Christensen J., Izatt R., Faux P. (1988). The Excess Enthalpies of (carbon dioxide + n-hexane + toluene) at 413.15 K and 7.50 and 12.50 MPa. *J. Chem. Thermodynamics* **20**, 503-512.

Clarke R.G.F. (2000). Amino Acids Under Hydrothermal Conditions: Apparent Molar Volumes, Apparent Molar Heat Capacities, and Acid/Base Dissociation Constants for Aqueous α -alanine, Glycine, and Proline at Temperatures from 25 to 250°C and Pressures Up to 30.0 MPa. *PhD. Thesis*, Memorial University of Newfoundland, St. John's, Newfoundland.

Cooper A.I., Londono J.D., Wignall G., McClain J.B., Samulski E.T., Lin J.S., Dobrynin A., Rubinstein M., Burke A.L.C., Frechet M.J.J., and DeSimone J.M. (1997). Extraction of a hydrophilic compound from water into liquid CO₂ using dendritic surfactants. *Nature* **389**, 368-371.

Cordfunke and Ouweltjes (1994) in *Solution Calorimetry*, Marsh K.N. and O'Hare P.A., eds. Blackwell Scientific Publications, Chapter 3.

Crovetto R., and Wood R.H. (1992). Solubility of CO₂ in water and density of aqueous CO₂ near the solvent critical temperature. *Fluid Phase Equilibria* **74**, 271-288.

Desnoyers J., Perron G. (1997). Treatment of excess thermodynamic quantities for liquid mixtures. *J. Soln. Chem.* **26**, 749-755.

Dombro R.A., McHugh M.A., Prentice G.A., and Westgate C.R. (1991). Dielectric constant behaviour of carbon dioxide-methanol mixtures in the mixture-critical and liquid phase regions. *Fluid Phase Equilibria* **61**, 227-241.

Friend D.G. (2001). Private communication.

Galicia-Luna L.A., Richon D., and Renon H. (1994). New loading technique for a vibrating tube densitometer and measurements of liquid densities up to 39.5 MPa for binary and ternary mixtures of the carbon dioxide-methanol-propane system. *J. Chem. Eng. Data* **39**, 424-431.

Gallagher J.S., Crovetto R., and Levelt Sengers J.M.H. (1993). The thermodynamic behaviour of the CO₂-H₂O system from 400 to 1000 K up to 100 MPa and 30% mole fraction of CO₂. *J. Phys. Chem. Ref. Data*, **22**, 431-513.

Goldfarb D.L., Fernandez D.P and Corti, H.R. (1999). Dielectric and volumetric properties of supercritical carbon dioxide (1) + methanol (2) mixtures at 323.15 K. *Fluid Phase Equilibria* **158-160**, 1011-1019.

Goodwin R.D. (1987). Methanol Thermodynamic Properties from 176 to 673 K at Pressures to 700 Bar. *J. Phys. Chem. Ref. Data* **16** (4), 799-810.

Gurdial, Foster, Yun and Tilly (1991) in *ACS Symposium Series 514: Supercritical Fluid Engineering Science. Fundamentals and Applications*. Kiran E. and Brennecke J.F., eds. American Chemical Society, Washington, Chapter 3.

Harvey A.H., Peskin A.P., and Klein S.A. (1996). NIST/ASME steam properties, version 2.11. *NIST Standard Reference Database* 10.

Hauser R.A., Zhao J.P., Tremaine P.R., Mather A.E. (1996). Excess molar enthalpies of six (carbon dioxide + a polar solvent) mixtures at the temperatures 298.15 K and 308.15 K and pressures from 7.5 MPa to 12.6 MPa. *J. Chem. Thermodynamics* **28**, 1303-1317.

Hawrylak B. (1999). Thermodynamics of Aqueous Methyl-diethanolamine and Methyl-diethanolammonium Chloride Over a Wide Range of Temperature and Pressure: Apparent Molar Volumes, Heat Capacities, Compressibilities, and Excess Molar Heat Capacities. *M.Sc. Thesis*, Memorial University of Newfoundland, St. John's, Newfoundland.

Hnedkovsky L., Wood R.H., and Majer V. (1996). Volumes of aqueous solutions of CH_4 , CO_2 , H_2S , and NH_3 at temperatures from 298.15 K to 705 K and pressures to 35 MPa. *J. Chem. Thermodynamics*, **28**, 125-142.

Jennings, Gude and Teja (1991) in *ACS Symposium Series 514: Supercritical Fluid Engineering Science. Fundamentals and Applications*. Kiran E. and Brennecke J.F., eds. American Chemical Society, Washington, Chapter 2.

Kohl A. and Riesenfeld F. (1974) *Introduction in Gas Purification*, 2nd Edition. Gulf Publishing Company, Houston. Chapter 1.

Kratky O., Leopold H., and Stabinger H. (1969). Density determinations of liquids and gases to an accuracy of $10^{-6} \text{ g cm}^{-3}$, with a sample volume of only 0.6 cm^3 (English Title from Chem. Abs.) *Angew. Phys.* **27**, 273-277.

Levelt-Sengers A. (1991) *Thermodynamics of Solutions Near the Solvent's Critical Point in Supercritical Fluid Technology: Reviews in Modern Theory and Application*. Bruno T.J. and Ely J.F., eds. CRC Press, Boca Raton, FL, Chapter 1.

Londono J.D., Dharmapurikar R., Cochran H.D., Wignall G.D., McClain J.B., Betts D.E., Canelas D.A., DeSimone J.M., Samulski E.T., Chilliva-Martino D., and Triolo R. (1997). The morphology of block copolymer micelles in supercritical carbon dioxide by small-angle neutron and X-ray scattering. *J. Appl. Cryst.* **30**, 690.

McCarty R.D., and Arp V. (1986). NIST thermophysical properties of pure fluids database, version 4.0. *NIST Standard Reference Database 12*.

Merkley K., Christensen J., Izatt R. (1987). Enthalpies of Absorption of Carbon Dioxide in Aqueous Methyl-diethanolamine Solutions. *Thermochim. Acta* **121**, 437-446.

Ohgaki K., and Katayama T. (1976). Isothermal vapour-liquid equilibrium data for binary systems containing carbon dioxide at high pressures: Methanol-carbon dioxide, n-hexane-carbon dioxide, and benzene-carbon dioxide systems. *J. Chem. Eng. Data* **21**, 1, 53-55.

- Oscarson J., Van Dam R., Christensen J., Izatt R. (1989). Enthalpies of Absorption of Carbon Dioxide in Aqueous Diethanolamine Solutions. *Thermochim. Acta* **146**, 107-114.
- Ott J.B and Boerio-Gates J. (2000). *Chemical Thermodynamics. Advanced Applications*. Academic Press, London, 2-13, 20-24, and 115-158.
- Ott J.B., Brown P.R., and Sipowska J.T. (1996). Comparison of excess molar enthalpies and excess molar volumes as a function of temperature and pressure for mixtures of (ethane, propane, and butane) with (methanol, ethanol, propan-1-ol, and butan-1-ol). *J. Chem. Thermodynamics*, **28**, 379-404.
- Ott J.B., Stouffer C.E., Cornett G.V., Woodfield B.F., Wirthlin R.C., and Christensen J.J. (1986). Excess enthalpies for (ethanol + water) at 298.15 K and pressures of 0.4, 5, 10, and 15 MPa. *J. Chem. Thermodynamics* **18**, 1-12.
- Ott J.B., Stouffer C.E., Vornett G.V., Woodfield B.F., Guanquan C.H.E. Christensen, J.J. (1987). Excess enthalpies for (ethanol + water) at 398.15, 423.15, 448.15, and 473.15 K and at pressures of 5 and 15 MPa. Recommendations for choosing (ethanol + water) as an H_m^E reference mixture. *J. Chem. Thermodynamics* **19**, 337-348.
- Ott J.B. and Wormald C.J. (1994) in *Solution Calorimetry*. Marsh K.N. and O'Hare P.A., eds. Blackwell Scientific Publications, Chapter 8.
- Palmer D.A. and van Eldik R. (1983). The chemistry of metal carbonato and carbon dioxide complexes. *Chem. Rev.*, **83**, 651-731.
- Pando C., Renuncio J., Izatt R., Christensen J. (1983). The Excess Enthalpies of (carbon dioxide + decane) from 283.15 to 323.15 K at 7.58 MPa. *J. Chem. Thermodynamics* **15**, 173-180.
- Pando C., Renuncio J., Izatt R., Christensen J. (1983). The Excess Enthalpies of (carbon dioxide + pentane) at 348.15, 373.15, 413.15, 470.15, and 573.15 K from 7.58 to 12.45 MPa. *J. Chem. Thermodynamics* **15**, 259-266.
- Pando C., Renuncio J., Schofield R.S., Izatt R., and Christensen J. (1983). The excess enthalpies of (CO₂ + toluene) at 308.15, 385.15, and 413.15 K from 7.60 to 12.67 MPa. *J. Chem. Thermodynamics*, **15**, 747-755.
- Peng D.Y., and Robinson D.B. (1976). A new two-constant equation of state. *Ind. Eng. Chem. Fundam.*, **15**, 1, 59-64.

- Perron G., Couture L., and Desnoyers J. (1992). Correlation of volumes and heat capacities of solutions with their solid-liquid phase diagrams. *J. Soln. Chem.*, **21**, 5, 433-443.
- Prausnitz J.M., Lichtenthaler R.N. and de Azevedo E.G. (1986). *Molecular Thermodynamics of Fluid-Phase Equilibria*, 2nd Edition. Prentice-Hall Inc. New Jersey, Chapter 1.
- Redlich O., and Kister A.T. (1948). Algebraic representation of thermodynamic properties and the classification of solutions. *Industrial and Engineering Chem.*, **40**, 2, 345-348.
- Reid R., Prausnitz J. and Poling B. *The Properties of Gases and Liquids*, 4th Edition. (1987). McGraw-Hill Book Company, New York, 29-73, 95-105, and 241-387.
- Reighard T.S., Lee S.T., and Olesik S.V. (1996). Determination of methanol/CO₂ and acetonitrile/CO₂ vapour-liquid phase equilibria using a variable-volume view cell. *Fluid Phase Equilibria* **123**, 215-230.
- de Reuck K.M., and Craven R.J.B. (1993). *Methanol. International Thermodynamic Tables of the Fluid State - 12*. Blackwell Scientific Publications, Oxford.
- Roskar V., Dombro R.A., Prentice G.A., Westgate C.R., and McHugh M.A. (1992). Comparison of the dielectric behaviour of mixtures of methanol with carbon dioxide and ethane in the mixture-critical and liquid regions. *Fluid Phase Equilibria* **77**, 241-259.
- Smith R.D., Fulton J.L., and Yee G.G. (1991). Hydrogen bonding of simple alcohols in supercritical fluids: An FTIR study. *J. Am. Chem. Soc* **113**, 8327-8334.
- Somsen (1994) in *Solution Calorimetry*; Marsh K.N. and O'Hare P.A., eds. Blackwell Scientific Publications, Chapter 1.
- Suzuki K., Sue H., Itou M., Smith R.L., Inomata H., Aral K., and Saito S. (1990). Isothermal vapour-liquid equilibrium data for binary systems at high pressures: Carbon dioxide-methanol, carbon dioxide-ethanol, carbon dioxide-1-propanol, methane-ethanol, methane-1-propanol, ethane-ethanol and ethane-1-propanol systems. *J. Chem. Eng. Data* **35**, 63-66.
- Takenouchi S., and Kennedy G.C. (1964). The binary system H₂O-CO₂ at high temperatures and pressures. *Am. J. Sci.* **262**, 1055-1074.

Taylor C.M.V, Bai S., Mayne C.L., and Grant D.M. (1997). Hydrogen bonding of methanol in supercritical CO₂ studied by ¹³C nuclear spin-lattice relaxation. *J. Phys. Chem.* **101**, 5652-5658.

Trevani L.N., Roberts J.C., and Tremaine P.R. (2001). Copper(II)-ammonia complexation equilibria in aqueous solutions from 30 to 250°C by visible spectroscopy. *J. Soln. Chem.*, **30**, 585-622.

van Konynenburg P.H., and Scott R.L. (1980). Critical lines and phase equilibria in binary van der Waals mixtures. *Philos. Trans. R. Soc.* **298**, 495-540.

Van Ness H.C. and Abbott M.M. (1982). *Classical Thermodynamics of Nonelectrolyte Solutions with Applications to Phase Equilibria*. McGraw-Hill Book Company, New York.

Wiebe R., and Gaddy V.L. (1940). The solubility of carbon dioxide in water at various temperatures from 12 to 40°C and at pressures to 500 atmospheres. Critical phenomena. *Bureau of Agricultural Chemistry and Engineering* **62**, 815-817.

Wormald C.J. (1986). Heats and volumes of mixing in the critical region. An exploration using the van der Waals equation. *Fluid Phase Equilibria* **28**, 137-153.

Xiao C., Bianchi H., and Tremaine P.R. (1997). Excess molar volumes and densities of (methanol + water) at temperatures between 323 K and 573 K and pressures of 7.0 MPa and 13.5 MPa. *J. Chem. Thermodynamics* **29**, 261-286.

Yang B.L. (1994) in *Methanol Production and Use*. Cheng W-H and Kung H-H, eds. Marcel Dekker Inc, New York, Chapter 2.

Zhao J.P. (1996). Excess Molar Enthalpies of Carbon Dioxide with Polar Solvents in the Vicinity of the Critical Point. *M.Sc. Thesis*. Memorial University of Newfoundland, St. John's, Newfoundland.

Ziegler J.W., Chester T.L., Innis D.P., Page S.H., and Dorsey J.G. (1995). Supercritical fluid flow injection method for mapping liquid-vapour critical loci of binary mixtures containing CO₂. *Innovations in Supercritical Fluids* in the 1995 American Chemical Society, 93-110.

Appendix I: Scoping Experiments on the CSC 4400 Isothermal Microcalorimeter

A.I-1 Calibration of Calorimeter and High Pressure Flow Cells With (Water + Ethanol) Mixtures

The CSC 4400 isothermal microcalorimeter and the high pressure flow cells were calibrated by pumping a known binary mixture through the calorimeter and measuring the heats of mixing as a function of flow rate. The mixture used was ($\text{H}_2\text{O} + \text{EtOH}$) having a composition of mole fraction $x = 0.5$ at $T = 298.15 \text{ K}$ and $p = 0.4 \text{ MPa}$. This not only enabled us to study the effects of flow rates on the calorimeter, but also to investigate the working range of the instrument.

Because of the growing interest in calorimetric measurements taken at high temperature and high pressure in laboratories around the world, there is a need for reference systems to compare calorimeters in the different laboratories. Christensen et al., (1986) have suggested using the ($\text{H}_2\text{O} + \text{EtOH}$) system as a reference, since a large volume of data already exist for this system at ambient temperatures and pressures. His group has extended this database to temperatures up to 473.15 K and pressures up to 15 MPa , making the ($\text{H}_2\text{O} + \text{EtOH}$) system a useful reference system for calorimetric studies. An attempt was made here using our new CSC 4400 commercial calorimeter with highly accurate Isco pumps to reproduce Christensen's data for our ($\text{H}_2\text{O} + \text{EtOH}$) mixtures.

Water flowed at a rate of $0.800 \text{ cm}^3 \cdot \text{min}^{-1}$ for an hour prior to mixing to ensure a stable baseline. At that time, the second pump was opened to the system and run at a flow rate of $0.611 \text{ cm}^3 \cdot \text{min}^{-1}$ while the flow rate from the water pump was reduced to $0.189 \text{ cm}^3 \cdot \text{min}^{-1}$ to keep the total flow rate at $0.800 \text{ cm}^3 \cdot \text{min}^{-1}$, the same as that at which the baseline was taken. The microcalorimeter required approximately 20 minutes for the mixed solution to produce a stable signal, and was allowed to run for a further hour to produce a long, stable plateau. The signal appeared to be completely flat with little fluctuation and indicated that the heat-flux detectors were saturated, i.e. the heat change occurring during the mixing process was too large to be measured by the calorimeter (see Section 2.2.2). The signal appeared to be cut off at $\pm 1.1 \cdot 10^5 \mu\text{W}$, this corresponds to the working power limit of the microcalorimeter.

To obtain a meaningful measurement we reduced the molar flow rates of the pumps and a second trial was attempted using a total flow rate of $0.600 \text{ cm}^3 \cdot \text{min}^{-1}$. For this mixture the water pump was run at $0.142 \text{ cm}^3 \cdot \text{min}^{-1}$ and the ethanol pump was set at $0.458 \text{ cm}^3 \cdot \text{min}^{-1}$ and a stable plateau was observed on the instrument output. Further runs were carried out at total flow rates of $0.400 \text{ cm}^3 \cdot \text{min}^{-1}$ (H_2O , $0.095 \text{ cm}^3 \cdot \text{min}^{-1}$; EtOH, $0.305 \text{ cm}^3 \cdot \text{min}^{-1}$) and $0.300 \text{ cm}^3 \cdot \text{min}^{-1}$ (H_2O , $0.071 \text{ cm}^3 \cdot \text{min}^{-1}$; EtOH, $0.229 \text{ cm}^3 \cdot \text{min}^{-1}$) and the signals compared. The calorimeter output signals are shown in Figure A-1 showing the flow rate dependence of the instrument. The signal obtained for the $0.300 \text{ cm}^3 \cdot \text{min}^{-1}$ run was noticeably more noisy than the results at higher flow rates. Further measurements at flow rates below $0.300 \text{ cm}^3 \cdot \text{min}^{-1}$ gave results that were too noisy to be

useful. This may be a result of laminar flow. At low velocity there may not have been enough turbulence to ensure that complete mixing was occurring inside the calorimeter. If so, the mixing process inside the microcalorimeter mixing chamber may be one where the two fluids are slowly diffusing into one another as a result of viscous fingering rather than quickly mixing, so that there was not enough time to achieve a homogeneous mixture in the small tubular mixing chamber of the instrument. To check the reproducibility of the CSC 4400 isothermal microcalorimeter, a second run at $0.600 \text{ cm}^3 \cdot \text{min}^{-1}$ was performed under the same conditions and compared to the first. The results shown in Figure A-2 show that the results obtained for the ($\text{H}_2\text{O} + \text{EtOH}$) mixture were reproducible.

From the power and the flow rates of the two pumps, we were able to determine the molar excess enthalpy, H_m^E , of the mixture, as described in Section 2.4.1. These results were compared with those obtained by Christensen's group (1987) and showed agreement to within 1 % of Christensen's results. The H_m^E values obtained for the 50-50 mixture at the various flow rates are listed in Table A-1.

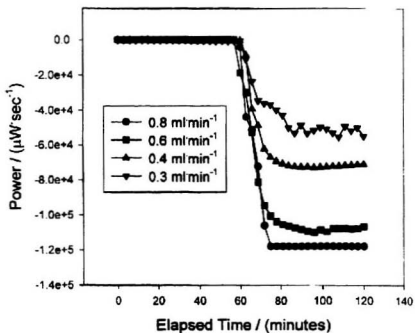


Figure A-1 CSC 4400 isothermal microcalorimeter power output for a 50-50 (water + ethanol) mixture at 298.15 K and 0.4 MPa as a function of flow rates.

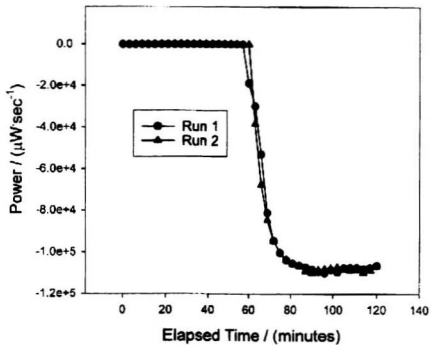


Figure A-2. (Water + ethanol) results for a 50-50 volume mixture at 298.15 K and 0.4 MPa and a total flow rate of $0.600 \text{ cm}^3\cdot\text{min}^{-1}$ taken during two different runs.

Table A-1 Commissioning results for the (water + ethanol) mixture on the CSC 4400 isothermal microcalorimeter at $x_{\text{H}_2\text{O}} = 0.50$ and at 298.15 K and 0.4 MPa.

Total Flow Rate	H_m^E
$\text{cm}^3 \cdot \text{min}^{-1}$	$\text{J} \cdot \text{mol}^{-1}$
	This Work
> 0.6	Saturated Signal
0.6	-412 ± 5
0.4	-410 ± 4
0.3	-399 ± 12
< 0.3	Noisy
	Christensen et al., 1986
0.5	-407 ± 2

A.I-2 (Carbon Dioxide + Propylene Carbonate) Mixtures

The flow system designed for use at high temperature and pressure in this work is described in Section 2.2.1. Corrosive chemicals were not placed directly inside the Isco pumps, but rather inside a Teflon bag contained in a high-pressure cylinder. To check whether the injection system and the microcalorimeter could produce reliable data for a carbon dioxide mixture, we measured the H_m^E values for the (CO₂ + propylene carbonate) system for comparison with those reported by Zhao (1996) from measurements made previously in our lab. The run was done at 298.15 K and 7.5 MPa with total flow rates of 0.300-0.500 cm³·min⁻¹ to ensure that the microcalorimeter signal did not saturate.

As is apparent from Figure A-3, the microcalorimeter can reliably reproduce literature values at high mole fractions of carbon dioxide. Unfortunately, literature values could not be reproduced at the lower CO₂ mole fractions. The discrepancies suggested that the carbon dioxide flow rate was too slow to ensure that complete mixing had occurred. The problem was further complicated in these mixtures because carbon dioxide is extremely compressible. Unless the flow rate of the Isco pump containing the carbon dioxide was fast enough, the carbon dioxide appeared to remain inside the pump and become more compressed until the pressure rose enough to force it to move. The erratic results suggested that squirts of carbon dioxide were coming from the pump rather than a smooth, continuous flow. Increasing the flow rates to overcome this problem resulted in a heat change that was so large that the microcalorimeter detectors were saturated and could not detect the change.

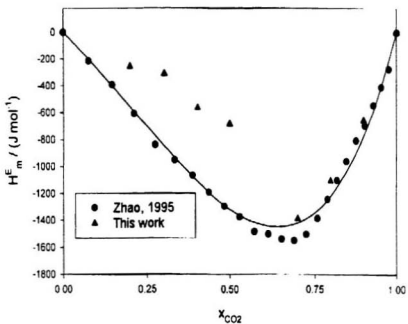


Figure A-3

Excess enthalpy results for the (carbon dioxide + propylene carbonate) system over the entire mole fraction range at 298.15 K and 7.5 MPa. The solid curve represents the solution to the Redlich-Kister fitting equation for Jian Ping Zhao's experimental points.

A.I-3 Scoping Experiments on Selected Dilute Systems

A.I-3.1 Introduction

Where measurements were possible, the results for the (CO₂ + propylene carbonate) mixtures agreed well with previous results obtained in our lab. This led us to believe that the microcalorimeter could be successfully used to obtain H_m^E data for near critical mixtures if an appropriate system could be found. We also sought to use it to study aqueous systems with solubilities in the range of 1 mol·kg⁻¹ to 5 mol·kg⁻¹. Several scoping experiments were carried out to find a system of interest for further work.

A.I-3.2(Carbon Dioxide + Aqueous Ethanolamine)

The use of alkanolamines as acidic gas absorbents was introduced in the 1930's by R.R. Bottoms (Somsen, 1994). Since that time much research has gone into the thermodynamic study of (CO₂ + amine) mixtures with applications to the gas and oil industries. Christensen's group at Brigham Young University has been a leader in developing calorimeters and experimental methods for such studies. This group has produced extensive data on the enthalpies of absorption for the binary mixtures of carbon dioxide with aqueous diethanolamine, methyldiethanolamine and diglycolamine solutions as a function of composition, temperature and pressure. (See, for example: Merkle et al., 1987)

Since aqueous monoethanolamine solutions were used almost exclusively for many years for the removal of carbon dioxide from natural gas, it was thought that this would be a good system to study with our microcalorimeter. The aqueous ethanolamine solutions (EA) were prepared by mass to make solutions with molalities of 1.82 mol kg^{-1} and $16.37 \text{ mol kg}^{-1}$ with nanopure water. The ethanolamine solutions were placed inside the Teflon bag as described previously. The microcalorimeter temperature was set to 298.15 K and the system pressure was maintained at 7.5 MPa. Carbon dioxide flowing at $0.500 \text{ cm}^3 \text{ min}^{-1}$ was used as the baseline.

A very large thermal effect was observed for the ($\text{CO}_2 + \text{aqueous ethanolamine}$) system, and the power change generated during the mixing process was too large to be measured by the microcalorimeter detectors regardless of the total flow rates. This would be a good system to study on a less sensitive instrument than ours, since the mixing problem associated with slow pump flow rates does not seem to be as severe in this case.

A.1-3.3(Carbon Dioxide + Aqueous Sodium Dodecyl Sulfate) Solutions

Surface active agents, commonly referred to as surfactants, are molecules that possess both hydrophobic and hydrophilic groups. Above a particular concentration of surfactant called the Critical Micellar Concentration (CMC), the molecules aggregate together to form spherical ensembles called micelles. The hydrophilic regions of the micelles extend into water or other polar solvents while the hydrophobic groups cluster together to form a spherical core. The reverse process happens in non-polar solvents to

form inverse micelles. This unique property of surfactants to form micelles is being exploited in supercritical fluid chemistry as a means of increasing the solubility of CO₂-insoluble molecules in liquid and supercritical carbon dioxide. This is achieved by solubilizing in the micelles which are more soluble in carbon dioxide. Cooper et al. (1997) describe how fluorinated dendritic surfactants were used to extract a polar ionic dye from water into carbon dioxide. Another study released by Londono et al. (1997) also describes the formation of micelle formations in supercritical carbon dioxide.

Probably the most extensively studied surfactant to date is sodium dodecyl sulfate, or SDS, and for this reason it was the surfactant chosen for this work. A one molal aqueous solution of SDS was prepared by mass and placed inside the Teflon bag compartment of the injection system. The surfactant solution was clear and colourless. The microcalorimeter temperature was kept at 298.15 K and the system was maintained at a pressure of 7.5 MPa. A carbon dioxide baseline was run at 0.500 cm³·min⁻¹ and then the flow rate was reduced to 0.250 cm³·min⁻¹ while the surfactant solution was also allowed to flow at a flow rate of 0.250 cm³·min⁻¹.

Figure A-4 shows the resulting signal obtained from the microcalorimeter. The signal was completely erratic and showed large jumps in the measurements. It was first thought that this was indicative of the formation of bubbles inside the microcalorimeter during the mixing process. However, at the end of the experiment the downstream pressure vessel was opened, to reveal an extremely thick, white foam that undoubtedly affected flow rate and back-pressure control. Two weeks of continual flushing with

water were required to clean the residual surfactant out of the injection system. This suggested that our erratic signals were due to the formation of foam that caused large pressure drops inside the microcalorimeter. It was decided not to continue with the surfactant experiments because the pressure drop associated with our backpressure control system is inherent to its design and will always generate foam.

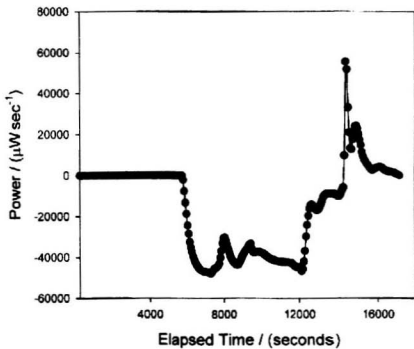


Figure A-4 Signal obtained from a one molal aqueous solution of SDS mixed with carbon dioxide at 298.15 K and 7.5 MPa.

A.I-3.4(Carbon Dioxide + Water)

Although not relevant to the applications mentioned in the introduction of this thesis, the ($\text{CO}_2 + \text{H}_2\text{O}$) system is of importance since it is fundamental to many geochemical processes. Much emphasis has been placed on studying the pVT properties and critical locus for this system at elevated temperatures and pressures, particularly near the critical point of carbon dioxide (Takenouchi and Kennedy, 1964). Although the solubility and pVT properties for this system have been well studied, the enthalpy of solution and heat capacities have not. This provides us with a challenging test case for our new calorimeter and an attempt to study these properties at 298.15 K and 7.5 MPa is presented in this work.

The signal obtained from the ($\text{CO}_2 + \text{H}_2\text{O}$) trials is shown on Figure 3.5. Again, the problem encountered here is one of poor mixing. Due to the low solubility of carbon dioxide in water ($\sim 1 \text{ mol}\cdot\text{kg}^{-1}$ at 10.0 MPa) a large difference in the flow rates between the two pumps was required. This apparently caused the carbon dioxide to flow too slowly, so that it compressed inside the pump rather than flowing smoothly into the microcalorimeter. This occurred regardless of the total flow rate used.

A literature search on the system showed that complete miscibility for this system could be expected at mole fractions up to approximately $x_{\text{CO}_2} = 0.1$ at the experimental temperature and pressure (Takenouchi and Kennedy, 1964). To determine if only a single phase was present in this system, a viewing cell was connected in-line at the outlet

of the microcalorimeter.

The procedure for measuring the H_m^E for ($\text{CO}_2 + \text{H}_2\text{O}$) was repeated, this time with the viewing cell in-line. Once the two fluids had mixed inside the microcalorimeter, the mixture flowed out of the flow cell and entered the viewing compartment of the viewing cell. Bubbles were observed through the sapphire windows, suggesting that a higher pressure was required to achieve a one-phase fluid. The ($\text{CO}_2 + \text{H}_2\text{O}$) experiments were ended because the low solubility of the carbon dioxide prevented us from adequately controlling the carbon dioxide flow rate.

At this point in the project, it became clear that reliable information for carbon dioxide mixtures could not be obtained from the microcalorimeter as it had been purchased. A newly designed flow cell with a longer thermal equilibrium chamber and an improved mixing chamber was obtained from CSC. As well, a gain switch was added to the microcalorimeter by CSC to extend the working range of the instrument. The results in the next section were obtained using the improved microcalorimeter.

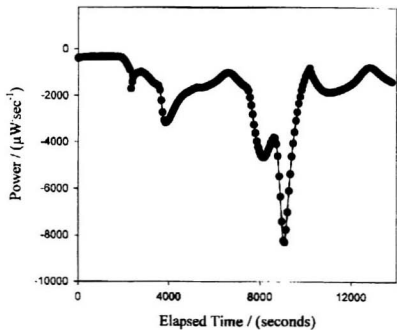


Figure A-5 Signal obtained for (carbon dioxide + water) at 298.15 K and 7.5 MPa.

Appendix II: Experimental results for the (CO₂ + MeOH) mixtures.

Table A-2 Volumetric results for (CO₂ + MeOH) mixtures at 298.15 K and 12.5 MPa.

x_{CO_2}	$10^2(\rho - \rho^*)$ g cm ⁻³	V_{sol} cm ³ mol ⁻¹	V_m^E cm ³ mol ⁻¹	$V_m^E/(x_1 x_2)$ cm ³ mol ⁻¹	$V\phi_{\text{MeOH}}$ cm ³ mol ⁻¹	$V\phi_{\text{CO}_2}$ cm ³ mol ⁻¹
1.0	0 ±0.003	51.649 ±0.003	0			
0.940	1.688 ±0.001	49.82 ±0.03	-1.135 ±0.001	-20.11 ±0.01	21 ±2	
0.909	1.740 ±0.003	49.37 ±0.09	-1.238 ±0.002	-15.07 ±0.03	26 ±1	
0.887	1.790 ±0.003	49.04 ±0.09	-1.317 ±0.002	-13.18 ±0.02	28 ±1	
0.849	1.640 ±0.004	48.6 ±0.1	-1.317 ±0.003	-10.33 ±0.02		
0.799	0.340 ±0.003	48.64 ±0.05	-0.704 ±0.008	-4.39 ±0.05		
0.599	-3.130 ±0.001	47.78 ±0.01	0.7364 ±0.0002	3.067 ±0.001		
0.398	-5.170 ±0.001	46.017 ±0.009	1.2647 ±0.0003	5.270 ±0.001		54.80 ±0.01
0.199	-5.301 ±0.004	43.10 ±0.03	0.6448 ±0.0005	4.031 ±0.003		54.83 ±0.04
0.098	-5.34 ±0.03	41.6 ±0.3	0.310 ±0.002	3.52 ±0.02		54.7 ±0.3
0 (Expt.)	-5.40 ±0.03	40.2 ±0.2	0			
0 (Lit.)	-5.420	40.17	0			

- Errors are experimental uncertainty in measuring τ , except for errors associated with $V\phi$, which are associated with the pressure uncertainty of the system.

Table A-3 Volumetric results for (CO₂ + MeOH) mixtures at 308.15 K and 12.5 MPa

x_{CO_2}	$\frac{10^4(\rho-\rho^*)}{\text{g cm}^{-3}}$	$\frac{V_{\text{soln}}}{\text{cm}^3 \text{mol}^{-1}}$	$\frac{V_m^E}{\text{cm}^3 \text{mol}^{-1}}$	$\frac{V_m^E/(x_1x_2)}{\text{cm}^3 \text{mol}^{-1}}$	$\frac{V\phi_{\text{-MeOH}}}{\text{cm}^3 \text{mol}^{-1}}$	$\frac{V\phi_{\text{-CO}_2}}{\text{cm}^3 \text{mol}^{-1}}$
1.0	0 ±0.005	56.582 ±0.005	0			
0.981	2.873 ±0.006	54.3 ±0.1	-1.991 ±0.004	-105.7 ±0.2	-63 ±10	
0.953	5.67 ±0.01	52.06 ±0.09	-3.767 ±0.007	-83.6 ±0.1	-39 ±5	
0.933	7.620 ±0.005	50.59 ±0.03	-4.912 ±0.003	-78.19 ±0.05	-32 ±4	
0.904	7.37 ±0.01	50.33 ±0.07	-4.707 ±0.006	-54.12 ±0.07	-8 ±2	
0.834	8.90 ±0.02	48.5 ±0.1	-5.44 ±0.01	-39.19 ±0.08	8 ±2	
0.758	8.940 ±0.009	47.41 ±0.05	-5.292 ±0.005	-28.85 ±0.03		
0.707	9.050 ±0.003	46.65 ±0.02	-5.237 ±0.002	-25.285 ±0.008		
0.659	8.26 ±0.03	46.4 ±0.2	-4.71 ±0.02	-20.94 ±0.08		
0.559	5.846 ±0.008	46.33 ±0.07	-3.193 ±0.004	-12.96 ±0.02		
0.511	5.46 ±0.01	45.84 ±0.08	-2.901 ±0.005	-11.61 ±0.02		
0.459	2.880 ±0.008	46.5 ±0.1	-1.37215 ±0.004	-5.53 ±0.02		

.....Continued on next page

x_{CO_2}	$10^2(\rho-\rho^*)$ g·cm ⁻³	V_{soln} cm ³ ·mol ⁻¹	V_m^E cm ³ ·mol ⁻¹	$V_m^E/(x_1x_2)$ cm ³ ·mol ⁻¹	$V\phi_{\text{MeOH}}$ cm ³ ·mol ⁻¹	$V\phi_{\text{CO}_2}$ cm ³ ·mol ⁻¹
0.412	2.301 ±0.005	46.2 ±0.1	-0.983 ±0.002	-4.060 ±0.009		
0.359	1.950 ±0.007	45.6 ±0.2	-0.727 ±0.003	-3.16 ±0.01		
0.309	1.830 ±0.006	44.9 ±0.1	-0.608 ±0.002	-2.845 ±0.009		
0.258	1.808 ±0.007	44.1 ±0.2	-0.544 ±0.002	-2.84 ±0.01		54.3 ±0.2
0.207	1.710 ±0.005	43.4 ±0.1	-0.439 ±0.001	-2.680 ±0.007		54.2 ±0.1
0.108	1.620 ±0.006	42.0 ±0.1	-0.296 ±0.001	-3.06 ±0.01		53.4 ±0.2
0.083	1.544 ±0.004	41.7 ±0.1	-0.232 ±0.001	-3.032 ±0.008		53.2 ±0.1
0.052	1.45 ±0.03	41.2 ±0.9	-0.153 ±0.003	-3.10 ±0.07		53 ±1
0 (Expt.)	1.27 ±0.07	40.53 ±0.01	0			
0 (Lit.)	1.130	40.603	0			

Table A-4 Volumetric results for (CO₂ + MeOH) mixtures at 323.15 K and 12.3 MPa.

x_{CO_2}	$10^3 \cdot (\rho - \rho^*)$ g cm ⁻³	V_{soln} cm ³ ·mol ⁻¹	V_m^E cm ³ ·mol ⁻¹	$V_m^E/(x_1x_2)$ cm ³ ·mol ⁻¹	$V\phi_{\text{MeOH}}$ cm ³ ·mol ⁻¹	$V\phi_{\text{CO}_2}$ cm ³ ·mol ⁻¹
1.0	0 ±0.006	71.631 ±0.006	0			
0.950	6.510 ±0.007	63.89 ±0.07	-6.228 ±0.006	-131.2 ±0.1	-809 ±3	
0.899	8.460 ±0.007	61.24 ±0.05	-7.344 ±0.006	-81.31 ±0.06	-642 ±2	
0.870	8.560 ±0.007	60.64 ±0.05	-7.036 ±0.005	-62.06 ±0.05	-436 ±1	
0.799	13.560 ±0.007	55.48 ±0.03	-10.072 ±0.005	-62.83 ±0.03		
0.749	17.052 ±0.007	52.26 ±0.02	-11.79 ±0.01	-62.86 ±0.03		
0.699	19.77 ±0.02	49.77 ±0.06	-12.76 ±0.02	-60.74 ±0.07		
0.600	19.98 ±0.03	48.17 ±0.06	-11.32 ±0.02	-47.16 ±0.06		
0.499	20.42 ±0.01	46.45 ±0.03	-10.015 ±0.004	-40.06 ±0.03		
0.399	20.15 ±0.01	45.13 ±0.02	-8.295 ±0.009	-34.57 ±0.02		
0.350	19.77 ±0.02	44.61 ±0.05	-7.312 ±0.002	-32.14 ±0.04		

...Continued on next page

x_{CO_2}	$\frac{10^3(\rho-\rho^*)}{\text{g}\cdot\text{cm}^{-3}}$	$\frac{V_{\text{soln}}}{\text{cm}^3\cdot\text{mol}^{-1}}$	$\frac{V_m^E}{\text{cm}^3\cdot\text{mol}^{-1}}$	$\frac{V_m^E/(x_1x_2)}{\text{cm}^3\cdot\text{mol}^{-1}}$	$\frac{V\phi_{\text{MeOH}}}{\text{cm}^3\cdot\text{mol}^{-1}}$	$\frac{V\phi_{\text{CO}_2}}{\text{cm}^3\cdot\text{mol}^{-1}}$
0.190	18.350 ± 0.007	43.15 ± 0.02	-4.216 ± 0.007	-26.37 ± 0.01		50.51 ± 0.02
0.100	18.34 ± 0.05	41.7 ± 0.1	-2.686 ± 0.007	-29.76 ± 0.08		44.81 ± 0.12
0 (Expt.)	16.12 ± 0.05	41.3 ± 0.1	0			
0 (Lit.)	16.11	41.315	0			

Table A-5: Volumetric results for (CO₂ + MeOH) mixtures at 373.15 K and 12.3 MPa.

x_{CO_2}	$10^{-3}(\rho-\rho^*)$ g cm ⁻³	V_{soln} cm ³ mol ⁻¹	V_m^E cm ³ mol ⁻¹	$V_m^E/(x_1x_2)$ cm ³ mol ⁻¹	$V\phi_{\text{MeOH}}$ cm ³ mol ⁻¹	$V\phi_{\text{CO}_2}$ cm ³ mol ⁻¹
1.0	0 ±0.001	175.899 ±0.001	0			
0.966	7.28 ±0.05	135.2 ±0.9	-36.4 ±0.3	-1106 ±8	-1024 ±80	
0.950	9.19 ±0.05	126.9 ±0.7	-42.4 ±0.2	-894 ±5	-806 ±50	
0.399	47.840 ±0.007	50.544 ±0.008	-46.198 ±0.007	-192.52 ±0.03		
0.350	47.820 ±0.004	49.743 ±0.004	-40.463 ±0.003	-177.79 ±0.01		
0.300	48.10 ±0.08	48.74 ±0.08	-34.89 ±0.06	-166.0 ±0.3		
0.250	51.59 ±0.04	45.73 ±0.04	-31.29 ±0.02	-166.7 ±0.1		50.8 ±0.4
0.200	49.03 ±0.09	46.50 ±0.08	-23.88 ±0.04	-149.3 ±0.3		56 ±1
0.150	48.82 ±0.01	45.83 ±0.01	-18.000 ±0.004	-140.95 ±0.04		56.0 ±0.1
0.100	48.79 ±0.01	45.04 ±0.01	-12.209 ±0.003	-135.19 ±0.04		54.1 ±0.1
0.050	47.91 ±0.01	44.76 ±0.01	-5.879 ±0.001	-123.11 ±0.03		58.5 ±0.1
0 (Expt.)	47.790 ±0.01	44.01 ±0.01	0			

...Continued on next page

x_{CO_2}	$\frac{10^3(\rho-\rho^*)}{\text{g cm}^{-3}}$	$\frac{V_{\text{soln}}}{\text{cm}^3 \cdot \text{mol}^{-1}}$	$\frac{V_m^E}{\text{cm}^3 \cdot \text{mol}^{-1}}$	$\frac{V_m^E/(x_1 x_2)}{\text{cm}^3 \cdot \text{mol}^{-1}}$	$\frac{V\phi_{\text{MeOH}}}{\text{cm}^3 \cdot \text{mol}^{-1}}$	$\frac{V\phi_{\text{CO}_2}}{\text{cm}^3 \cdot \text{mol}^{-1}}$
0 (Lit.)	47.76	44.02	0			
2-Phase						
0.801	47.7 ± 0.1	57.2 ± 0.1	-82.4 ± 0.2	-513 ± 1		
0.699	47.8 ± 0.1	55.5 ± 0.2	-76.8 ± 0.2	-366 ± 1		
0.599	47.7 ± 0.1	53.9 ± 0.1	-59.0 ± 0.2	-246 ± 7		
0.499	47.7 ± 0.5	55.2 ± 0.5	-53.0 ± 0.5	-212 ± 2		

Table A-6: Volumetric results for (CO₂ + MeOH) mixtures at 373.15 K and 19.8 MPa.

x_{CO_2}	$10^3(\rho-\rho^*)$ g·cm ⁻³	V_{soln} cm ³ ·mol ⁻¹	V_m^E cm ³ ·mol ⁻¹	$V_m^E/(x_1x_2)$ cm ³ ·mol ⁻¹	$V\phi_{\text{MeOH}}$ cm ³ ·mol ⁻¹	$V\phi_{\text{CO}_2}$ cm ³ ·mol ⁻¹
1.0	0 ±0.001	92.458 ±0.001	0			
0.950	10.75 ±0.001	74.387 ±0.007	-15.591 ±0.001	-326.83 ±0.04	-267 ±16	
0.900	16.900 ±0.007	66.38 ±0.03	-21.150 ±0.009	-235.0 ±0.1	-168 ±8	
0.799	26.780 ±0.004	55.945 ±0.008	-26.633 ±0.004	-166.23 ±0.02		
0.700	28.350 ±0.009	53.22 ±0.02	-24.446 ±0.008	-116.42 ±0.04		
0.600	26.660 ±0.001	52.819 ±0.002	-19.9184 ±0.0008	-83.002 ±0.003		
0.481	26.610 ±0.005	50.933 ±0.009	-15.929 ±0.003	-63.81 ±0.01		
0.450	26.741 ±0.002	50.347 ±0.003	-14.993 ±0.001	-60.574 ±0.004		
0.399	29.12 ±0.04	48.00 ±0.07	-14.86 ±0.02	-61.92 ±0.09		
0.349	29.19 ±0.05	47.18 ±0.07	-13.22 ±0.02	-58.10 ±0.09		
0.300	28.690 ±0.004	46.709 ±0.007	-11.242 ±0.002	-53.503 ±0.008		
0.250	28.570 ±0.006	45.99 ±0.01	-9.489 ±0.002	-50.57 ±0.01		53.5 ±0.1

...Continued on next page

x_{CO_2}	$10^3(\rho-\rho^*)$ g cm ⁻³	V_{soln} cm ³ mol ⁻¹	V_m^E cm ³ mol ⁻¹	$V_m^E/(x_1x_2)$ cm ³ mol ⁻¹	$V\phi_{\text{-MeOH}}$ cm ³ mol ⁻¹	$V\phi_{\text{-CO}_2}$ cm ³ mol ⁻¹
0.100	28.47 ±0.01	43.70 ±0.02	-4.393 ±0.002	-48.65 ±0.02		45.4 ±0.1
0 (Expt.)	26.7 ±0.1	43.1 ±0.2	0			
0 (Lit.)	26.64	43.16	0			

Table A-7 Volumetric results for (CO₂ + MeOH) mixtures at 473.15 K and 12.3 MPa.

x_{CO_2}	$\frac{10^2(\rho-\rho^*)}{\text{g}\cdot\text{cm}^{-3}}$	$\frac{V_{\text{soln}}}{\text{cm}^3\cdot\text{mol}^{-1}}$	$\frac{V_m^E}{\text{cm}^3\cdot\text{mol}^{-1}}$	$\frac{V_m^E/(x_1x_2)}{\text{cm}^3\cdot\text{mol}^{-1}}$	$\frac{V\phi_{\text{MeOH}}}{\text{cm}^3\cdot\text{mol}^{-1}}$	$\frac{V\phi_{\text{CO}_2}}{\text{cm}^3\cdot\text{mol}^{-1}}$
1.0	0 ±0.004	287.272 ±0.004	0			
0.968	4.763 ±0.004	217.2 ±0.2	-62.68 ±0.06	-2033 ±2	[-1912] ±100	
0.959	6.1 ±0.4	204 ±14	-74 ±5	-1894 ±120	[-1798] ±100	
0.899	12.0 ±0.4	156 ±5	-97 ±3	-1068 ±40	-1050 ±10	
0.800	12.3 ±0.5	150 ±6	-90 ±4	-569 ±20		
0.199	41.73 ±0.06	60.36 ±0.08	-42.29 ±0.06	-264.4 ±0.4		
0.100	41.68 ±0.06	58.32 ±0.09	-16.35 ±0.03	-181.7 ±0.4		75 ±1
0.050	41.68 ±0.05	57.27 ±0.07	-10.84 ±0.01	-226.9 ±0.3		71.0 ±0.8
0 (Expt.)	41.4 ±0.05	56.5 ±0.07	0			
0 (Lit.)	44.04	53.97	0			

Continued on next page

x_{CO_2}	$\frac{10^2(\rho-\rho^*)}{\text{g cm}^{-3}}$	$\frac{V_{\text{soln}}}{\text{cm}^3\text{-mol}^{-1}}$	$\frac{V_m^E}{\text{cm}^3\text{-mol}^{-1}}$	$\frac{V_m^E/(x_1x_2)}{\text{cm}^3\text{-mol}^{-1}}$	$\frac{V\phi_{\text{MeOH}}}{\text{cm}^3\text{-mol}^{-1}}$	$\frac{V\phi_{\text{CO}_2}}{\text{cm}^3\text{-mol}^{-1}}$
2-Phase						
0.699	13.8 ± 0.2	138 ± 2	-79 ± 1	-377 ± 5		
0.599	14.0 ± 0.3	156 ± 3	-69.0 ± 0.8	-287 ± 3		
0.500	39.869 ± 0.008	68.90 ± 0.01	-62.07 ± 0.02	-248 ± 0.09		
0.351	41.61 ± 0.01	63.65 ± 0.02	-73.69 ± 0.02	-323.8 ± 0.8		

* Square brackets are placed around values with large uncertainties and that showed questionable behaviour while obtaining their densities.

Table A-8 Volumetric results for (CO₂ + MeOH) mixtures at 473.15 K and 19.8 MPa.

x_{CO_2}	$10^3(\rho-\rho^*)$ g·cm ⁻³	V_{soln} cm ³ ·mol ⁻¹	V_m^E cm ³ ·mol ⁻¹	$V_m^E/(x_1x_2)$ cm ³ ·mol ⁻¹	$V\phi_{\text{MeOH}}$ cm ³ ·mol ⁻¹	$V\phi_{\text{CO}_2}$ cm ³ ·mol ⁻¹
1.0	0 ±0.001	171.579 ±0.001	0			
0.970	7.939 ±0.002	129.96 ±0.04	-38.11 ±0.01	-1317.6 ±0.4	-1444 ±40	
0.951	14.497 ±0.008	108.14 ±0.06	-57.60 ±0.03	-1222.1 ±0.7	-1312 ±30	
0.900	17.977 ±0.001	98.139 ±0.007	-61.701 ±0.005	-686.82 ±0.05	-763 ±10	
0.850	22.56 ±0.02	87.58 ±0.07	-66.42 ±0.05	-522.3 ±0.4	-581 ±6	
0.700	33.29 ±0.01	68.57 ±0.03	-67.73 ±0.03	-322.5 ±0.1		
0.599	35.704 ±0.006	63.92 ±0.01	-60.58 ±0.01	-252.37 ±0.04		
0.499	34.192 ±0.006	63.53 ±0.01	-49.178 ±0.009	-196.71 ±0.03		
0.400	35.13 ±0.01	60.60 ±0.02	-40.44 ±0.02	-168.46 ±0.06		
0.350	35.659 ±0.004	59.102 ±0.006	-36.074 ±0.004	-158.47 ±0.02		
0.300	35.612 ±0.004	58.165 ±0.007	-31.095 ±0.004	-148.03 ±0.02		67.97 ±0.08

...Continued on next page

x_{CO_2}	$\frac{10^3(\rho-\rho^*)}{\text{g cm}^{-3}}$	$\frac{V_{\text{soln}}}{\text{cm}^3\text{mol}^{-1}}$	$\frac{V_m^E}{\text{cm}^3\text{mol}^{-1}}$	$\frac{V_m^E/(X_1X_2)}{\text{cm}^3\text{mol}^{-1}}$	$\frac{V\phi_{\text{MeOH}}}{\text{cm}^3\text{mol}^{-1}}$	$\frac{V\phi_{\text{CO}_2}}{\text{cm}^3\text{mol}^{-1}}$
0.200	35.889 ± 0.004	55.958 ± 0.006	-21.541 ± 0.003	-134.54 ± 0.02		63.95 ± 0.07
0.100	35.766 ± 0.008	54.13 ± 0.01	-11.937 ± 0.003	-128.85 ± 0.03		55.6 ± 0.1
0.049	35.86 ± 0.02	53.06 ± 0.03	-6.767 ± 0.004	-142.63 ± 0.08		36.0 ± 0.2
0 (Expt.)	33.73 ± 0.02	53.95 ± 0.03	0			
1 (Lit.)	36.11	51.87	0			

Table A-9 Volumetric results for (CO₂ + MeOH) mixtures at 498.15 K and 12.3 MPa.

x_{CO_2}	$10^2 \cdot (\rho - \rho^*)$ g·cm ⁻³	V_{soln} cm ³ ·mol ⁻¹	V_m^E cm ³ ·mol ⁻¹	$V_m^E/(x_1x_2)$ cm ³ ·mol ⁻¹	$V\phi_{\text{MeOH}}$ cm ³ ·mol ⁻¹	$V\phi_{\text{CO}_2}$ cm ³ ·mol ⁻¹
1.0	0 ±0.001	310.148 ±0.001	0			
0.970	5.166 ±0.007	225.5 ±0.3	-77.1 ±0.1	-2683 ±3	[-2549] ±120	
0.951	8.88 ±0.01	188.2 ±0.3	-109.2 ±0.2	-2301 ±3	[-2131] ±100	
0.899	17.95 ±0.06	133.2 ±0.4	-151.3 ±0.5	-1675 ±5	-1452 ±20	
0.849	20.93 ±0.06	120.2 ±0.3	-151.6 ±0.4	-1187 ±3	-954 ±10	
0.801	27.97 ±0.06	98.7 ±0.2	-160.5 ±0.3	-1005 ±2	-750 ±8	
0.750	27.99 ±0.05	97.2 ±0.2	-149.0 ±0.3	-794 ±1		
0.700	27.99 ±0.06	95.8 ±0.3	-137.6 ±0.3	-655 ±1		
0.650	41.37 ±0.01	71.68 ±0.02	-149.17 ±0.04	-656.0 ±0.2		
0.599	42.16 ±0.07	69.6 ±0.1	-138.3 ±0.2	-575 ±1		
0.550	41.59 ±0.01	69.24 ±0.02	-126.06 ±0.04	-509.4 ±0.2		

...Continued on next page

x_{CO_2}	$10^3(\rho-\rho^*)$ $\text{g}\cdot\text{cm}^{-3}$	V_{soln} $\text{cm}^3\cdot\text{mol}^{-1}$	V_m^E $\text{cm}^3\cdot\text{mol}^{-1}$	$V_m^E/(x_1x_2)$ $\text{cm}^3\cdot\text{mol}^{-1}$	$V\phi_{\text{MeOH}}$ $\text{cm}^3\cdot\text{mol}^{-1}$	$V\phi_{\text{CO}_2}$ $\text{cm}^3\cdot\text{mol}^{-1}$
0.500	42.31 ± 0.06	67.29 ± 0.09	-115.1 ± 0.2	-460.4 ± 0.6		
0.449	41.55 ± 0.06	67.1 ± 0.1	-102.5 ± 0.2	-414.2 ± 0.7		
0.400	41.59 ± 0.09	66.0 ± 0.1	-90.8 ± 0.2	-378.5 ± 0.8		
0.350	-41.72 ± 0.03	64.80 ± 0.04	-79.38 ± 0.06	-348.8 ± 0.2		
0.301	41.72 ± 0.01	63.73 ± 0.02	-67.72 ± 0.02	-322.3 ± 0.1		
0.250	41.55 ± 0.07	62.9 0.1	-55.80 ± 0.09	-297.4 ± 0.5		87 ± 1
0.200	41.49 ± 0.01	61.84 ± 0.02	-43.95 ± 0.01	-274.85 ± 0.08		90.2 ± 0.3
0.150	41.56 ± 0.01	60.69 ± 0.02	-32.421 ± 0.009	-254.00 ± 0.07		94.3 ± 0.3
0.100	41.78 ± 0.01	59.39 ± 0.01	-20.981 ± 0.005	-232.45 ± 0.05		101.02 ± 0.02
0.050	44.12 ± 0.03	55.98 ± 0.03	-11.607 ± 0.007	-243.2 ± 0.2		79.2 ± 0.5
0 (Expt.)	44.33 ± 0.03	54.75 ± 0.03	0			
1 (Lit.)	39.43	59.75	0			

Table A-10 Volumetric results for (CO₂ + MeOH) mixtures at 498.15 K and 19.8 MPa

x_{CO_2}	$\frac{10^2(\rho-\rho^*)}{\text{g cm}^{-3}}$	$\frac{V_{\text{soln}}}{\text{cm}^3\text{-mol}^{-1}}$	$\frac{V_m^E}{\text{cm}^3\text{-mol}^{-1}}$	$\frac{V_m^E/(x_1x_2)}{\text{cm}^3\text{-mol}^{-1}}$	$\frac{V\phi_{\text{MeOH}}}{\text{cm}^3\text{-mol}^{-1}}$	$\frac{V\phi_{\text{CO}_2}}{\text{cm}^3\text{-mol}^{-1}}$
1.0	0 ±0.002	187.516 ±0.002	0			
0.970	5.197 ±0.004	152.3 ±0.1	-31.36 ±0.02	-1083.7 ±0.8	-994 ±50	
0.950	12.91 ±0.07	119.3 ±0.6	-61.7 ±0.3	-1309 ±7	-1186 ±20	
0.900	17.92 ±0.02	103.44 ±0.09	-71.09 ±0.06	-791.1 ±0.7	-655 ±10	
0.850	17.92 ±0.02	102.0 ±0.1	-66.06 ±0.06	-519.4 ±0.5	-384 ±5	
0.800	19.65 ±0.02	96.51 ±0.08	-65.00 ±0.06	-406.4 ±0.3		
0.750	21.53 ±0.03	91.2 ±0.1	-63.9 ±0.1	-341.0 ±0.5		
0.699	24.92 ±0.03	83.5 ±0.1	-64.96 ±0.09	-309.3 ±0.4		
0.599	32.401 ±0.007	70.19 ±0.01	-65.25 ±0.01	-271.79 ±0.06		
0.500	32.50 ±0.01	67.95 ±0.02	-54.58 ±0.02	-218.32 ±0.07		
0.400	32.50 ±0.01	65.81 ±0.02	-43.68 ±0.01	-181.99 ±0.06		
0.351	32.429 ±0.006	64.82 ±0.01	-38.188 ±0.007	-167.78 ±0.03		

...Continued on next page

x_{CO_2}	$\frac{10^3(\rho-\rho^*)}{\text{g cm}^{-3}}$	$\frac{V_{\text{soln}}}{\text{cm}^3\text{mol}^{-1}}$	$\frac{V_m^E}{\text{cm}^3\text{mol}^{-1}}$	$\frac{V_m^E/(x_1x_2)}{\text{cm}^3\text{mol}^{-1}}$	$\frac{V\phi_{\text{MeOH}}}{\text{cm}^3\text{mol}^{-1}}$	$\frac{V\phi_{\text{CO}_2}}{\text{cm}^3\text{mol}^{-1}}$
0.300	32.420 ± 0.008	63.75 ± 0.02	-32.714 ± 0.008	-155.76 ± 0.04		78.5 ± 0.2
0.200	32.406 ± 0.003	61.628 ± 0.007	-21.837 ± 0.002	-136.43 ± 0.01		78.38 ± 0.08
0.100	32.062 ± 0.004	59.859 ± 0.007	-10.632 ± 0.001	-117.75 ± 0.01		81.58 ± 0.09
0.049	32.132 ± 0.002	58.698 ± 0.003	-5.2308 ± 0.0003	-110.308 ± 0.006		82.71 ± 0.05
0 (Expt.)	32.314 ± 0.005	57.436 ± 0.009	0			
1 (Lit.)	33.93	55.82	0			

Table A-11 Volumetric results for (CO₂ + MeOH) mixtures at 523.15 K and 12.3 MPa.

x_{CO_2}	$10^2(\rho-\rho^*)$ $\text{g}\cdot\text{cm}^{-3}$	V_{soln} $\text{cm}^3\cdot\text{mol}^{-1}$	V_m^E $\text{cm}^3\cdot\text{mol}^{-1}$	$V_m^E/(x_1x_2)$ $\text{cm}^3\cdot\text{mol}^{-1}$	$V\phi_{\text{MeOH}}$ $\text{cm}^3\cdot\text{mol}^{-1}$	$V\phi_{\text{CO}_2}$ $\text{cm}^3\cdot\text{mol}^{-1}$
1.0	0 ±0.002	332.401 ±0.002	0			
0.950	7.849 ±0.005	205.8 ±0.1	-114.02 ±0.08	-2404 ±2	[-2203] ±100	
0.900	21.97 ±0.07	121.6 ±0.4	-185.6 ±0.6	-2056 ±6	[-1769] ±100	
0.849	23.750 ±0.009	114.12 ±0.04	-180.59 ±0.07	-1415.4 ±0.6	-1121.6 ±20	
0.801	25.35 ±0.03	107.8 ±0.1	-174.5 ±0.2	-1093 ±1		
0.750	25.503 ±0.002	105.870 ±0.009	-163.77 ±0.01	-873.43 ±0.07		
0.699	25.57 ±0.03	104.1 ±0.1	-152.9 ±0.2	-728 ±1		
0.651	26.370 ±0.002	100.545 ±0.006	-144.123 ±0.009	-633.94 ±0.04		
0.601	26.69 ±0.04	98.3 ±0.1	-133.9 ±0.2	-558.2 ±0.7		
0.550	26.359 ±0.002	97.551 ±0.008	-125.34 ±0.01	-506.52 ±0.04		
0.500	26.14 ±0.03	96.6 ±0.1	-115.3 ±0.1	-461.0 ±0.6		

...Continued on next page

x_{CO_2}	$\frac{10^3(\rho-\rho^*)}{\text{g cm}^{-3}}$	$\frac{V_{\text{soln}}}{\text{cm}^3 \text{mol}^{-1}}$	$\frac{V_m^E}{\text{cm}^3 \text{mol}^{-1}}$	$\frac{V_m^E/(x_1x_2)}{\text{cm}^3 \text{mol}^{-1}}$	$\frac{V\phi_{\text{MeOH}}}{\text{cm}^3 \text{mol}^{-1}}$	$\frac{V\phi_{\text{CO}_2}}{\text{cm}^3 \text{mol}^{-1}}$
0.451	25.334 ± 0.006	97.02 ± 0.02	-105.23 ± 0.02	-425.2 ± 0.1		
0.400	25.32 ± 0.04	95.5 ± 0.2	-95.1 ± 0.1	-396.2 ± 0.6		
0.350	25.37 ± 0.07	93.8 ± 0.3	-80.9 ± 0.2	-355 ± 1		
0.250	27.799 ± 0.002	85.373 ± 0.008	-60.981 ± 0.005	-324.95 ± 0.02		
0.200	26.02 ± 0.07	87.7 ± 0.2	-53.3 ± 0.1	-333.2 ± 0.7		
0.150	26.107 ± 0.006	86.00 ± 0.02	-43.891 ± 0.008	-313.69 ± 0.06		35.76 ± 0.09
0.100	26.26 ± 0.06	84.2 ± 0.2	-27.41 ± 0.05	-303.6 ± 0.5		-61.3 ± 0.2
0.050	26.411 ± 0.006	82.32 ± 0.02	-12.380 ± 0.002	-259.19 ± 0.05		-168.0 ± 0.3
0 (Expt.)	25.14 ± 0.06	81.4 ± 0.2	0			
1 (Lit.)	30.65	73.00	0			

Table A-12 Volumetric results for (CO₂ + MeOH) mixtures at 523.15 K and 19.8 MPa

x_{CO_2}	$\frac{10^3(\rho-\rho^*)}{\text{g}\cdot\text{cm}^{-3}}$	$\frac{V_{\text{soln}}}{\text{cm}^3\cdot\text{mol}^{-1}}$	$\frac{V_m^E}{\text{cm}^3\cdot\text{mol}^{-1}}$	$\frac{V_m^E/(x_1x_2)}{\text{cm}^3\cdot\text{mol}^{-1}}$	$\frac{V\phi_{\text{MeOH}}}{\text{cm}^3\cdot\text{mol}^{-1}}$	$\frac{V\phi_{\text{CO}_2}}{\text{cm}^3\cdot\text{mol}^{-1}}$
1.0	0 ±0.02	202.72 ±0.02	0			
0.950	10.29 ±0.03	135.7 ±0.4	-60.6 ±0.2	-1282 ±4	-1149 ±40	
0.900	16.29 ±0.03	112.7 ±0.2	-76.8 ±0.1	-854 ±1	-699 ±10	
0.850	20.167 ±0.005	100.82 ±0.03	-82.06 ±0.02	-645.1 ±0.2	-479 ±1	
0.800	19.91 ±0.02	100.0 ±0.1	-76.21 ±0.08	-476.5 ±0.5		
0.750	20.64 ±0.02	96.86 ±0.08	-72.73 ±0.06	-388.2 ±0.3		
0.699	23.30 ±0.02	89.79 ±0.08	-73.12 ±0.07	-348.1 ±0.3		
0.650	23.63 ±0.03	87.8 ±0.1	-68.46 ±0.09	-300.9 ±0.4		
0.599	25.69 ±0.03	82.7 ±0.1	-66.86 ±0.08	-278.5 ±0.3		
0.549	25.68 ±0.03	81.5 ±0.1	-61.50 ±0.07	-248.5 ±0.3		
0.500	25.69 ±0.02	80.23 ±0.06	-56.20 ±0.04	-224.8 ±0.2		
0.451	25.69 ±0.03	78.98 ±0.09	-50.84 ±0.06	-205.4 ±0.2		

... Continued on next page

x_{CO_2}	$\frac{10^4(\rho-\rho^*)}{\text{g}\cdot\text{cm}^{-3}}$	$\frac{V_{\text{soln}}}{\text{cm}^3\cdot\text{mol}^{-1}}$	$\frac{V_m^E}{\text{cm}^3\cdot\text{mol}^{-1}}$	$\frac{V_m^E/(X_1X_2)}{\text{cm}^3\cdot\text{mol}^{-1}}$	$\frac{V\phi_{\text{MeOH}}}{\text{cm}^3\cdot\text{mol}^{-1}}$	$\frac{V\phi_{\text{CO}_2}}{\text{cm}^3\cdot\text{mol}^{-1}}$
0.400	25.69 ± 0.01	77.70 ± 0.03	-45.43 ± 0.02	-189.26 ± 0.08		
0.351	25.69 ± 0.03	76.44 ± 0.09	-40.07 ± 0.05	-176.1 ± 0.2		
0.300	25.48 ± 0.04	75.5 ± 0.1	-34.35 ± 0.05	-163.6 ± 0.2		
0.250	25.082 ± 0.006	74.88 ± 0.02	-28.371 ± 0.007	-151.19 ± 0.04		
0.200	25.08 ± 0.04	73.6 ± 0.1	-22.99 ± 0.04	-143.7 ± 0.2		-116 ± 2
0.150	24.498 ± 0.007	72.48 ± 0.02	-17.520 ± 0.005	-137.09 ± 0.04		-202.2 ± 0.6
0.100	24.77 ± 0.03	71.50 ± 0.08	-11.85 ± 0.01	-131.2 ± 0.2		-373 ± 4
0.049	24.78 ± 0.01	70.20 ± 0.03	-6.456 ± 0.002	-136.15 ± 0.05		-899 ± 4
0 (Expt.)	24.04 ± 0.03	70.04 ± 0.09	0			
1 (Lit.)	30.04	61.91	0			

